The Dissertation Committee for Ramya Bhagavatula
certifies that this is the approved version of the following dissertation:

Limited Feedback for Multicell Cooperative Systems

Committee:

Robert W. Heath, Jr., Supervisor

Jeffrey Andrews

Brian Evans

John Hasenbein

Angel Lozano

Sriram Vishwanath

Limited Feedback for Multicell Cooperative Systems

by

Ramya Bhagavatula, B.E., M.S.E.

DISSERTATION

Presented to the Faculty of the Graduate School of

The University of Texas at Austin

in Partial Fulfillment

of the Requirements

for the Degree of

DOCTOR OF PHILOSOPHY

THE UNIVERSITY OF TEXAS AT AUSTIN

December 2010

Dedicated to my family.

Acknowledgments

I would like to start by thanking my advisor, Prof. Robert W. Heath, Jr., for giving me the opportunity to do a Ph.D. under his supervision. I can confidently say that I would not be where I am if it were not for his belief in me and demand for higher standards of research at every step. A special thanks goes out to my friends in and outside WNCG for their camaraderie.

I want to express my gratitude to my parents, Charumathi and Radha Krishna Bhagavatula, and my brother, Sravan Bhagavatula, for their love and, sometimes undeserved, support. I owe the person I am to my parents and brother. Finally, I would like to mention the one person who was as much a part of my Ph.D. as I was - Anand Dhulipala, my better half in the true sense of the word. His unconditional love, patience, and support remind me of my blessings every day.

Limited Feedback for Multicell Cooperative Systems

Publication No. _____

Ramya Bhagavatula, Ph.D.
The University of Texas at Austin, 2010

Supervisor: Robert W. Heath, Jr.

Cellular systems are interference limited in nature. This problem is further accentuated in upcoming commercial wireless standards, which intend to use all the available spectrum in every cell in the network to improve peak data rates. This, however, could lead to considerable interference among neighboring cells, decreasing data rates and causing outages at the cell-edge. Multicell cooperation offers a solution for reducing the high levels of interference. The basic idea is that base stations coordinate transmissions by sharing user information among themselves via backhaul links. With the backhaul being bandwidth limited, cooperative strategies that involve the exchange of only user channel state information (CSI) among base stations offer the best tradeoff between complexity, backhaul load and performance gains. This dissertation focuses on these partial cooperative techniques, known as *coordinated beamforming* in 3GPP LTE Advanced.

In existing frequency division duplex systems, users estimate and feedback the CSI of a single channel over a finite-bandwidth feedback link, using *limited feedback* techniques. In a multicell cooperative scenario, each user needs to transmit the CSI of *multiple* channels using the same feedback link. This implies that the available feedback bandwidth must be efficiently shared among different channels to maximize performance gains in the cellular network.

This dissertation develops three different approaches to limited feedback in multicell cooperative systems. The first technique, *separate quantization*, involves each channel being fed back individually using a different codebook. Closed-form expressions are derived to partition adaptively the available feedback bits, as a function of the signal strengths and delays associated with each of the multiple channels. The second strategy is known as *joint quantization*, where the CSI of all the channels are quantized together as a composite vector. It is shown that though this approach yields higher data rates with smaller feedback requirements than separate quantization, it requires the design and storage of special codebooks. Finally, *predictive joint quantization* is proposed to exploit the temporal correlation of the wireless channel to reduce feedback requirements significantly as compared to the other two strategies, at the cost of high complexity at the user terminals.

Table of Contents

List of Tables

List of Figures

Chapter 1

Introduction

The past few years have witnessed wireless communications become indispensable to everyday life. Smartphones have revolutionized cellular telephony by providing data connectivity on the go, resulting in unprecedented levels of data traffic in cellular networks. Achieving higher data rates and ubiquitous coverage requires overcoming challenges characteristic of wireless cellular systems. Rapid fluctuations in the received signal strength, referred to as *fading*, interference from transmissions in neighboring cells, and limited spectrum availability are factors that can affect the performance of a wireless communications link. The effects of fading can be combated by using multiple antennas at the base station and receiver units. Inter-cell interference arising due to transmissions on the same frequency, known as *co-channel interference* (CCI), can decrease data rates and increase outages in cellular systems. Earlier developed systems reduce CCI through frequency reuse, where the available spectrum is split among all the cells in the network. The idea is to geographically separate cells using the same frequency resources, as shown in Fig. 1.1(a). Since each cell is allocated only a fraction of the total bandwidth to decrease CCI, peak data rates that can be obtained are reduced.

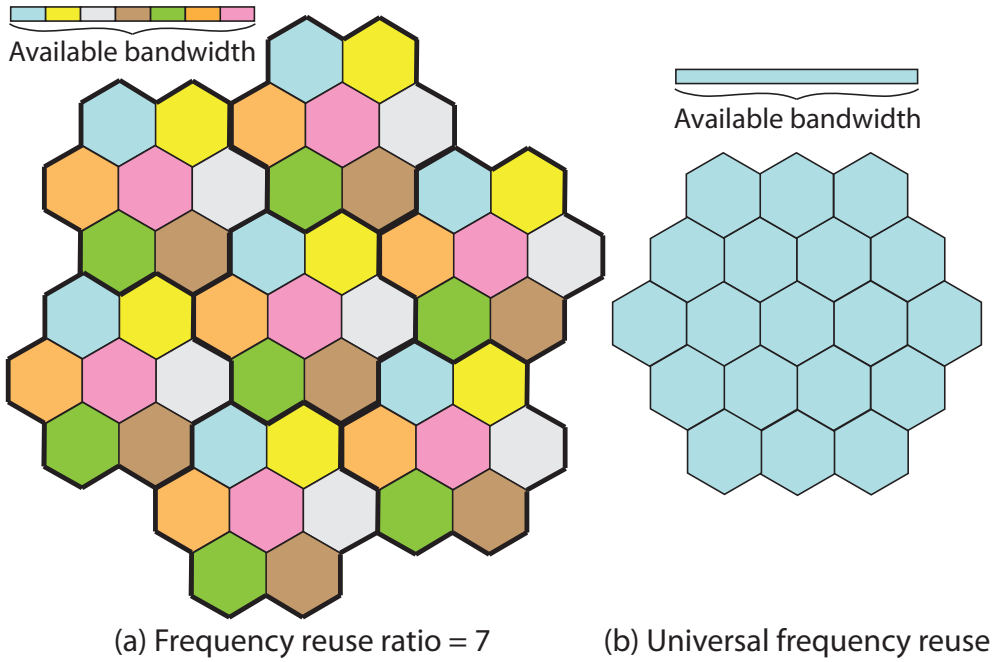

Figure 1.1: Illustration of a cellular system with (a) frequency reuse ratio = 7 and (b) universal frequency reuse.

Upcoming cellular standards, like the third generation partnership program (3GPP) long term evolution (LTE) Advanced [2] and IEEE 802.16m [65] aim to increase the peak data rates by employing universal frequency reuse, as shown in Fig. 1.1(b). Reusing frequencies in adjacent cells, however, can lead to very high levels of CCI. *Multicell cooperation* is a solution for managing CCI.

1.1 Multicell Cooperation

In multicell cooperation, base stations coordinate their transmissions to improve data rates and reduce outages in cellular systems. Known as *coordi-*

nated multipoint transmission (CoMP) in the 3GPP LTE Advanced literature, it involves the exchange of information among base stations using backhaul communication links, as illustrated in Fig. 1.2 for a three-cell system.

Multicell cooperation plays an important role in obtaining the high data rates promised by next generation wireless cellular systems. Depending on the transmission technique employed, base stations can exchange control-level signals, and/or transmit data, and/or user propagation information, known as channel state information (CSI) [50, 58, 77]. CSI refers to the radio channel information of the desired or interfering signals and incorporates fading effects. Knowledge of CSI can enable the transmitter to assign suitable weights to each of the transmit antennas. This is known as *beamforming* for single-stream transmission; the transmitter designs *beamforming vectors* to adapt its transmission to overcome the impact of fading, thus increasing received signal strength and improving link reliability and data rates. In cooperative systems, base stations can exploit information of the desired and interfering channels at the users to coordinate transmissions effectively. For example, if a base station is informed of the CSI of the interference that it causes to a user in an adjacent cell, it can transmit in a direction orthogonal to the interfering channel, thereby nulling out the interference it causes to the user. This strategy is known as inter-cell interference nulling (ICIN) [99].

Successful implementation of multicell cooperation in upcoming cellular systems requires identifying and addressing practical constraints that can degrade performance gains. The delay associated with backhaul links

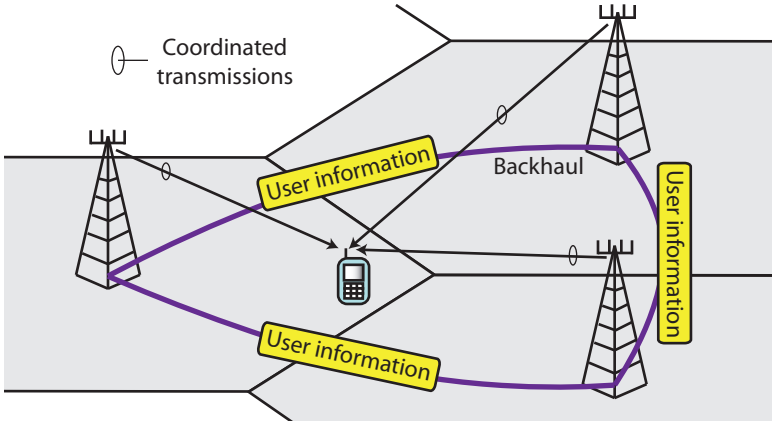

Figure 1.2: Base station cooperation for a three-cell system.

[8, 10, 38] plays an important role in obtaining performance gains from cooperation. While communication links are typically associated with delays due to signal processing, protocol overhead, scheduling etc. [4, 39, 45, 64, 101], the backhaul introduces an additional source of delay in multicell cooperative strategies. This causes the CSI available at base stations via the backhaul to be outdated, reducing performance gains. The bandwidth of the backhaul link is another factor that can affect how much data is exchanged between base stations, which in turn determines the *level of cooperation* and the data rates achieved. Backhaul capacity is limited in practice due to the prohibitive expenditure involved in establishing high-capacity wired links by network providers [74, 79, 80]. Most of the literature on base station cooperation assumes ideal backhaul with zero-delay and no bandwidth restrictions. This dissertation analyzes the impact of delay on the performance of transmission strategies that impose reasonable loads on the backhaul by requiring the exchange of

only CSI among base stations [73]. These techniques are referred to as *partial cooperation* in the remainder of this text and as *coordinated beamforming* in 3GPP LTE Advanced.

Users in multicell cooperative systems estimate CSI of multiple channels using orthogonal training sequences from each of the different base stations [33, 53, 56, 87, 100]. This increases downlink overhead and reduces the potential performance gains from multicell cooperation. Overhead from CSI estimation can be reduced by grouping a reasonable number of cooperating cells into a cluster and cooperating only among base stations in the cluster [100]. This way, each user has to estimate the CSI of channels from only a few base stations. Different techniques to manage the overhead resulting from CSI estimation in the downlink are proposed in [56, 87]. Measurement results in [53] confirm that coordinated multipoint transmission can yield improvements in the sum-rate for low to moderate user velocities, where larger coherence times make frequent CSI estimation unnecessary and reduce downlink overhead.

The availability of CSI at the transmitter(s) is also an important consideration in multicell cooperation. There are two approaches to provide CSI at base stations. The first is applicable in time division duplex (TDD) systems, where the principle of reciprocity is used to obtain CSI from the uplink channel. In frequency division duplex (FDD) systems, however, uplink and downlink transmissions take place over different frequencies, causing reciprocity to be invalid. FDD-based multicell cooperative system is, however, being considered in 3GPP LTE-Advanced for integration with the legacy 3GPP LTE standard

[2]. The feedback overhead associated with sending back CSI of multiple channels from each user to the base station could limit performance gains in FDD-based cooperative systems. This dissertation develops techniques for reducing the feedback requirements involved with providing base stations with the desired and interfering CSI, which is important for realizing the performance gains promised by base station cooperation.

The requirement for synchronizing transmissions across the coordinating base stations is important to manage CCI through cooperation. Asynchronous interference can reduce the data rates obtained [98]. Global positioning systems and network synchronization protocols can be used to synchronize the clocks in different base stations [52]. Most of the existing literature on base station cooperation assumes synchronization among base stations. This dissertation also assumes that the network is synchronized perfectly.

1.2 Limited Feedback

In networks that use FDD, the uplink channel used for feeding back CSI to the base station is finite-bandwidth. Hence, CSI is quantized at the user terminal using a codebook known at both the transmitter and receiver, and the index corresponding to the selected codeword is transmitted over the uplink to the base station. The existing literature on limited feedback considers single-cell non-cooperative systems, which do not take into account inter-cell interference (ICI), and hence, require the CSI of only the desired channel to be fed back over the uplink, as shown in Fig. 1.3(a). This is known

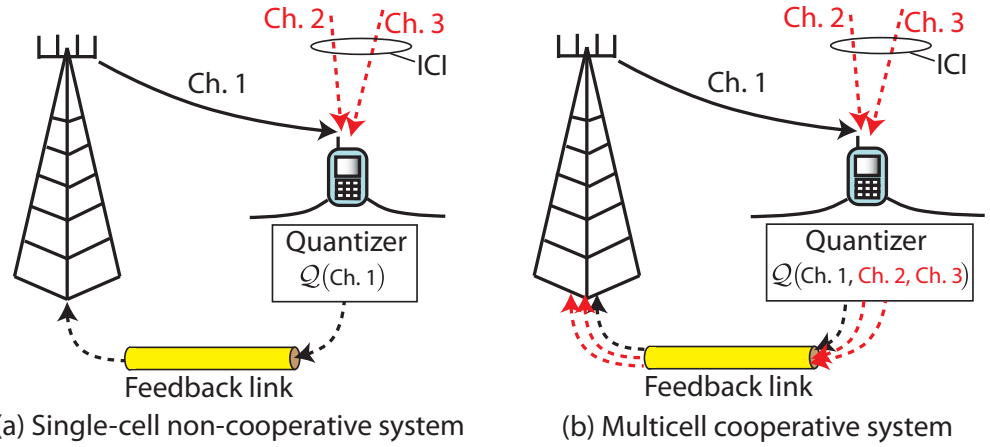

Figure 1.3: Illustration of limited feedback in (a) single-cell non-cooperative and (b) multicell cooperative systems.

as *limited feedback* and is a very well investigated topic for non-cooperative systems (please refer to [63] and the references within). Unfortunately, results from single-cell limited feedback [63] are not directly applicable to the multicell scenario.

While the CSI of only one channel is fed back in the single-cell case, cooperative strategies require feedback of CSI from *multiple* base stations over the uplink, as illustrated in Fig. 1.3(b). Each of the multiple channels might be associated with different signal strengths and channel statistics. In single-cell transmission, quantized CSI reaches the base station after experiencing a delay due to signal processing and propagation [45, 101]. In the multicell cooperative framework, however, quantized CSI is subject to an *additional* source of delay in the backhaul link. The impact of delayed CSI on the performance of (single-cell) non-cooperative systems [45, 101] has been investigated extensively. The

Table 1.1: Comparison between limited CSI feedback for single-cell and cooperative systems.

Single-cell systems	**Cooperative systems**
CSI of *single* channel	CSI of *multiple* channels
Delay in feedback link	Delay in feedback *and backchaul* links
Feedback a single channel	Feedback channels with different signal strengths, statistics, delays

effect of delayed limited feedback on the performance of cooperative systems has received comparatively less attention. Also, the multiple channels might suffer from different delays. The differences between single-cell and cooperative systems are summarized in Table 1.1. Note that most of the literature on multicell cooperation assumes that full CSI is available at the transmitters.

The performance of multicell cooperative transmission strategies is highly dependent on the quality of the CSI fed back by the users. Limited feedback for multicell systems is a topic of ongoing research [9–12, 99]. This dissertation proposes the following three techniques to quantize the CSI of multiple channels.

1. **Separate quantization** - In this approach, available feedback bits are partitioned among the different channels to be fed back. Each channel is individually quantized using separate codebooks. Feedback bits can either be allocated equally or partitioned adaptively in proportion to the signal strengths and delays associated with each of the channels. Separate quantization allows existing codebooks (for single CSI feedback)

to be used, making it the most practical solution given the current state-of-the-art. The disadvantage, however, is that separate quantization requires higher feedback requirements and yields the least data rates as compared to the other strategies proposed in this dissertation.

2. **Joint quantization** - In joint quantization, all the estimated channels are concatenated to form a *net channel vector*, which is quantized using a single codebook. Adaptive inherent biases introduced in quantizing different parts of the net channel vector with varying resolutions make this technique different from single-cell limited feedback. While this strategy yields higher data rates than separate quantization, it requires the design of special codebooks that can implement the different biases.

3. **Predictive quantization** - Exploiting the temporal correlation in radio channels can help significantly decrease the distortion associated with CSI quantization and reduce feedback requirements. While this approach yields the highest data rates and least feedback requirements as compared to the other two strategies, it also requires special codebook designs and possesses higher complexity.

The three strategies are compared in Table 1.2. This dissertation develops limited feedback models and techniques, using these three approaches to feedback the CSI of multiple channels over a finite-bandwidth link for multicell base station cooperation.

Table 1.2: Comparison of the three approaches for limited CSI feedback for multicell cooperation.

Feature	Data Rates	Feedback Requirements	Ease of Implementation
Sep. quant.	✓	✓	✓✓✓
Joint quant.	✓✓	✓✓	✓✓
Pred. quant.	✓✓✓	✓✓✓	✓

1.3 Thesis Statement

Knowledge of high resolution CSI of multiple channels is necessary at base stations to obtain the high data rates and reduced outages promised by multicell cooperation.

1.4 Contributions

The contributions of this dissertation can be classified into three categories - separate, joint, and predictive quantization.

- **Separate quantization** - Feedback-bit partitioning is motivated by first considering a single interferer system [9]. Separate quantization is then considered for the more realistic case of multiple interferers, assuming delay in communication links [10]. In both instances, feedback bits are assigned adaptively as a function of signal strengths (and delays, in the second case) of the channels involved. The contributions in this approach are listed below.

    1. A limited CSI feedback model is proposed for the (single and) mul-

tiple interferer scenario with delays in the feedback and backhaul links. In the proposed model, each user feeds back quantized CSI of the desired and interfering channels to its own base station [9, 10]. The neighboring base stations exchange only the quantized interfering CSI, making the load on the backhaul link manageable.

2. The loss in performance gains due to limited feedback is quantified by deriving an upper bound on the mean loss in sum-rate in a multiple-input single-output (MISO) system [9, 10]. The bound is a function of the number of feedback bits allocated to each of the channels, the relative strengths, and delays of the channels.

3. A novel feedback-bit partitioning algorithm is presented to allocate the available feedback bits between the desired and interfering channels to reduce the mean loss in sum-rate due to limited feedback, as a function of their relative strengths and delays [9, 10].

4. Simulations verify that the proposed feedback-bit allocation algorithms reduce the mean-loss in sum-rate associated with delayed limited feedback. It is also shown that adaptively partitioning the feedback bits yield much better performance than equal-bit allocation.

- **Joint quantization** - The CSI of multiple channels is quantized as a net channel vector in joint quantization [12]. A multiple interferer scenario is considered with zero-delays associated with the communication links.

The selection criterion derived in this dissertation quantizes stronger channels more finely than the weaker ones, thus ensuring that available feedback resources are efficiently utilized towards reducing the loss in data rate as a result of limited feedback. The contributions in joint quantization can be summarized as follows.

1. A limited CSI feedback model is proposed for joint quantization, where users concatenate the CSI of multiple channels and feed back the net channel vector using a single codebook.
2. A joint quantization approach is presented for informing the base station of the error vectors. A *selection criterion* is derived to select adaptively appropriate codewords, as a function of the signal strengths of the channels [12].
3. Simulation results illustrate the potential benefits of jointly quantizing the CSI of multiple channels over separate quantization approaches.

- **Predictive joint quantization** - Since the CSI of multiple channels is required to be fed back in a multicell cooperative system, feedback requirements are much higher than those in single-cell non-cooperative systems. In this dissertation, predictive quantization is used to improve CSI resolution (and thereby, increase data rates) by exploiting the temporal correlation in wireless propagation channels [11]. It is proposed to concatenate the *error vectors* between the predicted and actual CSI into

a *net error vector*, which is quantized using a single codebook [12].

1. A limited CSI feedback model is proposed for joint predictive quantization, where users predict desired and interfering channels and feed back the errors between the actual and predicted channels. Base stations then exchange this information over the backhaul [11].
2. Joint quantization is used for informing the base station of the error vectors. A selection criterion is derived to select codewords from a codebook, as a function of the signal strengths and delays associated with each of the channels. The selection criterion does not impose any restrictions on the predictor, error estimator, channel statistics, or even the transmit strategy, implying that it can be used as a universal selection criterion for joint quantization in multicell limited CSI feedback [11].
3. A predictor based on subspace-tracking on the Grassmann manifold is proposed. The feedback overhead associated with feeding back the norm of the error vectors is eliminated by means of the presented approach.
4. Simulation results show that joint predictive quantization reduces feedback requirements and improves data rates in multicell cooperative systems.

1.5 Organization

The rest of this dissertation is orgarnized as follows. Chapter 2 provides a brief background on multicell base station cooperation and the feedback strategies proposed in this dissertation. In Chapter 3, feedback-bit partitioning is proposed for a single-interferer, zero-delay case using generalized eigenvector beamforming. In Chapter 4, separate quantization is considered for the more realistic multiple interferers and finite-delay scenarios, using ICIN as the cooperative transmit strategy. Joint quantization is introduced in Chapter 5 for a multiple interferer scenario with zero-delay communication links. Predictive joint quantization is presented in Chapter 6 for the multiple-interferer and finite-delay multicell system to improve data rates and reduce feedback requirements considerably. Chapter 7 draws conclusions from the technical contents of this dissertation and presents directions for future work.

1.6 Notation

In this dissertation, $\mathbf{X}$ refers to a matrix and $\mathbf{x}$ to a column vector. $\mathbf{X}^T$ and $\mathbf{X}^c$ denote the transpose and conjugate, respectively. The Hermitian transpose and pseudo-inverse of $\mathbf{X}$ are given by $\mathbf{X}^*$ and $\mathbf{X}^\dagger$, respectively. An identity matrix of size $R \times R$ is denoted by $\mathbf{I}_R$. $\mathbb{E}\{.\}$ refers to the expectation. $\|\mathbf{x}\|$ stands for the Frobenius norm of $\mathbf{x}$. $\mathcal{N}_c(\mu, \sigma^2)$ refers to a complex Gaussian distribution with mean μ and variance σ^2. The n^{th} column $\mathbf{X}$ is denoted by $\mathbf{X}(:, n)$. The $(m, n)^{\text{th}}$ element in a matrix $\mathbf{X}$ is denoted by $[\mathbf{X}]_{m,n}$. $\mathbb{C}$ and $\mathbb{R}$ denote the field of all complex and all real numbers, respectively. The angle

between two vectors, $\mathbf{x}$ and $\mathbf{y}$ is denoted by $\theta_{\mathbf{x},\mathbf{y}}$. The cardinality of a set $\mathcal{S}$ is denoted by $|\mathcal{S}|$. Further notation is introduced in the chapters, as the need arises.

Chapter 2

Background

This chapter provides a brief background and literature survey on base station cooperation. Multicell limited feedback is discussed and separate, joint and predictive quantization are described in more detail.

2.1 Base Station Cooperation

Multicell cooperation entails sharing control signals, user propagation channel information, and/or transmit data via high-capacity wired backhaul links to coordinate transmissions [5, 9–12, 17, 24, 46, 50, 54, 58, 59, 68, 69, 74, 77, 79, 80, 82, 83, 95, 97, 99]. Based on the amount of information exchanged between base stations over the backhaul, base station cooperation can be broadly classified into the following three categories

1. control-level cooperation,
2. full cooperation, and
3. partial cooperation.

Cooperative strategies that jointly allocate frequency and/or time resources to users in adjacent cells by exchanging control-level information among

base stations lead to a small load on the backhaul link. For example, dynamic and fractional frequency reuse [5] and inter-cell scheduling [17] strategies orthogonalize user transmissions by assigning different frequency bands of operation and timing cycles, respectively. While these techniques yield higher sum-rates than static transmission algorithms, they do not utilize all the available frequency and time resources and do not realize the performance gains that can be potentially obtained using base station cooperation [17].

Full cooperation (known as *joint transmission* in the 3GPP LTE literature) leads to the highest sum-rates at the cost of increased overhead due to global CSI requirements and the exchange of a greater amount of information among base stations, like CSI, transmit data and precoding information. Dirty paper coding (DPC) was shown theoretically to be the sum-capacity achieving solution for single [77] and multiple antenna cellular systems [97]. Note that [77] and [97] used sum-power constraints across all base stations. More realistic per-base and per-antenna power constraints were considered for DPC in [46] and [95], respectively. Multicell DPC is difficult to implement in practice due to the complexity involved with successive encoding, which increases significantly with the number of users [54, 97]. Consequently, low-complexity strategies were proposed in [50, 97] that include zero-forcing, minimum mean square error, and null-space decomposition. It was shown in [50, 97] that though these sub-optimal linear techniques reduce encoding complexity, they still involve the exchange of a large amount of information among base stations, resulting in a prohibitive load on the finite-capacity backhaul

links, similar to DPC [50, 80, 97].

Partial cooperative strategies (known as *coordinated beamforming* in the 3GPP LTE Advanced literature), where base stations exchange only the CSI of active users, offer a fair balance between ensuring a reasonable load on the backhaul links and attaining the performance gains using cooperation [80]. The shared CSI can be used by base stations to design individual precoding matrices (or beamforming vectors, for single-stream transmission) on site to transmit exclusively to users within their own cell [9, 12, 24, 58, 59, 68, 69, 99]. Distributed transmit beamforming was investigated in [24], where an iterative algorithm was proposed to minimize transmit power and not necessarily maximize sum-rate. A distributed beamforming approach was studied in [68, 69] where transmit symbol vectors were designed using linear minimum mean square error estimation techniques such as iterative forward-backward and the sum-product Kalman smoothing algorithms. The convergence of these approaches is, however, not guaranteed. The authors of [58, 59] propose a non-iterative solution to design precoding matrices for multicell systems, which will maximize the sum-rates for only a two-cell system at high signal-to-noise ratio (SNR), using a per base power constraint.

This dissertation considers partial cooperative strategies such as generalized eigenvector beamforming (GEBF) [9, 12] for single-interferer systems, which is based on [58, 59], and inter-cell interference nulling (ICIN) [10, 11, 51, 62, 99] for multiple interferer systems. GEBF and ICIN, introduced in Chapters 3 and 4, respectively, yield reasonable sum rate improvements and require

Table 2.1: Comparison between different levels of cooperation.

Level	Performance gains	Backhaul load	Complexity
Control-level	✓	✓ ✓ ✓	✓ ✓ ✓
Partial	✓ ✓	✓ ✓	✓ ✓
Full	✓ ✓ ✓	✓	✓

only a small amount of additional backhaul bandwidth for moderate Doppler spreads [73]. The three levels of cooperation are compared in Table 2.1.

2.2 Limited Feedback for Multicell Cooperation

Full and partial cooperation requires that base stations have the knowledge of CSI experienced at the users [9–12, 24, 46, 50, 54, 58, 59, 68, 69, 74, 77, 79, 80, 82, 83, 95, 97, 99]. Users can estimate CSI through training symbols transmitted from base stations at regular intervals. As discussed in Section 1.2, limited feedback techniques are used in FDD systems to make CSI available at the base stations using finite-bandwidth feedback links. This dissertation proposes separate, joint, and predictive quantization techniques for multicell limited feedback.

2.2.1 Separate Quantization

Of the three approaches, separate quantization is the most natural extension of single-CSI feedback literature, to quantize multiple channels in a cooperative limited feedback system. Since each channel is quantized individually (as shown in Fig. 2.1), existing single-CSI codebook designs can be

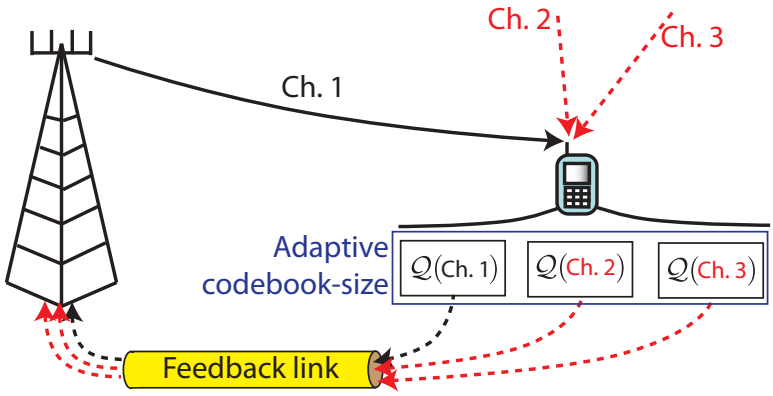

Figure 2.1: Separate CSI quantization for multicell limited feedback.

exploited, making this approach easily adaptable to the current state-of-art.

Equal bit allocation (EBA) is a straightforward solution for separate quantization, where uplink bandwidth is uniformly partitioned among all the channels. It can, however, lead to inefficient utilization of the available feedback resources. For example, if the interference is very weak and does not affect the data rate significantly, few or no bits can be assigned to quantize and feedback the interfering channel. In contrast, if interference is very strong (at cell-edge), more bits can be assigned to the interfering channel to quantize it with high resolution and reduce the quantization error associated with mitigating interference. This is illustrated in Fig. 2.2(a) [9, 10]. Since the uplink channel in a multicell cooperative system must be used for transmitting the CSI of multiple channels, efficiently utilizing the available feedback bits is very important.

Adaptively partitioning feedback bits as a function of the desired and

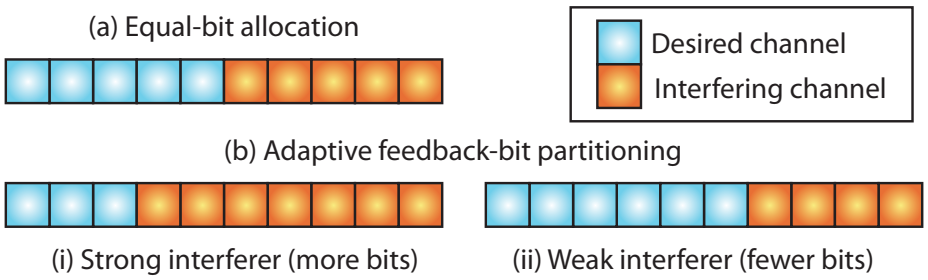

Figure 2.2: Illustration of two separate quantization approaches (a) equal-bit allocation and (b) adaptive feedback-bit partitioning.

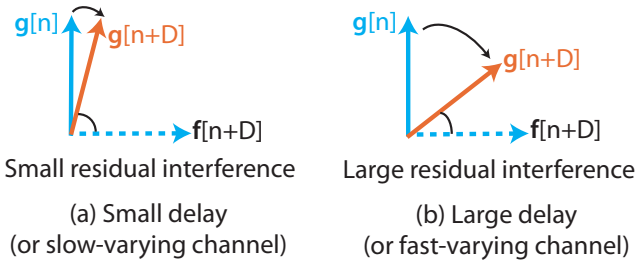

Figure 2.3: Impact of delay in communication links: (a) small delay (or slow-varying channels) and (b) large delay (or fast-varying channels).

interfering channel strengths can efficiently utilize feedback resources. This allows stronger channels that have a larger impact on the data rate to be quantized and fed back with a higher resolution than the weaker channels that do not impact performance as much, as shown in Fig. 2.2(b). In addition to signal strength, feedback bits can also be assigned as a function of the delays associated with each channel. The impact of delay on the performance of wireless system is illustrated in Fig. 2.3, assuming a simple interference nulling strategy. The interference channel is denoted by $\mathbf{g}[n]$ at time instant n. Since information about $\mathbf{g}[n]$ reaches the base station after a delay D, the

beamforming vector at the time instant $n + D$, $\mathbf{f}[n + D]$ is designed so that $|\mathbf{g}^*[n]\mathbf{f}[n + D]| = 0$. If the channel is slowly time varying, then the residual interference caused by $|\mathbf{g}^*[n + D]\mathbf{f}[n + D]|$ is small. In contrast, if $\mathbf{g}[n + D]$ is significantly different than $\mathbf{g}[n]$, the residual interference, $|\mathbf{g}^*[n + D]\mathbf{f}[n + D]|$, can be large, reducing the signal to interference noise ratio (SINR) and thus, decreasing the data rate obtained. In techniques like ICIN, residual interference arising from delayed limited feedback of multiple interferers can significantly degrade SINR.

It is seen from Fig. 2.3 that if a channel suffers from a large delay, the beamforming vector will be designed using outdated information. Due to this reason, quantizing the outdated channel information finely will not decrease the residual interference. Hence, few or no bits can be allocated to feedback channels with large delays. In contrast, high resolution CSI for channels with small delays can help to reduce the associated interference and improve data rates. This dissertation proposes adaptive separate quantization to distribute feedback resources among the desired and interfering channels in proportion to their signal strengths and delays, and utilize feedback bandwidth more efficiently than equal-bit allocation [9, 10].

Quantizing each channel individually can lead to very large feedback requirements, as will be shown in Chapters 3 and 4. Further, the data rates obtained using separate quantization are less than that compared to joint and predictive limited feedback approaches. Separate quantization, however, is still an attractive solution for multicell limited feedback since it offers a

practical and natural extension of the current state-of-the-art, and can exploit the well-researched single-CSI codebook designs.

2.2.2 Joint Quantization

A fundamental result of vector quantization states that the distortion resulting from quantizing a vector may be smaller than that arising from quantizing each component separately, even when the entries are statistically independent [27]. Vector quantization has the ability to exploit linear and nonlinear dependence among the coordinates and hence, has the extra freedom in choosing the multi-dimensional quantizer cell shapes or Voronoi regions [27]. In the multicell cooperative scenario, this result implies that for a given number of feedback bits, quantizing the desired and interfering channels' error vectors *jointly* as a composite vector could yield a lower distortion (or, higher data rate) as compared to separate quantization for the same number of feedback bits. Fig. 2.4 illustrates the principle of joint quantization in a three-cell system. CSI of the three channels is concatenated and quantized using a single codebook.

In separate quantization, available bandwidth is utilized efficiently by allocating feedback bits to the desired and interfering channels in proportion to their signals strengths and delays. In joint quantization, stronger channels are quantized with finer resolution by introducing a bias in the way that codewords are selected from the codebook. For example, in Fig. 2.4, if channel 1 (Ch.1) is stronger than the other two channels, then the codeword is chosen such

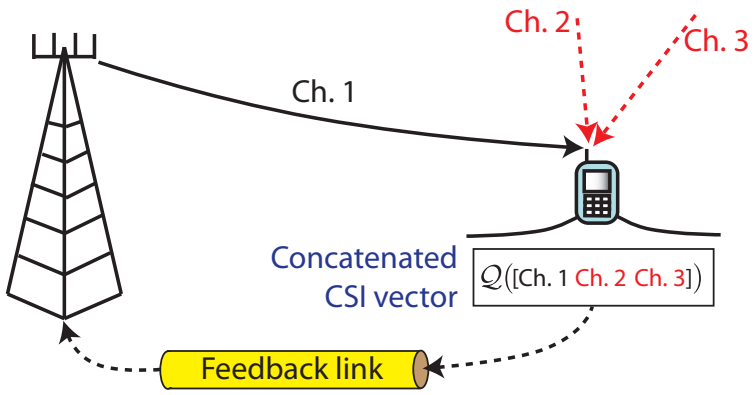

Figure 2.4: Joint CSI quantization for multicell limited feedback.

that the corresponding portion of the concatenated quantization vector is most closely aligned to Ch.1. Hence, the *selection criterion* generates a bias towards choosing the closest alignment to the strongest channels. A selection criterion is derived in Chapter 5 for joint quantization [12]. Note that this approach differs from single-CSI feedback, where the selection criterion corresponds to choosing a codeword that has the smallest angular separation with the single CSI.

Joint quantization using the selection criterion proposed in this dissertation yields larger data rates than when channels are fed back using separate codebooks. It, however, requires special codebook designs for multiple CSI transmission. Further, the selection criterion chooses codewords based on the relative strengths of the different channels, implying that the optimal codebook designs will vary as a function of the received signal energies. Hence, a large number of codebooks need to be stored at the user terminal, increasing

memory requirements [12].

2.2.3 Predictive Quantization

Memory-based vector quantization techniques have received attention in the literature as efficient limited feedback strategies for slowly-varying signals [13, 42, 43, 55, 57, 72, 81, 86, 93, 96]. These approaches exploit correlation in observed data and are applied widely to quantize signals that exhibit high levels of redundancy, such as voice, images, and videos [27, 31, 32]. Since real-life wireless propagation channels exhibit temporal correlation, there has been a considerable amount of research on memory-based limited CSI feedback [13, 42–44, 55, 57, 72, 81, 86, 93, 96]. Note that Chapters 3, 4, and 5 consider single-shot memoryless multicell limited feedback, which does not account for correlation between consecutive samples and can lead to larger distortions.

Predictive vector quantization (PVQ) is a memory-based quantization technique that has gained popularity for CSI quantization in temporally correlated channels [43, 44, 57, 81, 86, 93]. At every time instant, the channel vector is predicted at both the user terminal and base station by exploiting channel characteristics such as statistics and temporal correlation. The user, which can estimate the actual channel, quantizes the residual error between the estimated channel vector and *predicted channel* vector. The *error vector* is then fed back to the base station, as shown in Fig. 2.5(a). When there is zero delay associated with the feedback link, the error vector is added back to the predicted vector to get a *reconstructed* estimate of the actual channel at the base station.

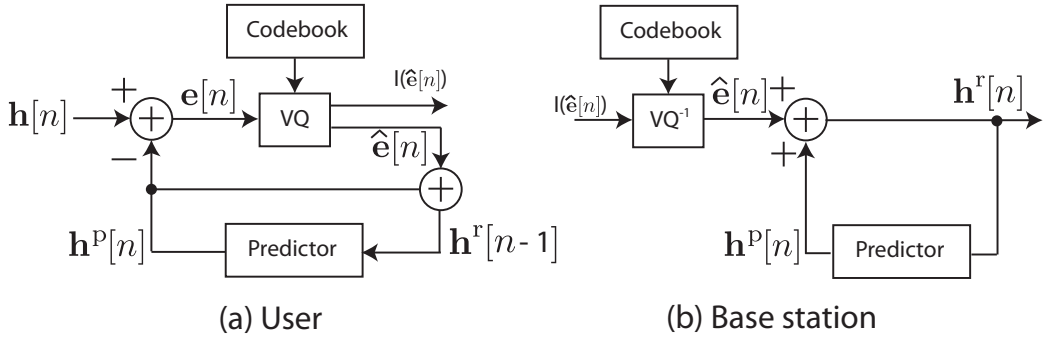

Figure 2.5: Predictive vector quantization for communication links with zero-delay.

The transmitter structure for PVQ is illustrated in Fig. 2.5(b). In channels with a high degree of temporal correlation, error vectors typically have small variances, implying that fewer number of bits can be used for feedback.

The performance of PVQ is dependent on the quality of the predictor used at the user and base station. Linear and non-linear predictors have been well researched in the literature [57, 81, 86, 93]. For example, linear vector predictors are used in [81] and [57] for zero-forcing beamforming in broadcast channels, and in [93] for minimum mean squared error (MMSE) precoding. Linear predictors are typically low-complexity compared to their non-linear counterparts, but result in performance degradation for long-range prediction [22]. A non-linear Kalman filter approach is used in [86], to predict CSI in a broadcast channel, by modeling temporally correlated channels as autoregressive (AR) random processes.

A more recent development is predicting CSI on the Grassmann manifold. It was shown in [23] that the normalized MISO channel directions lie on

a one-dimensional Grammann manifold, under the sum-rate performance metric. In the presence of temporal correlation, the unit-norm and phase-invariant (channel) vectors form a correlated sequence on the manifold [43, 44, 63, 71]. *Grassmannian predictive coding* (GPC) was proposed in [43, 44] for a multiuser system using zero-forcing beamforming. A new signal processing framework was developed for the locally Euclidean Grassmannian space in [43] and a linear predictor was derived assuming instantaneous feedback. Delayed GPC, considered in [44] by optimizing the prediction step size, was shown to yield improvements in the sum-rates for multiuser systems. GPC exploits the redundancy inherent in temporally correlated channels to reduce feedback requirements and yield higher data rates. Prediction via subspace tracking using particle filerting was explored in [71] for a single-user system.

When there is a non-zero delay associated with communication links, base stations cannot generate the reconstructed current channel instantaneously. Instead, the predicted channel vector can be used for designing beamforming vectors at the base station. The delayed error vector is used to reconstruct the past channel and then predict the channel at the current time instant. Delayed limited feedback for a broadcast channel was considered in [44] where a predictor was derived using properties of the Grassmann manifold and shown to yield considerable performance improvement as compared to traditional prediction in the presence of delay. It is to be noted that most of the existing literature on predictive CSI quantization focusses on single-CSI limited feedback [43, 44, 57, 81, 86, 93].

This dissertation develops a PVQ-based limited CSI feedback framework for multicell base station cooperation with multiple interferers and delays in communication links. Error vectors are quantized jointly as a *net error vector*, to obtain the benefits of joint quantization in reducing distortion further and improving the data rates obtained. A prediction algorithm based on subspace tracking on the Grassmann manifold is also presented in Chapter 6 [11]. Simulations confirm that the multicell joint PVQ approach developed in this dissertation reduces feedback requirements significantly in multicell systems, while yielding data rates that are reasonably close to the full CSI case even for delayed limited feedback. The primary disadvantage of the proposed technique, however, is the increased complexity at the base station and user terminals, which grows as the number of cooperating cells increases [11]. Also, jointly quantizing the error vectors requires special codebook designs for maximum performance gains.

Chapter 3

Separate CSI Feedback for Single Interferer Systems with No Delay

This chapter motivates separate CSI quantization for multicell cooperative limited feedback, using a single-interferer model with zero-delay communication links. A feedback-bit partitioning algorithm is proposed to allocate feedback bits adaptively to the desired and interfering channels, as a function of the received signal strengths. Simulation results are used to confirm that the technique reduces the mean loss in sum-rate due to limited feedback and provides an efficient limited feedback approach for multicell cooperation.

3.1 Overview and Contributions

In [58, 59], the authors propose a partial cooperative strategy to maximize the sum-rates for a two-cell system at high signal-to-noise ratio (SNR), using a per base power constraint. This chapter extends the linear beamforming strategy in [58, 59] to maximize the sum-rates (at high SNR) in a *multicell* system for the *soft handoff model*, which considers a linear array of cells with a single user per cell and one dominant interferer at each user location [50, 60, 61, 79, 80, 82, 83]. Beamforming vectors are designed using a general-

ized eigenvector approach by taking into account variations in the desired and interfering signal strengths. The technique is, hence, referred to as generalized eigenvector beamforming (GEBF). GEBF is non-iterative in nature and does not have convergence issues unlike the solutions in other partial-cooperative beamforming solutions like [68, 69]. Further, it uses explicit per-base power constraints, in contrast to distributed zero-forcing beamforming in [82]. GEBF also possesses low-complexity and results in a smaller burden on the backhaul link, in comparison to the full cooperation strategies in [46, 50, 77, 97], while yielding reasonable gains in sum-rates.

Most of the existing work on multicell cooperation assumes the availability of full CSI at the base stations [24, 46, 50, 54, 58–61, 68, 69, 77, 79, 80, 82, 83, 97]. The authors of the two-cell solution in [58, 59] invoke reciprocity to assume full CSI at transmitters in a TDD system. In FDD systems, however, finite bandwidth feedback channels are used to feedback quantized CSI to the base stations using the concept of limited feedback [63]. The fundamental differences between limited CSI feedback for single-cell non-cooperative and multicell cooperative systems, highlighted in Table 1.1, make it unclear how to apply the existing multiuser limited CSI feedback techniques [63, 88, 101] to multicell systems.

This chapter develops a novel adaptive limited feedback strategy, which takes into account the difference in signal strengths to distribute feedback bits among the desired and interfering channels, in a multicell cooperative system, assuming single-interferer and zero-delay communication links. For analytical

reasons, the desired and interfering channels are quantized using random vector quantization (RVQ), i.e. the quantization vectors are independently chosen from the isotropic distribution on a unit hypersphere [49, 75, 76].

This chapter presents analytical results that will be important to understand and design multicell limited feedback strategies. The contributions of this chapter are as follows.

1. Assuming the soft handoff model, a simple limited feedback model is presented for the multicell cooperative system using GEBF. The model requires each user to feedback quantized CSI to its own base station. Adjacent base stations are connected by a backhaul link, which is used to transfer the quantized CSI of only the interfering channels [9]. Hence, the requirement of a global high-capacity backhaul link is eliminated and the load on the backhaul link is manageable.

2. Quantization of CSI can lead to a loss in the sum-rate obtained. This chapter quantifies the mean loss in sum-rate arising due to CSI quantization with RVQ by deriving an upper bound. Shown to be a reliable representation of the mean loss in sum-rate, the upper bound is a function of the codebook sizes of the desired and interfering CSI, in addition to the relative strengths of the two channels.

3. A feedback-bit partitioning algorithm is then proposed to minimize the upper bound on the mean loss in sum-rate. Closed-form expressions are presented that allocate bits to the desired and interfering CSI as a

function of the relative strengths of the two signals. This enables efficient utilization of the available feedback resources [9].

4. Simulation results are presented to show that the proposed adaptive feedback algorithm yields higher mean sum-rates using GEBF than equal bit partitioning technique.

Note that the single-interferer, zero-delay assumptions help in understanding the dependence of the mean sum-rate on the quantization of the desired and interfering channels and their relative strengths. These assumptions are relaxed in the subsequent chapters.

3.2 System Description

This section describes the system model and the partial cooperative transmit strategy, GEBF, adopted in this chapter. The limited feedback model for cooperative multicell systems is also presented.

3.2.1 System Model

The multicell system used in this chapter (shown in Fig. 3.1) is popularly known as the 'soft handoff model'. First introduced in [82, 83], it was later used by other authors for analyzing multicell cooperation [50, 60, 61, 79, 80]. A (possibly finite) linear array of cells is assumed where users are located close to the cell-edge and hence, are subjected to interference primarily from a single base station. This model is based on the Wyner model [91], which is known to

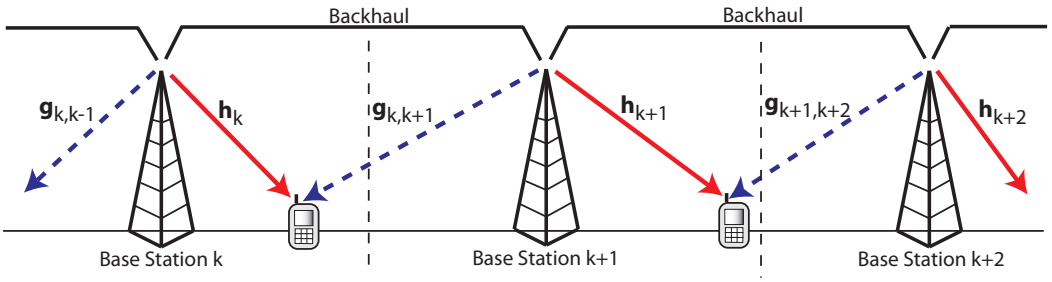

Figure 3.1: Pictorial depiction of the soft handoff model.

capture most real-life effects such as pathloss, fading and intercell interference while retaining analytical tractability [77, 79, 80, 82, 83]. The backhaul and feedback links are assumed to be error-free and zero-delay. It is also assumed that each base station serves a single active user, using intra-cell time division multiple access (TDMA) or a comparable orthogonal access strategy. This is a common assumption in multicell cooperative literature due to the popularity of the Wyner model and the analytical tractability afforded by the single user model [77, 79, 80, 82, 83, 92]. Note that the Wyner model is not accurate representation of the multicell system [92] and the assumptions will be relaxed in the subsequent chapters.

The number of cells in the multicell system is denoted by K, where K goes to infinity for the Wyner model. The k^{th} base station is assumed to service the k^{th} user, for $k = 1, \ldots, K$. All the base stations are equipped with N_t antennas each, while each user supports a single receive antenna. The channel corresponding to the desired signal between the k^{th} base station and k^{th} user is denoted by $\mathbf{h}_k \in \mathbb{C}^{N_t \times 1}$. The interfering channel between the k^{th}

user and the $(k+1)^{\text{th}}$ base station is given by $\mathbf{g}_{k,k+1} \in \mathbb{C}^{N_t \times 1}$. This is illustrated in Fig. 3.1. The solid line represents the desired signal and the dashed line represents the interfering signal. The symbol transmitted from the k^{th} base station (to the k^{th} user) is denoted by s_k, where the transmit power, $\mathbb{E}\{|s_k|^2\}$ is normalized to one. The desired and interfering signal powers at the k^{th} user after large-scale fading effects are given by $\gamma_k^{(\text{d})}$ and $\gamma_{k,k+1}^{(\text{i})}$, respectively. We denote $\gamma_{k,k+1}^{(\text{i})} = \alpha_{k,k+1}\gamma_k^{(\text{d})}$, where $\alpha_{k,k+1}$ denotes the the interfering to signal ratio (ISR)[1]. A similar parameter is used in [50, 82] to model the SNR of the interfering signal with respect to the received signal. Using the narrowband flat-fading model and assuming that the channels remain constant over the codeword transmission, the baseband discrete-time input-output relation for the user in the k^{th} cell is given by

$$y_k = \sqrt{\gamma_k^{(\text{d})}}\mathbf{h}_k^* \mathbf{f}_k s_k + \sqrt{\gamma_{k,k+1}^{(\text{i})}}\mathbf{g}_{k,k+1}^* \mathbf{f}_{k+1} s_{k+1} + v_k,$$

where $y_k \in \mathbb{C}$ is the received signal at the k^{th} user and $\mathbf{f}_k \in \mathbb{C}^{N_t \times 1}$ is the beamforming vector at the k^{th} base station. Note that we drop the discrete-time index for sake of convenience. Finally, $v_k \in \mathbb{C}$ is complex additive zero-mean white Gaussian noise at the receive antennas, with $\mathbb{E}\{|v_k|^2\} = N_0$.

[1]Note that typically $\alpha_{k,\ell} \in (0, 6]$ dB due to the hysteresis effect during handoff [70]. The analysis presented in this dissertation is applicable to hard-handoffs since we assume that the user receives its desired signal from only one base station at a given time instant. The proposed results are not directly applicable to soft-handoff, which is a form of joint transmission.

The signal to interference noise ratio (SINR) of the k^{th} user is given by

$$\begin{aligned} \mathsf{SINR}_k &= \frac{\gamma_k^{(\mathrm{d})} |\mathbf{h}_k^* \mathbf{f}_k|^2}{\alpha_{k,k+1} \gamma_k^{(\mathrm{d})} |\mathbf{g}_{k,k+1}^* \mathbf{f}_{k+1}|^2 + N_0} \\ &= \frac{|\mathbf{h}_k^* \mathbf{f}_k|^2}{\alpha_{k,k+1} |\mathbf{g}_{k,k+1}^* \mathbf{f}_{k+1}|^2 + \frac{1}{\rho_{k,(\mathrm{d})}}} \ . \end{aligned} \tag{3.1}$$

Note that $\rho_{k,(\mathrm{d})} = \frac{\gamma_k^{(\mathrm{d})}}{N_0}$ is the average received SNR of the desired signal, which is independent of the beamforming vectors. It is popularly assumed in the literature that base stations have perfect knowledge of $\rho_{k,(\mathrm{d})}$ [18, 41, 78]. This assumption is justified since cellular standards like 3GPP LTE [3] and HSDPA [2] require users to periodically transmit 'channel quality indicators', in the form of SNR (or SINR) measures to the respective base stations for scheduling and adaptive modulation and coding purposes. Also, it was shown in [41] that SNR quantization does not effect the sum-rates of a single-cell multiuser MIMO system signicantly. Hence, we assume that the base stations have perfect knowledge of the SNR.

The sum-rate of all the users within the system, R_s, is expressed as

$$R_s = \sum_k \log_2 \left(1 + \mathsf{SINR}_k\right) \ . \tag{3.2}$$

It is evident that the design of the beamforming vectors $\{\mathbf{f}_k\}_{k=1}^K$ influences the sum-rate of the multicell system. The dependence of SINR_k on both, $\mathbf{f}_k$ and $\mathbf{f}_{k+1}$ (as given in (3.1)) implies that a joint optimization across all the active users is required to maximize the sum-rate. In this chapter, we use a high SINR approximation to remove this interdependency of users and thereby avoid an explicit joint maximization.

3.2.2 Generalized Eigenvector Beamforming

It can be shown that $\log(1+\mathsf{SINR}) = \log(\mathsf{SINR}) + \mathcal{O}(1/\mathsf{SINR})$. Since $\mathcal{O}(1/\mathsf{SINR}) \to 0$ as SINR increases, $\log(1+\mathsf{SINR}) \approx \log(\mathsf{SINR})$ at high SINR. Hence, (3.2) can be given by [48, 49]

$$R_s \approx \sum_k \log_2\left(\mathsf{SINR}_k\right) = \log_2\left(\prod_k \mathsf{SINR}_k\right) \ . \tag{3.3}$$

Thus, maximizing the sum-rate, R_s, at high SINR involves maximizing the product of the SINRs. We would like to emphasize that GEBF is strictly sub-optimal at low SINR since $\log(1+\mathsf{SINR}) = \mathcal{O}(\mathsf{SINR}) \to 0$ for $\mathsf{SINR} \to 0$, invalidating the high SINR approximation used in (3.3). Using GEBF, the beamforming vectors $\{\mathbf{f}_k\}_{k=1}^K$ are found by solving

$$\begin{aligned} R_{s,\text{opt}} = \max_{\{\mathbf{f}_k\}_{k=1}^K} & \log_2\left(\prod_{k=1}^K \frac{|\mathbf{h}_k^*\mathbf{f}_k|^2}{\alpha_{k,k+1}|\mathbf{g}_{k,k+1}^*\mathbf{f}_{k+1}|^2 + \frac{1}{\rho_{k,(\mathrm{d})}}}\right) \\ & \text{s.t.} \|\mathbf{f}_\mathrm{k}\|^2 = 1, \mathrm{k} = 1, \ldots, \mathrm{K} \ . \end{aligned} \tag{3.4}$$

Taking advantage of the commutativity of the multiplication operation, the objective function in (3.4) can be rewritten as

$$\begin{aligned} R_{s,\text{opt}} = \max_{\{\mathbf{f}_k\}_{k=1}^K} & \sum_k \log_2\left(\frac{|\mathbf{h}_k^*\mathbf{f}_k|^2}{\alpha_{k-1,k}|\mathbf{g}_{k-1,k}^*\mathbf{f}_k|^2 + \frac{1}{\rho_{k-1,(\mathrm{d})}}}\right) \\ & \text{s.t. } \|\mathbf{f}_\mathrm{k}\|^2 = 1, \mathrm{k} = 1, \ldots, \mathrm{K}, \end{aligned} \tag{3.5}$$

for the soft handoff model. In the single interferer case, the k^{th} base station has knowledge of both $\mathbf{h}_k$ and $\mathbf{g}_{k-1,k}$ (obtained from the $(k-1)^{\text{th}}$ base station using the backhaul link) and can 'locally' maximize (3.5). Thus, the high

SINR approximation is used to reduce the global optimization in (3.4) to a local maximization problem in (3.5), without universal CSI knowledge [9].

Now, (3.5) deals with maximizing a function consisting of K independent variables, $\{\mathbf{f}_k\}_{k=1}^{K}$. The optimal linear beamforming vector, $\mathbf{f}_{k,\text{opt}}$, is the solution to

$$\mathbf{f}_{k,\text{opt}} = \arg \max_{\mathbf{f}:\|\mathbf{f}\|^2=1} \quad \frac{\mathbf{f}^* \mathbf{R}_{\mathbf{h}_k} \mathbf{f}}{\mathbf{f}^* \mathbf{R}_{\mathbf{g}_{k-1,k}} \mathbf{f}}, \tag{3.6}$$

where $\mathbf{R}_{\mathbf{h}_k} = \mathbf{h}_k \mathbf{h}_k^*$ and $\mathbf{R}_{\mathbf{g}_{k-1,k}} = \rho_{k-1,(\text{i})} \mathbf{g}_{k-1,k} \mathbf{g}_{k-1,k}^* + \mathbf{I}_{N_t}$. The expression in (3.6) is the well known generalized Rayleigh quotient [14]. Note that $\mathbf{R}_{\mathbf{g}_{k-1,k}}$ is positive definite (and hence, full rank) as $\mathbf{x}^* \mathbf{R}_{\mathbf{g}_{k-1,k}} \mathbf{x} = \mathbf{x}^* (\rho_{k-1,(\text{i})} \mathbf{g}_{k-1,k} \mathbf{g}_{k-1,k}^* + \mathbf{I}_{N_t}) \mathbf{x} > 0$, for all $\mathbf{x} \neq \mathbf{0}$. Since $\mathbf{R}_{\mathbf{h}_k}$ and $\mathbf{R}_{\mathbf{g}_{k-1,k}}$ are Hermitian, the solution to (3.6) is given by the generalized eigenvalue decomposition:

$$\mathbf{R}_{\mathbf{h}_k} \mathbf{f} = \lambda_k \mathbf{R}_{\mathbf{g}_{k-1,k}} \mathbf{f}, \tag{3.7}$$

where λ_k denotes the eigenvalues of $\mathbf{R}_{\mathbf{g}_{k-1,k}}^{-1} \mathbf{R}_{\mathbf{h}_k}$ [16]. Due to the rank deficient nature of $\mathbf{R}_{\mathbf{h}_k} (= \mathbf{h}_k \mathbf{h}_k^*)$, there exists only one non-zero eigenvalue. The solution to (3.6) will then be equal to the generalized eigenvector corresponding to the non-zero (maximum) eigenvalue. Note that there can be infinitely many solutions to (3.6) since $\mathbf{f}_{k,\text{opt}}$ is invariant to an angular rotation, θ [9].

While (3.7) can be used to maximize the sum-rate for an infinite linear array (in Fig. 3.1), it can also be used for a finite cellular array by accounting for edge effects and using (3.7) for $k = 2, \ldots, K$. The base station in the first cell of the array does not cause interference, implying that optimal beamforming vector is given by eigen-beamforming solution in (3.7) with $\mathbf{R}_{\mathbf{g}_1} = \mathbf{I}_{N_t}$.

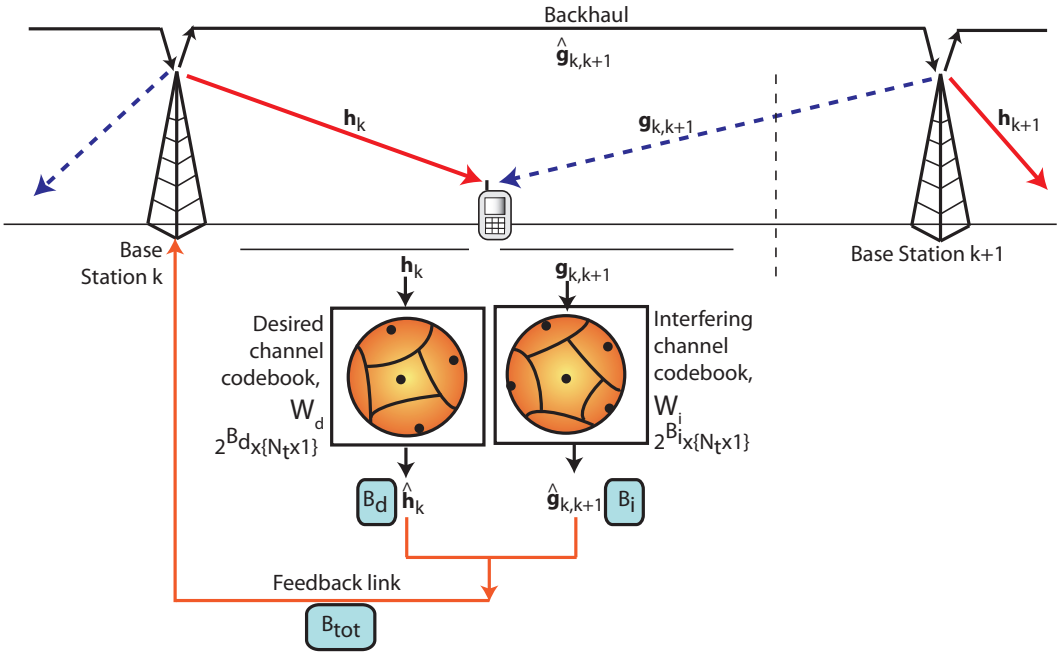

Figure 3.2: The limited feedback model to feedback quantized CSI of the desired and interfering channels using two separate codebooks.

Hence, (3.7) can be used for any K, while the solution in [58, 59] maximizes sum-rates at high SINR for only $K = 2$.

3.2.3 Limited Feedback Model

The limited feedback model for the multicell setup in Section 3.2.1 is described in Fig. 4.2. It is assumed that the k^{th} user can perfectly estimate the desired and interfering channels, $\mathbf{h}_k$ and $\mathbf{g}_{k,k+1}$, using separate training symbols from the k^{th} and $(k+1)^{\text{th}}$ base stations, respectively. For the single-interferer soft handoff model, the k^{th} receiver uses $B_{k,(\text{d})}$ and $B_{k,(\text{i})}$ bits to feed back

quantized versions of $\mathbf{h}_k$ and $\mathbf{g}_{k,k+1}$, respectively, where $B_{k,(\mathrm{d})} + B_{k,(\mathrm{i})} = B_{\mathrm{tot}}$ is fixed. Note that $B_{k,(\mathrm{d})}$ and $B_{k,(\mathrm{i})}$ will depend on the relative strengths of the interfering and desired signals, i.e. $\alpha_{k,k+1}$. For example, when $\alpha_{k,k+1} \to 0$, the contribution of the desired channel towards the SINR is greater than that of the interfering channel and it is more important to reduce the loss due to quantization of $\mathbf{h}_k$ as compared to that due to $\mathbf{g}_{k,k+1}$. This can be done by setting $B_{k,(\mathrm{d})} \approx B_{\mathrm{tot}}$. Hence, $\mathbf{h}_k$ and $\mathbf{g}_{k,k+1}$ are quantized using two separate codebooks of (variable) sizes $2^{B_{k,(\mathrm{d})}}$ (denoted by $\mathcal{W}_{k,(\mathrm{d})}$) and $2^{B_{k,(\mathrm{i})}}$ (given by $\mathcal{W}_{k,(\mathrm{i})}$), respectively [9].

As codebook design for multicell systems is a topic of ongoing research, we use RVQ for channel quantization to facilitate analysis. If we use $B_{k,(\mathrm{d})}$ (or $B_{k,(\mathrm{i})}$) bits for feedback, then each of the $2^{B_{k,(\mathrm{d})}}$ ($2^{B_{k,(\mathrm{i})}}$) codebook vectors is independently chosen from the isotropic distribution on the N_t dimensional unit sphere [75, 76]. The unit-norm desired and interfering channel directions are given by $\tilde{\mathbf{h}}_k = \mathbf{h}_k/\|\mathbf{h}_k\|$ ($\tilde{\mathbf{g}}_{k,k+1} = \mathbf{g}_{k,k+1}/\|\mathbf{g}_{k,k+1}\|$). The quantized vectors for $\tilde{\mathbf{h}}_k$ and $\tilde{\mathbf{g}}_{k,k+1}$, given by $\hat{\mathbf{h}}_k$ and $\hat{\mathbf{g}}_{k,k+1}$, respectively, are mapped to codebook entries with the smallest angular separations, using

$$\hat{\mathbf{h}}_k = \arg \max_{\mathbf{w} \in \mathcal{W}_{k,(\mathrm{d})}} |\tilde{\mathbf{h}}_k^* \mathbf{w}|^2 = \arg \max_{\mathbf{w} \in \mathcal{W}_{k,(\mathrm{d})}} \cos^2\left(\theta_{\tilde{\mathbf{h}}_k, \mathbf{w}}\right), \text{ and}$$
$$\hat{\mathbf{g}}_{k,k+1} = \arg \max_{\mathbf{w} \in \mathcal{W}_{k,(\mathrm{i})}} |\tilde{\mathbf{g}}_{k,k+1}^* \mathbf{w}|^2 = \arg \max_{\mathbf{w} \in \mathcal{W}_{k,(\mathrm{i})}} \cos^2\left(\theta_{\tilde{\mathbf{g}}_{k,k+1}, \mathbf{w}}\right).$$

The k^{th} base station has information about both $\hat{\mathbf{h}}_k$ and $\hat{\mathbf{g}}_{k,k+1}$ and uses the backhaul link to inform the $(k+1)^{\mathrm{th}}$ base station about the interfering channel. Thus, each base station has knowledge of not only its own desired channel,

Table 3.1: Notation

Symbol	What it stands for
K	Number of cooperating cells in the system
$\mathbf{h}_k$	Desired channel between k^{th} user and k^{th} base station
$\mathbf{g}_{k,\ell}$	Desired channel between k^{th} user and ℓ^{th} base station
$\mathbf{f}_k$	Unit-norm beamforming vector at the k^{th} base station
$\rho_{k,(\text{d})}$	Desired signal SNR at the k^{th} user
$\alpha_{k,\ell}$	Interference to signal ratio at k^{th} user from the ℓ^{th} base station
$\tilde{\mathbf{h}}_k$	Unit-norm channel direction between k^{th} user and k^{th} base station
$\tilde{\mathbf{g}}_{k,\ell}$	Unit-norm channel direction between k^{th} user and ℓ^{th} base station
$\hat{\mathbf{h}}_k$	Unit-norm quantization vector for $\tilde{\mathbf{h}}_k$
$\hat{\mathbf{g}}_{k,\ell}$	Unit-norm quantization vector for $\tilde{\mathbf{g}}_{k,\ell}$

but also of the interference that it is causing to the user in the adjacent cell. A summary of the system model-related notation is given in Table 3.1. Note that subsequent chapters use the same notation.

3.3 Impact of Limited Feedback

The k^{th} base station computes the beamforming vector at the k^{th} base station, $\hat{\mathbf{f}}_k$, using $\hat{\mathbf{h}}_k$ and $\hat{\mathbf{g}}_{k-1,k}$, as the generalized eigenvector satisfying

$$\mathbf{R}_{\hat{\mathbf{h}}_k}\hat{\mathbf{f}}_k = \lambda_k \mathbf{R}_{\hat{\mathbf{g}}_{k-1,k}}\hat{\mathbf{f}}_k$$

where $\mathbf{R}_{\hat{\mathbf{h}}_k} = \|\mathbf{h}_k\|^2\hat{\mathbf{h}}_k\hat{\mathbf{h}}_k^*$ and $\mathbf{R}_{\hat{\mathbf{g}}_{k-1,k}} = \rho_{k-1,(\text{i})}\|\mathbf{g}_{k-1,k}\|^2\hat{\mathbf{g}}_{k-1,k}\hat{\mathbf{g}}_{k-1,k}^* + \mathbf{I}_{N_t}$. Note that $\|\mathbf{h}_k\|^2$ can be absorbed as a constant into λ_k. Hence, the k^{th} base station only requires the channel gain information of the interfering channel, i.e. $\|\mathbf{g}_{k-1,k}\|$. Since $\|\mathbf{g}_{k-1,k}\|$ is a scalar and can be quantized easily, in this chapter, we concentrate on quantizing the channel directions, and use simulations to

show that for $N_t = 2$, one bit of feedback for the channel norm is sufficient to achieve data rates that are very close to the full CSI case. Note that most of the literature on multiuser MIMO assumes that base stations have perfect knowledge of the channel gains [18, 41, 78]. To the best of our knowledge, quantizing channel gain has not been investigated for multicell systems.

Quantization of CSI leads to a loss in the sum-rate. In this chapter, we develop a feedback-bit partitioning strategy to reduce the mean loss in sum-rate given by [9]

$$\begin{aligned}\mathbb{E}\{\Delta R_s\} &= \mathbb{E}\{R_{s,\text{full}} - R_{s,\text{LF}}\} \\ &= \mathbb{E}\left\{\sum_k \log_2\left(\frac{|\mathbf{h}_k^*\mathbf{f}_{k,\text{full}}|^2}{\alpha_{k-1,k}|\mathbf{g}_{k-1,k}^*\mathbf{f}_{k,\text{full}}|^2 + \frac{1}{\rho_{k,(\text{d})}}}\right)\right. \\ &\quad \left. - \sum_k \log_2\left(\frac{|\mathbf{h}_k^*\hat{\mathbf{f}}_k|^2}{\alpha_{k-1,k}|\mathbf{g}_{k-1,k}^*\hat{\mathbf{f}}_k|^2 + \frac{1}{\rho_{k,(\text{d})}}}\right)\right\}, \end{aligned} \tag{3.8}$$

where $R_{s,\text{full}}$ is given in (3.5) and $R_{s,\text{LF}}$ is the sum-rate using limited feedback. Also, $\mathbf{f}_{k,\text{full}}$ corresponds to the full CSI beamforming vector (from (3.7)).

3.4 Feedback Bit Partitioning

Generalized eigenvector beamforming requires both the desired and interfering CSI at the base station. As the number of available feedback bits, B_{tot} is fixed, it is possible that allocating feedback bits between the desired and interfering channels can further improve the limited feedback sum-rate. In this section, we propose a feedback-bit allocation strategy to numerically evaluate the number of bits required to quantize the desired and interfering

channels using RVQ, denoted by $B_{k,(\mathrm{d})}$ and $B_{k,(\mathrm{i})}$, respectively. We model all the channels by the Rayleigh fading model, where each entry is a zero-mean unit-variance complex Gaussian independent and identically distributed (i.i.d.) random variable according to $\mathcal{N}_c(0,1)$. While it is recognized that Rayleigh fading does not model realistic propagation channels accurately, we use the i.i.d. assumption to obtain closed-form expressions of the mean loss in sum-rate and feedback-bit partitioning algorithms.

Maximizing the mean sum-rate at high SINR using GEBF with limited feedback is equivalent to minimizing $\mathbb{E}\{\Delta R_s\}$ in (3.8), which is rewritten as

$$\mathbb{E}\{\Delta R_s\} = \sum_k \underbrace{\mathbb{E}\left\{\log_2\left(\frac{|\mathbf{h}_k^*\mathbf{f}_{k,\mathrm{full}}|^2}{|\mathbf{h}_k^*\hat{\mathbf{f}}_k|^2}\right)\right\}}_{R_{k,(\mathrm{d})}} + \sum_k \underbrace{\mathbb{E}\left\{\log_2\left(\frac{\rho_{k,(\mathrm{i})}|\mathbf{g}_{k,k+1}^*\hat{\mathbf{f}}_{k+1}|^2+1}{\rho_{k,(\mathrm{i})}|\mathbf{g}_{k,k+1}^*\mathbf{f}_{k+1,\mathrm{full}}|^2+1}\right)\right\}}_{R_{k,(\mathrm{i})}}, \tag{3.9}$$

for the case of a single interferer (the soft handoff model). The mean loss in sum-rate can be viewed to be a contribution of two terms, $R_{k,(\mathrm{d})}$ and $R_{k,(\mathrm{i})}$, corresponding to the mean loss resulting from quantizing the desired and interfering channels, respectively. Note that $R_{k,(\mathrm{d})}$ and $R_{k,(\mathrm{i})}$ depend only on $B_{k,(\mathrm{d})}$ and $B_{k,(\mathrm{i})}$, respectively, and are independent of $R_{l,(\mathrm{d})}$ and $R_{l,(\mathrm{i})}$, for $k \neq l$. Therefore, minimizing (3.9) is equivalent to minimizing $\Delta_k = R_{k,(\mathrm{d})} + R_{k,(\mathrm{i})}$ for each k. Since obtaining a closed form expression for (3.9) is complicated, we derive an upper bound for $\mathbb{E}\{\Delta R_s\}$ in terms of bounds on $R_{k,(\mathrm{d})}$ and $R_{k,(\mathrm{i})}$ [9]. The following proposition presents an upper bound on $R_{k,(\mathrm{d})}$.

Proposition 3.4.1. *The upper bound on the mean loss in sum-rate due to*

quantizing desired channel of the k^{th} user, $R_{k,(\text{d})}$, in (3.9) is approximated by

$$-\mathbb{E}\left\{\log_2(\cos^2(\theta_{\tilde{\mathbf{h}_k},\hat{\mathbf{h}_k}})\right\} \ .$$

Proof. The proof is given in Appendix 3.7.1. □

Proposition 3.4.1 relates the mean loss in sum-rate to the mean error due to the desired channel quantization. The following two lemmas are used to simplify the expression in Proposition 3.4.1 [9]. Let $\mathcal{H}$ denote the set of all unit-norm channel directions, $\tilde{\mathbf{h}}$.

Lemma 3.4.2. *The mean of* $\log_2\left(\cos^2\left(\theta_{\tilde{\mathbf{h}},\hat{\mathbf{h}}}\right)\right)$ *is given by*

$$\mathbb{E}_{\mathcal{H},\mathcal{W}}\left\{\log_2\left(\cos^2\left(\theta_{\tilde{\mathbf{h}},\hat{\mathbf{h}}}\right)\right)\right\} = \log_2(e)\sum_{i=0}^{2^B}\binom{2^B}{i}(-1)^i\sum_{l=1}^{i(N_t-1)}\frac{1}{l} \ .$$

Proof. The proof is given in Appendix 3.7.2. □

To further simplify Lemma 3.4.2, $\sum_{i=0}^{2^{B_{k,(\text{d})}}}\binom{2^{B_{k,(\text{d})}}}{i}(-1)^i\sum_{n=1}^{i(N_t-1)}\frac{1}{n}$ is expressed as the sum of beta functions, as shown by Lemma 3.4.3.

Lemma 3.4.3. *The contribution of the desired channel delay and quantization towards the loss in sum-rate,* $\sum_{i=0}^{2^{B_{k,(\text{d})}}}\binom{2^{B_{k,(\text{d})}}}{i}(-1)^i\sum_{n=1}^{i(N_t-1)}\frac{1}{n}$ *is given by*

$$\sum_{i=0}^{2^{B_{k,(\text{d})}}}\binom{2^{B_{k,(\text{d})}}}{i}(-1)^i\sum_{n=1}^{i(N_t-1)}\frac{1}{n} = \frac{1}{N_t-1}\sum_{i=1}^{N_t-1}\beta\left(2^{B_{k,(\text{d})}},\frac{i}{N_t-1}\right).$$

Proof. The proof is given in Appendix 3.7.3. □

Hence, $R_{k,(\mathrm{d})}$ can be expressed as

$$R_{k,(\mathrm{d})} \leq \frac{-\log_2(e)}{N_t - 1} \sum_{i=1}^{N_t - 1} \beta\left(2^{B_{k,(\mathrm{d})}}, \frac{i}{N_t - 1}\right). \tag{3.10}$$

It is intuitive that larger N_t will result in a larger quantization error, for fixed $B_{k,(\mathrm{d})}$. This is verified through (3.10), where the sum of the beta functions in will increase with N_t for a fixed $B_{k,(\mathrm{d})}$. Proposition 3.4.1 and Lemmas 3.4.2-3.4.3 translate this increase in quantization error to the loss in mean sum-rate. We now present an upper bound on $R_{k,(\mathrm{i})}$ in Proposition 3.4.4.

Proposition 3.4.4. *The upper bound on the mean loss in sum-rate due to quantizing interfering channel of the* k^{th} *user,* $R_{k,(\mathrm{i})}$ *in* (3.9) *is approximated by*

$$\log_2\left(1 + \rho_{k,(\mathrm{i})} N_t 2^{B_{k,(\mathrm{i})}} \beta\left(2^{B_{k,(\mathrm{i})}}, \frac{N_t}{N_t - 1}\right)\right),$$

where $\beta(x, y) = \int_0^1 t^{x-1}(1-t)^{y-1} dt$.

Proof. The proof is given in Appendix 3.7.4. □

Using Stirling's approximation, $\beta(a, b) \approx \Gamma(b) a^{-b}$, when a is large and b is fixed [26, 30]. Hence, for large $B_{k,(\mathrm{i})}$, the beta function in Proposition 3.4.4, $\beta\left(2^{B_{k,(\mathrm{i})}}, \frac{N_t}{N_t - 1}\right) \approx \Gamma\left(\frac{N_t}{N_t - 1}\right) 2^{B_{k,(\mathrm{i})} \frac{-N_t}{N_t - 1}}$. As $B_{k,(\mathrm{i})}$ increases, $2^{B_{k,(\mathrm{i})} \frac{-N_t}{N_t - 1}} \to 0$, implying that the contribution of $R_{k,(\mathrm{i})}$ to mean loss in sum-rate approaches zero [9]. This makes intuitive sense. Using Propositions 3.4.1 and 3.4.4, $\mathbb{E}\{\Delta R_s\}$

is upper bounded by

$$\mathbb{E}\{\Delta R_s\} \leq \sum_k \log_2\left(1+\rho_{k,(\mathrm{i})}N_t 2^{B_{k,(\mathrm{i})}}\beta\left(2^{B_{k,(\mathrm{i})}},\frac{N_t}{N_t-1}\right)\right) - \frac{\log_2(e)}{N_t-1}\sum_{i=1}^{N_t-1}\beta\left(2^{B_{k,(\mathrm{d})}},\frac{i}{N_t-1}\right) . \quad (3.11)$$

Substituting $N_t = 2$ in (3.11), we get

$$\mathbb{E}\{\Delta R_s\} \leq \sum_k \log_2\left(1+2\rho_{k,(\mathrm{i})}2^{B_{k,(\mathrm{i})}}\beta\left(2^{B_{k,(\mathrm{i})}},2\right)\right) - \log_2(e)\beta\left(2^{B_{k,(\mathrm{d})}},1\right), \quad (3.12)$$

where $\beta\left(2^{B_{k,(\mathrm{d})}},1\right) = -2^{-B_{k,(\mathrm{d})}}$. Further, $\beta\left(2^{B_{k,(\mathrm{i})}},2\right) = 1/(2^{B_{k,(\mathrm{i})}}(2^{B_{k,(\mathrm{i})}}+1))$ and $B_{k,(\mathrm{i})} = B_{\mathrm{tot}} - B_{k,(\mathrm{d})}$. Hence, (3.12) is rewritten as

$$\mathbb{E}\{\Delta R_s\} \leq \sum_k \underbrace{\log_2\left(1+2\rho_{k,(\mathrm{i})}\frac{1}{2^{B_{\mathrm{tot}}-B_{k,(\mathrm{d})}}+1}\right) + 2^{-B_{k,(\mathrm{d})}}\log_2(e)}_{\tilde{\Delta}_k} . \quad (3.13)$$

For simplicity, we denote the right hand side of expression (3.13) by $\tilde{\Delta}_k$. Treating $B_{k,(\mathrm{d})}$ as a real number, we first show in Theorem 3.4.5 that $\tilde{\Delta}_k$ is convex in $B_{k,(\mathrm{d})} \in [0, B_{\mathrm{tot}}]$, and then use the result to compute the optimum number of desired and interfering feedback bits for the soft handoff model.

Theorem 3.4.5. *The minimum value of the upper bound, $\tilde{\Delta}_k$ in (3.13), is obtained at $B_{k,(\mathrm{d})}$ equal to*

$$B_{k,(\mathrm{d})}{}^{\mathrm{real}} = B_{\mathrm{tot}} - \log_2\left(1+\rho_{k,(\mathrm{i})}+\sqrt{\rho_{k,(\mathrm{i})}2^{B_{\mathrm{tot}}+1}+(\rho_{k,(\mathrm{i})})^2}\right),$$

where $B_{k,(\mathrm{d})}{}^{\mathrm{real}} \in [0, B_{\mathrm{tot}}]$ is a real number.

Proof. The proof is given in Appendix 3.7.5. □

Since $\rho_{k,(\mathrm{i})} = \rho_{k,(\mathrm{d})}\alpha_{k,k+1}$, it is clear from Theorem 3.4.5 that ${B_{k,(\mathrm{d})}}^{\mathrm{real}}$ is a function of $\rho_{k,(\mathrm{d})}$, $\alpha_{k,k+1}$, and B_{tot}. As $\rho_{k,(\mathrm{i})}$ increases, more bits are assigned to quantize the interfering channel to mitigate the strong interference. In contrast, when $\rho_{k,(\mathrm{d})}$ is small, most of the bits are assigned to the desired channel. This is understandable at low SNR regimes, where the objective of GEBF is to first increase the desired signal strength, since the interfering signal is weak as well (note that $\rho_{k,(\mathrm{i})} \leq \rho_{k,(\mathrm{d})}$). When the interfering signal has zero power or there is no interferer transmitting, i.e. $\alpha_{k,k+1} = 0$, ${B_{k,(\mathrm{d})}}^{\mathrm{real}} = B_{\mathrm{tot}}$. In the absence of interference, it is evident that the strength of the received signal, $\rho_{k,(\mathrm{d})}$ does not affect the bits allocated. Thus, the bit partitioning algorithm presented in Theorem 3.4.5 makes intuitive sense.

Since the minimization in Theorem 3.4.5 is over the set of real values, ${B_{k,(\mathrm{d})}}^{\mathrm{real}}$ is not necessarily an interger. Since the upper bound $\tilde{\Delta}_k$ is convex in ${B_{k,(\mathrm{d})}}^{\mathrm{real}}$, we only need to consider the ceiling and floor of ${B_{k,(\mathrm{d})}}^{\mathrm{real}}$ (denoted by $\lfloor {B_{k,(\mathrm{d})}}^{\mathrm{real}} \rfloor$ and $\lceil {B_{k,(\mathrm{d})}}^{\mathrm{real}} \rceil$, respectively) to find the optimal number of bits to minimize $\tilde{\Delta}_k$ [28, 67].

Corollary 3.4.6. *The optimum number of desired and interfering feedback bits are given by* ${B_{k,(\mathrm{d})}}^{\mathrm{opt}}$ *and* ${B_{k,(\mathrm{i})}}^{\mathrm{opt}} = B_{\mathrm{tot}} - {B_{k,(\mathrm{d})}}^{\mathrm{opt}}$ *respectively, where* ${B_{k,(\mathrm{d})}}^{\mathrm{opt}}$ *is either* $\lfloor {B_{k,(\mathrm{d})}}^{\mathrm{real}} \rfloor$ *or* $\lceil {B_{k,(\mathrm{d})}}^{\mathrm{real}} \rceil$.

Note from Theorem 3.4.5 and Corollary 3.4.6 that the proposed adaptive bit-partitioning is a function of B_{tot} and the interfering signal strength

received at the user, $\rho_{k,(\mathrm{i})}$, and does not depend on the instantaneous channel realizations. This implies that users do not have to feedback the bit-partitions to the base station for every channel instant. Further, base stations have information about $\rho_{k,(\mathrm{i})}$ through the channel quality indicator feedback [2, 3]. Since B_{tot} is fixed, the bit assignments for users can be computed at the transmitter side without any significant additional feedback overhead requirements.

3.5 Simulation Results

In this section, we show that the proposed feedback-bit allocation strategy reduces the mean loss in data rate due to quantization. Simulations are also used to verify that the partitioning of feedback bits between the desired and interfering channels proposed in Theorem 3.4.5 and Corollary 3.4.6 matches numerical results for the soft handoff model using a linear array of cells. Unless otherwise stated, we assume that all K users have the same received desired and interfering signal strengths, i.e., $\rho_{k,(\mathrm{d})} = \rho_{(\mathrm{d})}$ and $\alpha_k = \alpha$, for all k, for simplicity. We provide simulation results for the asymmetric case at the end of this section.

The upper bound on the mean loss in sum-rate (in (3.13)) was derived by assuming that the number of bits available for both the desired and interfering channels are large enough to ignore quantization errors. In Fig. 3.3, we plot the actual mean data rate per cell and the lower bound obtained using (3.13). It is seen that for $\rho_{(\mathrm{d})} = 10$ dB, $B_{\mathrm{tot}} = 10$, $K = N_t = 2$ and $\alpha = \{0.1, 1\}$, the maxima of the actual mean data rate and the lower bound

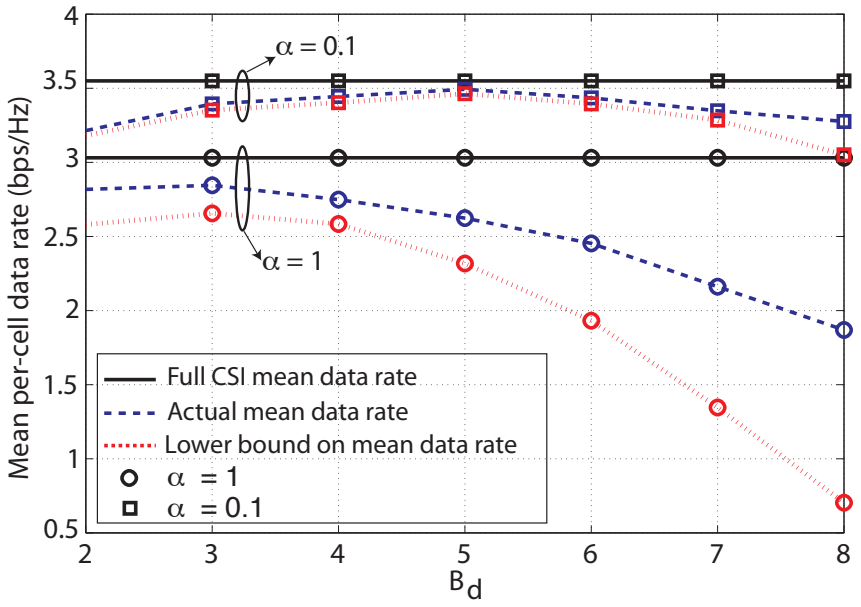

Figure 3.3: Per-cell data rate for $\alpha = \{0.1, 1\}$, $N_t = K = 2$, $\rho_{(\mathrm{d})} = 10$ dB and $B_{\mathrm{tot}} = 10$.

are reasonably close and more importantly, occur at the same value of $B_{k,(\mathrm{d})}$. Hence, partitioning adaptively the feedback bits, as a function of the location of the mobile terminal (α), is an effective method to increase the sum-rates obtained in limited feedback systems. This implies that the upper bound derived in (3.13) can be used to evaluate the number of quantization bits needed to minimize the mean sum-rate loss, for the setup considered in the chapter. Further, Fig. 3.3 clearly demonstrates the concavity of the lower bound on the per-cell data rate, thereby illustrating the convexity of the upper bound in (3.13).

Next, we present simulation results to show that GEBF with the proposed feedback-bit partitioning algorithm outperforms non-cooperative eigen-

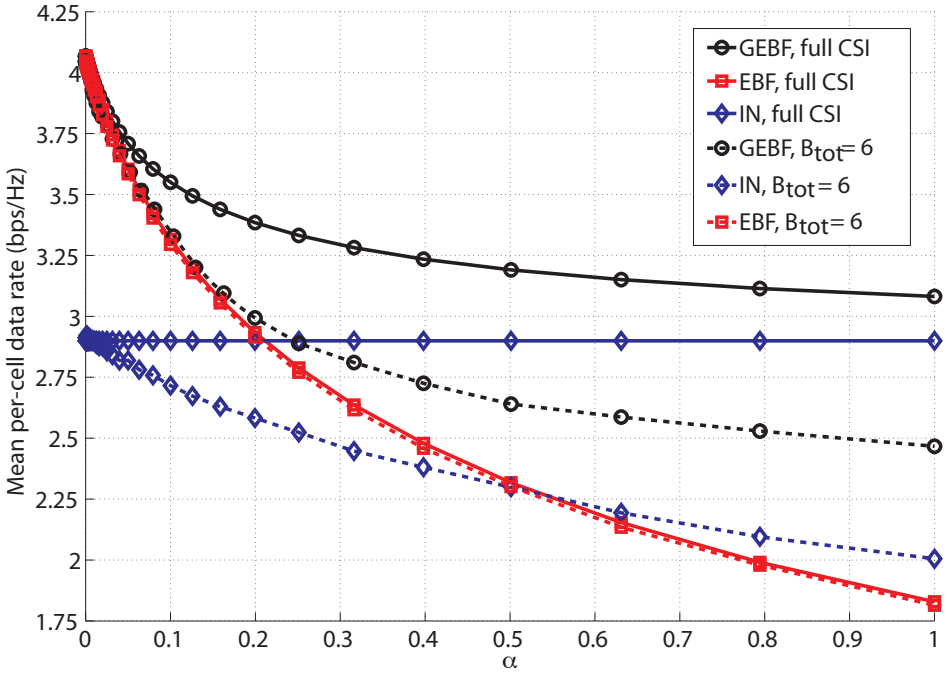

Figure 3.4: Comparison of the mean per cell data rate obtained using the proposed beamforming strategy, non-cooperative eigenbeamforming and (co-operative) interference nulling, for $\rho_{(\mathrm{d})} = 10$ dB, $N_t = K = 2$ and $B_{\mathrm{tot}} = 6$.

beamforming (EBF) and multicell interference nulling (IN) beamforming strategies with limited CSI feedback. In EBF, each base station transmits in a non-cooperative manner by ignoring the co-channel interference from neighboring base stations, as in the case of single-cell single-user beamforming [66]. For MIMO systems, the beamforming vector is chosen to be the eigenvector corresponding to the maximum eigenvalue of the MIMO channel. For a MISO system, the eigen-beamforming vector, $\mathbf{f}_k$, is reduced to

$$\mathbf{f}_k^{\mathrm{EBF}} = \frac{\mathbf{h}_k^c}{\|\mathbf{h}_k\|} \ .$$

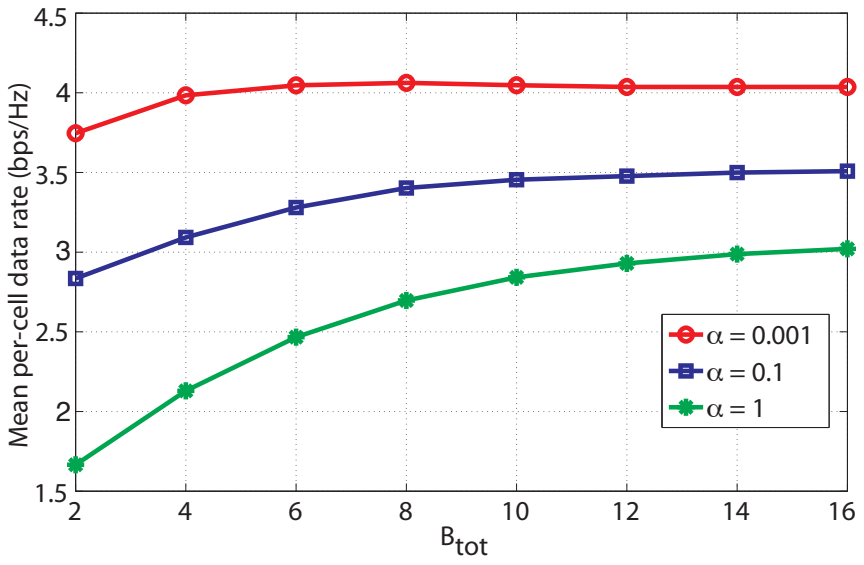

Figure 3.5: Comparison of the mean per-cell data rates obtained using GEBF for $\alpha = \{0.001, 0.1, 1\}$ as a function of B_{tot}, for $\rho_{(\text{d})} = 10$ dB, $N_t = K = 2$.

The intercell interference nulling approach in [99] requires that $|\mathbf{g}_{k-1,k}^{*}\mathbf{f}_{k}^{\text{IN}}|^2 = 0$, where $(\mathbf{f}_{k}^{\text{IN}})^{*}\mathbf{f}_{k}^{\text{IN}} = 1$. Denoting $\mathbf{X}_k = [\mathbf{h}_k^{*},\ \mathbf{g}_{k-1,k}^{*}]$ and $\mathbf{W}_k = (\mathbf{X}_k^{*}\mathbf{X}_k)^{-1}\mathbf{X}_k^{*}$ the beamforming vector is designed by setting

$$\mathbf{f}_{k}^{\text{IN}} \;=\; \frac{\mathbf{W}_{k}^{[1]}}{\|\mathbf{W}_{k}^{[1]}\|}$$

Since EBF is non-cooperative, ${B_{k,(\text{d})}}^{\text{EBF}} = B_{\text{tot}}$, whereas for intercell interference nulling approach, ${B_{k,(\text{d})}}^{\text{IN}} = {B_{k,(\text{i})}}^{\text{IN}} = B_{\text{tot}}/2$ is assumed. Fig. 3.4 shows the sum-rates that can be obtained using the three transmission strategies for a two-cell (two-user) scenario with $B_{\text{tot}} = 6$ and $\rho_{(\text{d})} = 10$ dB and $K = N_t = 2$. Fig. 3.4 helps to illustrate that the proposed limited feedback algorithm with GEBF yields higher sum-rates than those obtained with other transmission strategies like eigen-beamforming and interference nulling.

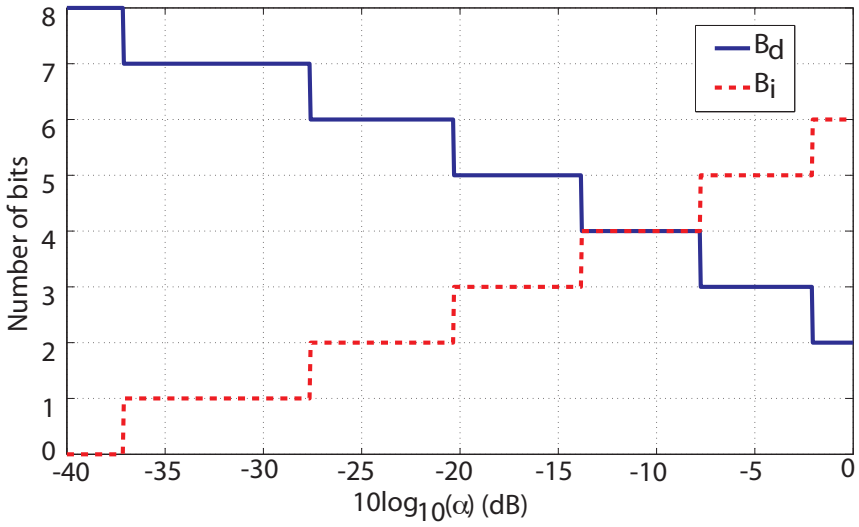

Figure 3.6: (B_d, B_i) partitioning for $\rho_{(\mathrm{d})} = 10$ dBW, $N_t = K = 2$ and $B_{\mathrm{tot}} = 8$.

The sum-rates obtained using the proposed bit-partitioning technique as B_{tot} increases are compared in Fig. 3.5 for $N_t = K = 2$ and $\rho_{(\mathrm{d})} = 10$ dB for $\alpha = \{0.001, 0.1, 1\}$. It is seen that the cell-edge users ($\alpha \to 1$) require a larger B_{tot} as compared to users in the cell-center ($\alpha \to 0$). This is due to the requirement of cell-edge users to quantize the interfering channel (in addition to the desired channel) with a sufficiently high resolution. In contrast, users in the cell-center that have weak interfering signals have to only ensure that the desired channel is allocated sufficient number of feedback bits. Hence, the feedback-bits, B_{tot} can be varied adaptively as a function of the user location within the cell to yield a given sum-rate.

In Fig. 3.6, we show the variation in the number of bits allocated to the desired and interfering channels as a function of the interfering to desired signal

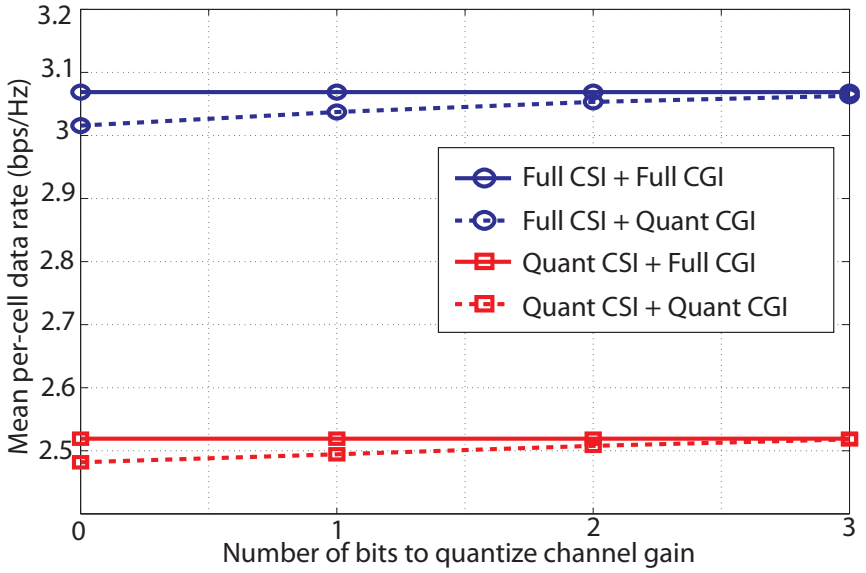

Figure 3.7: Impact of CGI quantization for $\rho_{(\mathrm{d})} = 10$ dBW, $\alpha = 0$ dB, $N_t = K = 2$, and $B_{\mathrm{tot}} = 6$.

ratio, given by $\tilde{\alpha} = 10\log_{10}(\alpha)$ dB. In Fig. 3.6, for $K = N_t = 2$ and $\rho_{(\mathrm{d})} = 10$ dBW, we can see that when the difference in path-loss is greater than 37 dB, $(B_{k,(\mathrm{d})}, B_{k,(\mathrm{i})}) = (8, 0)$. As the path-loss difference decreases, $B_{k,(\mathrm{d})}$ reduces and $B_{k,(\mathrm{i})}$ increases, due to an increasing need to quantize the interfering channel with greater resolution. When both the desired and interfering channels have the same signal strength, it is seen that $(B_{k,(\mathrm{d})}, B_{k,(\mathrm{i})}) = (2, 6)$, i.e. reducing the interfering signal strength is 'more important' to maximize the sum-rate than increasing the desired signal strength. Note that these results are valid for the soft handoff model, which assumes a single interferer to each user. In Fig. 3.7, we use the Lloyd algorithm [27] to show that channel gain quantization (CGI) has a very small impact on the overall mean data rate. In particular,

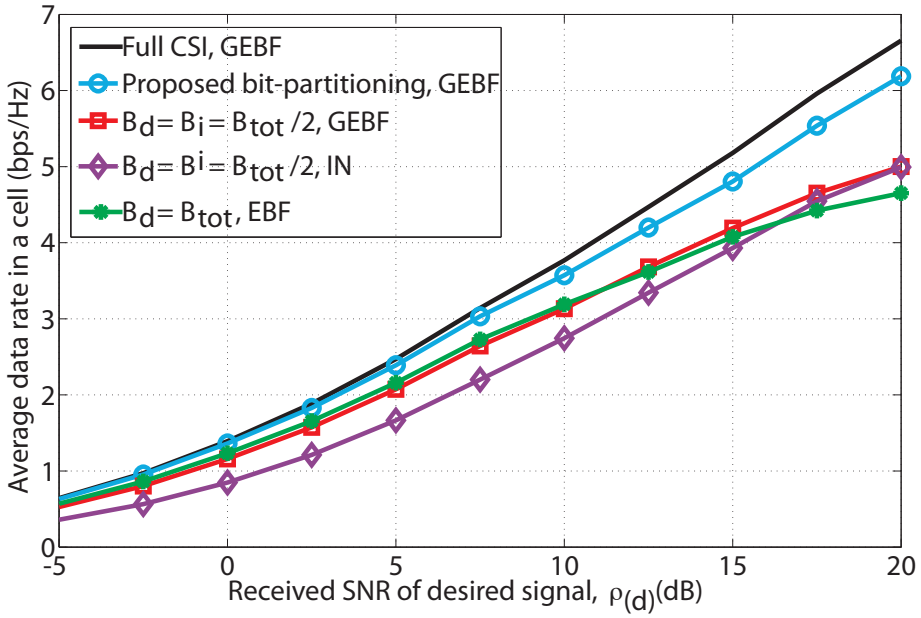

Figure 3.8: Average data rate in a cell as a function of the received desired signal power for $N_t = K = 2$ and $B_{\text{tot}} = 6$.

for a $K = N_t = 2$ system with $\rho_{(\text{d})} = 10$ dBW, $\alpha = 0$ dB, and $B_{\text{tot}} = 6$, quantizing the interfering channel gain with one bit is sufficient. The reason is that the quantization error in the channel gain does not significantly affect the beamformer design, unless the gain registered is an extreme value that is $>> 1/\rho_{(\text{d})}$. Since this happens with a low probability, the mean data rate is not drastically influenced by the channel gain quantization.

Finally, we consider the case where the users are randomly located in their cells and have different interfering to desired signal ratios, i.e. $\tilde{\alpha}_k \neq \tilde{\alpha}_l, k \neq l$. Hence, the users can have different feedback bit allocations. The performance of the proposed feedback-bit allocation strategy with GEBF can

be examined for the asymmetric scenario by evaluating the average data-rate in a cell, where the average is taken over all possible user locations in the cell. Assuming $B_{\text{tot}} = 6$ at each user, we consider 1000 cells (users) arranged in a linear fashion, with $\tilde{\alpha}_k$ uniformly distributed between $[-40\ dB, 0\ dB]$, for all k. Adjacent cells cooperate by sharing the interfering channel CSI to compute the bit partitions for each user independently. In Fig. 3.8, it is seen that the average data-rate in a cell using the proposed feedback-bit allocation strategy is reasonably close to that obtained using GEBF with full CSI. We also show that the data rate obtained using equal bit partitioning in GEBF, i.e. $B_{k,(\text{d})} = B_{k,(\text{i})} = B_{\text{tot}}/2$ for all k is less than that obtained using the proposed bit allocation, especially for larger $\rho_{(\text{d})}$. This makes intuitive sense as the equal bit allocation does not reduce the quantization error, which grows with larger $\rho_{(\text{d})}$, while the proposed strategy allocates bit adaptively to minimize the overall impact of quantization error. We also plot the average data rates obtained using the non-cooperative eigenbeamforming and multicell interference nulling approaches with limited feedback. The proposed feedback-bit strategy with GEBF outperforms both, EBF and IN, especially at larger values of $\rho_{(\text{d})}$. Hence, it can be concluded that the proposed limited feedback strategy is effective for the soft handoff multicell model using GEBF.

3.6 Conclusion

We first presented a beamforming strategy that uses cooperation among base stations in a multicell MISO system to maximize the sum-rate at high

SINR for the soft handoff model. For the limited feedback scenario, we presented a feedback-bit allocation strategy to reduce the mean loss in sum-rate caused due to quantization using RVQ. The proposed technique relies on the relative strength between the desired and interfering signals within the cell to allocate bits adaptively to each of the two channels, assuming a single interferer. A closed form expression for the number of feedback bits was derived. The average data rate in a cell using the feedback-bit allocation strategy was also shown to reasonably close to the full CSI case for the soft handoff model, verifying that the proposed multicell limited feedback algorithm reduces the mean loss in sum-rates due to CSI quantization.

3.7 Appendix

3.7.1 Proof of Proposition 3.4.1

Dropping the index k for the sake of convenience, the first term of (3.9), $R_{k,(\mathrm{d})}$ is rewritten in terms of the channel directions, $\tilde{\mathbf{h}}$ as

$$\mathbb{E}\left\{\log_2\left(\frac{|\mathbf{h}^*\mathbf{f}_{\text{full}}|^2}{|\mathbf{h}^*\hat{\mathbf{f}}|^2}\right)\right\} = \mathbb{E}\left\{\log_2(|\tilde{\mathbf{h}}^*\mathbf{f}_{\text{full}}|^2)\right\} - \mathbb{E}\left\{\log_2(|\tilde{\mathbf{h}}^*\hat{\mathbf{f}}|^2)\right\} \ . \quad (3.14)$$

Now, since $|\mathbf{h}^*\mathbf{f}_{\text{full}}| \in [0,1]$, and $|\mathbf{h}^*\hat{\mathbf{f}}| \in [0,1]$, we can safely assume that the angles $\theta_{\tilde{\mathbf{h}}^c,\hat{\mathbf{f}}}, \theta_{\hat{\mathbf{h}}^c,\hat{\mathbf{f}}} \in [0,\pi/2]$. Using the triangle inequality for angles [90], we write

$$\begin{aligned} \theta_{\tilde{\mathbf{h}}^c,\hat{\mathbf{f}}} &\leq \theta_{\tilde{\mathbf{h}}^c,\hat{\mathbf{h}}^c} + \theta_{\hat{\mathbf{h}}^c,\hat{\mathbf{f}}}, \\ &= \theta_{\tilde{\mathbf{h}},\hat{\mathbf{h}}} + \theta_{\hat{\mathbf{h}}^c,\hat{\mathbf{f}}}, \end{aligned} \quad (3.15)$$

where $\theta_{\tilde{\mathbf{h}},\hat{\mathbf{h}}} = \theta_{\tilde{\mathbf{h}}^c,\hat{\mathbf{h}}^c}$ is used to obtain (3.15). We can lower bound $|\tilde{\mathbf{h}}^*\hat{\mathbf{f}}|^2 = \cos^2(\theta_{\tilde{\mathbf{h}}^c,\hat{\mathbf{f}}})$ by

$$\begin{aligned}
\cos^2(\theta_{\tilde{\mathbf{h}}^c,\hat{\mathbf{f}}}) &\geq \left[\cos(\theta_{\tilde{\mathbf{h}},\hat{\mathbf{h}}})\cos(\theta_{\hat{\mathbf{h}}^c,\hat{\mathbf{f}}}) - \sin(\theta_{\tilde{\mathbf{h}},\hat{\mathbf{h}}})\sin(\theta_{\hat{\mathbf{h}}^c,\hat{\mathbf{f}}})\right]^2 \\
&= \left[\cos(\theta_{\tilde{\mathbf{h}},\hat{\mathbf{h}}})\cos(\theta_{\hat{\mathbf{h}}^c,\hat{\mathbf{f}}})(1 - \tan(\theta_{\tilde{\mathbf{h}},\hat{\mathbf{h}}})\tan(\theta_{\hat{\mathbf{h}}^c,\hat{\mathbf{f}}}))\right]^2 \\
&= \left[\cos(\theta_{\tilde{\mathbf{h}},\hat{\mathbf{h}}})\cos(\theta_{\hat{\mathbf{h}}^c,\hat{\mathbf{f}}})(1 - \mathcal{O}(\theta_{\tilde{\mathbf{h}},\hat{\mathbf{h}}}))\right]^2 \\
&\approx \left[\cos(\theta_{\tilde{\mathbf{h}},\hat{\mathbf{h}}})\cos(\theta_{\hat{\mathbf{h}}^c,\hat{\mathbf{f}}})\right]^2 \qquad (3.16) \\
&= \cos^2(\theta_{\tilde{\mathbf{h}},\hat{\mathbf{h}}})|\hat{\mathbf{h}}^*\hat{\mathbf{f}}|^2 \qquad (3.17)
\end{aligned}$$

where (3.16) is obtained by understanding that as the number of quantization bits increase, $\theta_{\tilde{\mathbf{h}},\hat{\mathbf{h}}}$ and hence $\mathcal{O}(\theta_{\tilde{\mathbf{h}},\hat{\mathbf{h}}}) \to 0$. This small quantization error approximation is often used in the literature on RVQ for analytical purposes [102].

Substituting (3.17) in (3.14), we get

$$\begin{aligned}
\mathbb{E}\left\{\log_2\left(\frac{|\mathbf{h}^*\mathbf{f}_{\text{full}}|^2}{|\mathbf{h}^*\hat{\mathbf{f}}|^2}\right)\right\} &\leq \mathbb{E}\left\{\log_2(|\tilde{\mathbf{h}}^*\mathbf{f}_{\text{full}}|^2)\right\} - \mathbb{E}\left\{\log_2(\cos^2(\theta_{\tilde{\mathbf{h}},\hat{\mathbf{h}}})|\hat{\mathbf{h}}^*\hat{\mathbf{f}}|^2)\right\} \\
&= -\mathbb{E}\left\{\log_2(\cos^2(\theta_{\tilde{\mathbf{h}},\hat{\mathbf{h}}})\right\} \qquad (3.18)
\end{aligned}$$

where (3.18) was obtained using $\mathbb{E}\left\{\log_2(|\tilde{\mathbf{h}}^*\mathbf{f}_{\text{full}}|^2)\right\} = \mathbb{E}\left\{\log_2(|\hat{\mathbf{h}}^*\hat{\mathbf{f}}|^2)\right\}$.

3.7.2 Proof of Lemma 3.4.2

It was shown in [6] that the probability density function of $\nu = \cos^2\left(\theta_{\tilde{\mathbf{h}},\hat{\mathbf{h}}}\right)$ is given by

$$f_\nu(\nu) = \sum_{i=0}^{N}\sum_{j=1}^{i(N_t-1)}\binom{N}{i}\binom{i(N_t-1)}{j}(-1)^{i+j}j\nu^{j-1},$$

where $N = 2^{B_{k,(\mathrm{i})}}$ is the size of the RVQ codebook. The mean, $\mathbb{E}\{\log_2(\nu)\}$, is then computed as

$$\mathbb{E}\{\log_2(\nu)\} = \log_2(e) \int_0^1 \ln(\nu) f_\nu(\nu) d\nu, \tag{3.19}$$

which is written as

$$\mathbb{E}\{\log_2(\nu)\} = \log_2(e) \sum_{i=0}^{N} \binom{N}{i} (-1)^i \sum_{j=1}^{i(N_t-1)} \binom{i(N_t-1)}{j} (-1)^j j \int_0^1 \ln(\nu) \nu^{j-1} d\nu \tag{3.20}$$

$$= \log_2(e) \sum_{i=0}^{N} \binom{N}{i} (-1)^i \sum_{j=1}^{i(N_t-1)} \binom{i(N_t-1)}{j} \frac{(-1)^{j+1}}{j^2} \tag{3.21}$$

$$= \log_2(e) \sum_{i=0}^{N} \binom{N}{i} (-1)^i \sum_{l=1}^{i(N_t-1)} \frac{1}{l} \tag{3.22}$$

where substituting $f_\nu(\nu)$ in (3.19) leads to (3.20). Also, (3.21) is obtained by solving for $\int_0^1 \ln(\nu)\nu^{j-1} d\nu$ in (3.20). Finally, (3.22) is given in [30].

3.7.3 Proof of Lemma 3.4.3

Denoting $N_t - 1 = M$, $\sum_{i=1}^{2^{B_{k,(\mathrm{d})}}} \binom{2^{B_{k,(\mathrm{d})}}}{i} (-1)^i \sum_{n=1}^{iM} \frac{1}{n}$ can be written as

$$\sum_{i=1}^{2^{B_{k,(\mathrm{d})}}} \binom{2^{B_{k,(\mathrm{d})}}}{i} (-1)^i \sum_{n=1}^{iM} \frac{1}{n} = \sum_{i=1}^{2^{B_{k,(\mathrm{d})}}} \binom{2^{B_{k,(\mathrm{d})}}}{i} (-1)^i \int_0^1 \frac{1 - x^{iM}}{1 - x} dx.$$

Since $\frac{1-x^{iM}}{1-x} \geq 0$, $i = 1, \ldots, 2^{B_{k,(\mathrm{d})}}$ and $x \in [0,1]$, we exchange the integrand and summations to yield

$$\begin{aligned}\sum_{i=1}^{2^{B_{k,(\mathrm{d})}}} \binom{2^{B_{k,(\mathrm{d})}}}{i} (-1)^i \sum_{n=1}^{iM} \frac{1}{n} &= \int_0^1 \frac{1}{1-x} \sum_{i=1}^{2^{B_{k,(\mathrm{d})}}} \binom{2^{B_{k,(\mathrm{d})}}}{i} (-1)^i (1-x^{iM}) dx \\ &= \int_0^1 \frac{1}{1-x} \sum_{i=1}^{2^{B_{k,(\mathrm{d})}}} \left[\binom{2^{B_{k,(\mathrm{d})}}}{i} (-1)^i - \binom{2^{B_{k,(\mathrm{d})}}}{i} (-x^M)^i \right] dx \\ &= -\int_0^1 \frac{(1-x^M)^{2^{B_{k,(\mathrm{d})}}}}{1-x} dx, \end{aligned} \tag{3.23}$$

where (3.23) was obtained using $\sum_{i=1}^{2^{B_{k,(\mathrm{d})}}} \binom{2^{B_{k,(\mathrm{d})}}}{i} (-1)^i = (1+(-1))^{2^{B_{k,(\mathrm{d})}}} = 0$ and $\sum_{i=1}^{2^{B_{k,(\mathrm{d})}}} \binom{2^{B_{k,(\mathrm{d})}}}{i} (-x^M)^i = (1-x^M)^{2^{B_{k,(\mathrm{d})}}}$. The relation $1 - x^M = (1-x)\sum_{k=0}^{M-1} x^k$ is used to further simplify (3.23) as

$$\sum_{i=1}^{2^{B_{k,(\mathrm{d})}}} \binom{2^{B_{k,(\mathrm{d})}}}{i} (-1)^i \sum_{n=1}^{iM} \frac{1}{n} = -\int_0^1 (1-x^M)^{2^{B_{k,(\mathrm{d})}}-1} \sum_{k=0}^{M-1} x^k dx$$

Since $x^k \geq 0$ for all $k = 1, \ldots, M-1$ and $x \in [0,1]$, we again interchange the summation and integrals

$$\begin{aligned}\sum_{i=1}^{2^{B_{k,(\mathrm{d})}}} \binom{2^{B_{k,(\mathrm{d})}}}{i} (-1)^i \sum_{n=1}^{iM} \frac{1}{n} &= -\sum_{k=0}^{M-1} \int_0^1 (1-x^M)^{2^{B_{k,(\mathrm{d})}}-1} x^k dx \\ &= -\sum_{k=0}^{M-1} \int_0^1 u^{\frac{k+1}{M}-1} (1-u)^{2^{B_{k,(\mathrm{d})}}-1} du, \end{aligned} \tag{3.24}$$

where $u = x^M$. Note that the expression in (3.24) is that of a beta function with parameters given by $\frac{k+1}{M}$ and $2^{B_{k,(\mathrm{d})}}$. Hence, (3.24) is given by the sum of beta functions

$$\sum_{i=1}^{2^{B_{k,(\mathrm{d})}}} \binom{2^{B_{k,(\mathrm{d})}}}{i} (-1)^i \sum_{n=1}^{iM} \frac{1}{n} = -\sum_{k=1}^{N_t-1} \beta\left(2^{B_{k,(\mathrm{d})}}, \frac{k}{N_t-1}\right)$$

3.7.4 Proof of Proposition 3.4.4

Dropping the index k (and $(k-1)$) for the sake of convenience, the second term of (3.9), $R_{k,(\mathrm{i})}$, is upper bounded by

$$\begin{aligned}
\mathbb{E}\left\{\log_2\left(\frac{\rho_{(\mathrm{d})}\alpha|\mathbf{g}^*\hat{\mathbf{f}}|^2+1}{\rho_{(\mathrm{d})}\alpha|\mathbf{g}^*\mathbf{f}_{\mathrm{full}}|^2+1}\right)\right\} &\leq \mathbb{E}\left\{\log_2(\rho_{(\mathrm{d})}\alpha|\mathbf{g}^*\hat{\mathbf{f}}|^2+1)\right\} \\
&\leq \log_2(1+\rho_{(\mathrm{d})}\alpha\mathbb{E}\{|\mathbf{g}^*\hat{\mathbf{f}}|^2\}) \qquad (3.25)\\
&= \log_2(1+\rho_{(\mathrm{d})}\alpha\mathbb{E}\{\|\mathbf{g}\|^2\}\mathbb{E}\{|\tilde{\mathbf{g}}^*\hat{\mathbf{f}}|^2\}) \qquad (3.26)\\
&= \log_2(1+\rho_{(\mathrm{d})}\alpha N_t\mathbb{E}\{|\tilde{\mathbf{g}}^*\hat{\mathbf{f}}|^2\})\ . \qquad (3.27)
\end{aligned}$$

Here, (3.25) is obtained from Jensen's inequality. In (3.26) and (3.27), we use the relations $\mathbf{g}=\|\mathbf{g}\|^2\tilde{\mathbf{g}}$ and $\mathbb{E}\{\|\mathbf{g}\|^2\}=N_t$, respectively.

Now, the triangle inequality for angles is rewritten as [90],

$$\begin{aligned}
\theta_{\tilde{\mathbf{g}}^c,\hat{\mathbf{f}}} &\geq |\theta_{\tilde{\mathbf{g}}^c,\hat{\mathbf{g}}^c}-\theta_{\hat{\mathbf{g}}^c,\hat{\mathbf{f}}}|,\\
&= |\theta_{\tilde{\mathbf{g}},\hat{\mathbf{g}}}-\theta_{\hat{\mathbf{g}}^c,\hat{\mathbf{f}}}|,
\end{aligned}$$

since the angles are all positive and lie between $[0,\pi/2]$.

Using trigonometry, $\sin^2(\theta_{\tilde{\mathbf{g}}^c,\hat{\mathbf{f}}})$ is lower-bounded by

$$\begin{aligned}
\sin^2(\theta_{\tilde{\mathbf{g}}^c,\hat{\mathbf{f}}}) &\geq \left[\sin(\theta_{\tilde{\mathbf{g}},\hat{\mathbf{g}}})\cos(\theta_{\hat{\mathbf{g}}^c,\hat{\mathbf{f}}}) - \cos(\theta_{\tilde{\mathbf{g}},\hat{\mathbf{g}}})\sin(\theta_{\hat{\mathbf{g}}^c,\hat{\mathbf{f}}})\right]^2 && (3.28)\\
&= \left[(\cos(\theta_{\tilde{\mathbf{g}},\hat{\mathbf{g}}})\sin(\theta_{\hat{\mathbf{g}}^c,\hat{\mathbf{f}}}))(\tan(\theta_{\tilde{\mathbf{g}},\hat{\mathbf{g}}})\cot(\theta_{\hat{\mathbf{g}}^c,\hat{\mathbf{f}}}) - 1)\right]^2 \\
&= \left[(\cos(\theta_{\tilde{\mathbf{g}},\hat{\mathbf{g}}})\sin(\theta_{\hat{\mathbf{g}}^c,\hat{\mathbf{f}}}))(\mathcal{O}(\theta_{\tilde{\mathbf{g}},\hat{\mathbf{g}}}) - 1)\right]^2 && (3.29)\\
&\approx \left[-\cos(\theta_{\tilde{\mathbf{g}},\hat{\mathbf{g}}})\sin(\theta_{\hat{\mathbf{g}}^c,\hat{\mathbf{f}}})\right]^2 && (3.30)\\
&= \cos^2(\theta_{\tilde{\mathbf{g}},\hat{\mathbf{g}}})(1 - \sin^2(\theta_{\hat{\mathbf{g}}^c,\hat{\mathbf{f}}})) && (3.31)\\
&= \cos^2(\theta_{\tilde{\mathbf{g}},\hat{\mathbf{g}}})(1 - \mathcal{O}(\theta^2_{\hat{\mathbf{g}}^c,\hat{\mathbf{f}}})) && (3.32)\\
&\approx \cos^2(\theta_{\tilde{\mathbf{g}},\hat{\mathbf{g}}}) && (3.33)
\end{aligned}$$

where (3.28) is obtained from the relations $\sin^2(|\theta|) = \sin^2(\theta)$ and $\sin(A-B) = \sin(A)\cos(B) - \sin(B)\cos(A)$. Also, in (3.29) when sufficient quantization bits are used, $\theta_{\tilde{\mathbf{g}},\hat{\mathbf{g}}}$ and hence $\mathcal{O}(\theta_{\tilde{\mathbf{g}},\hat{\mathbf{g}}}) \to 0$, leading to (3.30). Note also that in (3.31) and (3.32) $\theta_{\hat{\mathbf{g}}^c,\hat{\mathbf{f}}} \to 0$, due to the generalized eigenvector relation that minimizes the value of $|\hat{\mathbf{g}}^*\hat{\mathbf{f}}|$. This leads to (3.33).

We know that $|\tilde{\mathbf{g}}^*\hat{\mathbf{f}}|^2 = \cos^2(\theta_{\tilde{\mathbf{g}}^c,\hat{\mathbf{f}}})$. Using (3.33), we have

$$\begin{aligned}
\mathbb{E}\{|\tilde{\mathbf{g}}^*\hat{\mathbf{f}}|^2\} &\leq \mathbb{E}\{1 - \cos^2(\theta_{\tilde{\mathbf{g}},\hat{\mathbf{g}}}\} \\
&= 2^B\beta\left(2^B, \frac{N_t}{N_t - 1}\right) && (3.34)
\end{aligned}$$

where (3.34) is obtained from [6].

3.7.5 Proof of Theorem 3.4.5

We denote (from (3.13))

$$\tilde{\Delta}_k = \log_2\left(1 + 2\rho_{k,(\mathrm{i})}\frac{1}{2^{B_{\mathrm{tot}} - B_{k,(\mathrm{d})}} + 1}\right) + 2^{-B_{k,(\mathrm{d})}}\log_2(e)$$

Note that $\tilde{\Delta}_k$ is continuous and differentiable in $B_{k,(\mathrm{d})}$. The partial derivative of $\tilde{\Delta}_k$ in terms of $B_{k,(\mathrm{d})}$ is obtained as

$$\frac{\partial \tilde{\Delta}_k}{\partial B_{k,(\mathrm{d})}} = 2\rho_{k,(\mathrm{i})} \frac{2^{B_{\mathrm{tot}}-B_{k,(\mathrm{d})}}}{\left(2^{B_{\mathrm{tot}}-B_{k,(\mathrm{d})}} + 2\rho_{k,(\mathrm{i})} + 1\right)\left(1 + 2^{B_{\mathrm{tot}}-B_{k,(\mathrm{d})}}\right)} - 2^{-B_{k,(\mathrm{d})}} \ . \quad (3.35)$$

Now, $\tilde{\Delta}_k$ is convex on the convex set $\mathbb{C}^{2\times 1}$ iff its gradient $\partial\tilde{\Delta}_k/\partial B_{k,(\mathrm{d})}$ is monotone, i.e.

$$\left(\frac{\partial \tilde{\Delta}_k}{\partial {B_{k,(\mathrm{d})}}^{(1)}} - \frac{\partial \tilde{\Delta}_k}{\partial {B_{k,(\mathrm{d})}}^{(2)}})\right)\left({B_{k,(\mathrm{d})}}^{(1)} - {B_{k,(\mathrm{d})}}^{(2)}\right) \geq 0 \ .$$

From (3.35), it is shown using simple algebra that if ${B_{k,(\mathrm{d})}}^{(1)} < {B_{k,(\mathrm{d})}}^{(2)}$, then

$$\begin{aligned} -2^{-{B_{k,(\mathrm{d})}}^{(1)}} + 2\rho_{k,(\mathrm{i})} \frac{2^{B_{\mathrm{tot}}-{B_{k,(\mathrm{d})}}^{(1)}}}{\left(2^{B_{\mathrm{tot}}-{B_{k,(\mathrm{d})}}^{(1)}} + 2\rho_{k,(\mathrm{i})} + 1\right)\left(1 + 2^{B_{\mathrm{tot}}-{B_{k,(\mathrm{d})}}^{(1)}}\right)} < \\ - 2^{-{B_{k,(\mathrm{d})}}^{(2)}} + 2\rho_{k,(\mathrm{i})} \frac{2^{B_{\mathrm{tot}}-{B_{k,(\mathrm{d})}}^{(2)}}}{\left(2^{B_{\mathrm{tot}}-{B_{k,(\mathrm{d})}}^{(2)}} + 2\rho_{k,(\mathrm{i})} + 1\right)\left(1 + 2^{B_{\mathrm{tot}}-{B_{k,(\mathrm{d})}}^{(2)}}\right)}, \end{aligned}$$

implying that the condition for convexity stated in this section is satisfied and $\tilde{\Delta}_k$ is convex in $B_{k,(\mathrm{d})}$. Hence, the value of $B_{k,(\mathrm{d})}$ that minimizes $\tilde{\Delta}_k$ will be a global optimal value and is obtained by equating (3.35) to zero. A closed-form expression for the optimal $B_{k,(\mathrm{d})}$ is given by

$$B_{k,(\mathrm{d})} = B_{\mathrm{tot}} - \log_2\left(1 + \rho_{k,(\mathrm{i})} + \sqrt{\rho_{k,(\mathrm{i})} 2^{B_{\mathrm{tot}}+1} + (\rho_{k,(\mathrm{i})})^2}\right).$$

Chapter 4

Delayed Separate CSI Feedback for Multiple Interferer Systems

In the previous chapter, we introduced the notion of separate CSI feedback, by assuming single interferer multicell cooperative systems with delay-free communication links. In this chapter, we develop a feedback-bit partitioning algorithm for separate CSI quantization for *multiple* interferer scenarios with delays in the feedback and backhaul links. Simulations are used to confirm that the adaptive strategy proposed outperforms equal-bit allocation and leads to a more efficient utilization of the available feedback resources.

4.1 Overview and Contributions

The cooperative strategy used in Chapter 3, GEBF, maximizes sum-rates at high SNR for a single-interferer per user [9, 12]. While the single-interferer assumption was useful to motivate and understand separate quantization, it does not model practical wireless systems where users face interference from several neighboring base stations. This chapter considers ICIN, a partial cooperative strategy for multiple interferer scenarios, where each base station transmits in the null-space of the interference it generates [51, 62, 99].

It is to be noted that ICIN is a non-iterative solution and involves the exchange of only CSI over the backhaul.

In multicell cooperative strategies like ICIN, interference is perfectly nulled out when *full CSI* is available *instantaneously* at the base stations (zero-delay). Realistic wireless communication links are, however, typically associated with delays arising due to signal processing at the transceivers, propagation and channel access protocols, which can degrade the data rates obtained and increase outages in cellular systems [4, 39, 45, 64, 101]. Multicell cooperative strategies are faced with an additional source of delay in the backhaul links, which causes base stations to receive the CSI of the generated interference after an extra delay. It is important to consider the impact of the delays incurred in CSI acquisition at base stations. This chapter deals with partitioning the available feedback bits adaptively based on not only the signal strengths but also the delays associated with each of the channels. Towards this end, a set of *effective interferers* is defined in this chapter, which includes only those channels that affect the data rate most significantly. By distributing feedback resources only among the desired channel and effective interferers in proportion to their signal strengths and delays, the proposed algorithm utilizes the feedback bandwidth more efficiently than equal-bit allocation [10]. It is also shown that designing beamforming vectors by accounting for only the effective interferers yields higher sum-rates due to an increase in the availability degrees of freedom.

Since the performance of a multicell cooperative strategy depends strongly

on the quality of CSI at the base stations, it is important to investigate the impact of delayed limited feedback on multicell systems. The extensive literature on the effect of delay on the performance of single-cell non-cooperative systems cannot be directly applied to the multicell case, since the multiple channels in the cooperative scenario may suffer from different delays. Further, the interfering channels suffer from an additional source of delay in the backhaul link. This chapter uses background from Chapter 3 to develop a framework for limited feedback in multicell cooperative systems with multiple interferers and non-zero delays. The impact of delayed limited feedback in multicell cooperative systems using ICIN is quantified and a feedback-bit partitioning algorithm is presented to reduce the resulting mean loss in sum-rate [10].

The contributions of this chapter are as follows.

1. A limited feedback model is presented for a multicell cooperative scenario, with multiple interferers and delay in feedback and backhaul links. Similar to the limited feedback model in Chapter 3, each user is assumed to estimate and feedback quantized versions of the desired and interfering channels to its own base station. The backhaul link is then used to inform each neighboring base station of the interference that it is causing. Thus, exchanging only the interfering CSI ensures that the load on the backhaul link is manageable.

2. A set of effective interferers is defined, which consists of a subset of interferers that are strong enough and/or have small delays to affect the

sum-rate [10]. The idea is that feedback bits will only be partitioned among the desired channel and the effective interferers, since the other interfering channels are too weak and/or have large delays to reduce the data rate.

3. Assuming that feedback bits are only partitioned among the desired and effective interfering channels, the mean loss in sum-rate arising due to delayed limited feedback is quantified by means of an upper bound. The bound is a function of the relative signal strengths, delays, and codebook sizes of the desired and interfering CSI.

4. Feedback-bit partitions are then derived to assign available feedback bits between the desired and interfering channels to reduce the mean loss in sum-rate, using the upper bound derived [10]. The expressions confirm that the mean sum-rate can be increased by allocating bits in a *water-filling fashion*, i.e. strong channels with smaller delays are assigned more bits than the weaker ones with larger delays.

5. Finally, simulation results are presented to show that the proposed adaptive feedback algorithm yields higher mean sum-rates using ICIN than equal bit partitioning technique.

4.2 System Description

This section briefly summarizes the notation introduced in Section 3.2.1 (and Table 3.1) and presents some chapter-specific terminology. The temporal

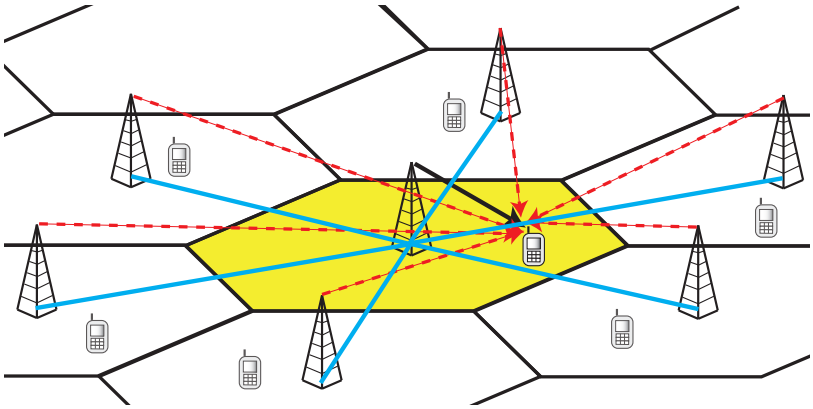

Figure 4.1: Multicell cooperative model described in Section 4.2.

correlation channel model is then described, followed by the multicell cooperative transmit strategy and the limited feedback setup.

4.2.1 System Model

The cellular system adopted in this chapter is illustrated in Fig. 4.1. The solid line with an arrow represents the desired signal, while the dashed lines denote the interfering signals. The solid line between base stations represents the backhaul links connecting base stations. Similar to Chapter 3, a single active user in each of the K cells is assumed, using intra-cell TDMA or a comparable orthogonal access strategy. Each base station and mobile terminal is equipped with N_t and 1 antennas, respectively. The notation in Table 3.1 is also followed in this chapter. At the n^{th} time instant, $\mathbf{h}_k[n]$ refers to the desired channel between the k^{th} user and base stations and $\mathbf{g}_{k,\ell}[n]$ is the interfering channel between the k^{th} user and the ℓ^{th} base station for

$k, \ell \in \{1, \ldots, K\}, k \neq \ell$. In this chapter, we model the desired and interfering channels by the i.i.d. Rayleigh fading model, where each entry is unit variance complex Gaussian independent and identically distributed (i.i.d.) according to $\mathcal{N}_c(0,1)$. While it is recognized that the Rayleigh fading model does not model realistic propagation channels accurately, we use the i.i.d. Gaussian assumption to facilitate the limited feedback analysis.

The symbol transmitted from the k^{th} base station (intended for the k^{th} user) is denoted by s_k, where $\mathbb{E}\{|s_k|^2\} = 1$. Each user is assumed to face interference from $K-1$ neighboring base stations, each transmitting with energy E_s. At the k^{th} user, the *received* desired signal power is denoted by γ_k and the power of the interfering signal from base station ℓ is given by $\gamma_{k,\ell}$. The ISR of the ℓ^{th} interferer to the k^{th} user by $\alpha_{k,\ell} = \gamma_{k,\ell}/\gamma_k$, where $\ell = 1, \ldots, K$, $\ell \neq k$. Using the narrowband flat-fading model, the baseband discrete-time input-output relation for the user in the k^{th} cell is given by

$$y_k[n] = \sqrt{\gamma_k}\mathbf{h}_k^*[n]\mathbf{f}_k[n]s_k[n] + \sum_{\substack{\ell=1 \\ \ell \neq k}}^{K} \sqrt{\alpha_{k,\ell}\gamma_k}\mathbf{g}_{k,\ell}^*[n]\mathbf{f}_\ell[n]s_\ell[n] + v_k[n], \qquad (4.1)$$

where $y_k[n] \in \mathbb{C}$ is the received signal at the k^{th} user and $\mathbf{f}_k[n] \in \mathbb{C}^{N_t \times 1}$ is the unit-norm beamforming vector at the k^{th} base station, at the n^{th} time instant. Finally, $v_k[n] \in \mathbb{C}$ is complex additive zero-mean white Gaussian noise at the k^{th} user, with $\mathbb{E}\{|v_k|^2\} = N_0$. We denote the received desired and interfering signal to noise ratios (SNR) as $\rho_k = \gamma_k/N_0$ and $\alpha_{k,\ell}\rho_k$, respectively. As in Chapter 3, base stations are assumed to have perfect knowledge of ρ_k.

The SINR of the k^{th} user at the n^{th} instant is given by

$$\mathsf{SINR}_k[n] = \frac{\rho_k |\mathbf{h}_k^*[n]\mathbf{f}_k[n]|^2}{1 + \sum_{\substack{\ell=1 \\ \ell \neq k}}^{K} \alpha_{k,\ell}\rho_k |\mathbf{g}_{k,\ell}^*[n]\mathbf{f}_\ell[n]|^2} \tag{4.2}$$

The sum-rate of all the users within the system is

$$R_s[n] = \sum_k \log_2 \left(1 + \mathsf{SINR}_k[n]\right).$$

The sum-rate, hence, depends on beamforming vectors $\mathbf{f}_k[n]$, which are designed using quantized and delayed channel state information. Note that in the remainder of this chapter, we assume that $k \neq \ell$ unless otherwise mentioned.

4.2.2 Limited Feedback Model

The channel directions, denoted by $\tilde{\mathbf{h}}_k[n] := \mathbf{h}_k[n]/\|\mathbf{h}_k[n]\|$ and $\tilde{\mathbf{g}}_{k,\ell}[n] := \mathbf{g}_{k,\ell}[n]/\|\mathbf{g}_{k,\ell}[n]\|$, are quantized to the unit-norm vectors given by $\hat{\mathbf{h}}_k[n]$ and $\hat{\mathbf{g}}_{k,\ell}[n]$, respectively, at the k^{th} user in the n^{th} time instant. Using ICIN, the cooperative strategy used in this chapter, beamforming vectors are designed to lie in the null space of the interfering channel *directions*. Since base stations do not require knowledge of the channel gains, users feedback only the estimated channel directions. The limited feedback model is illustrated in Fig. 4.2.

We assume that each user can utilize B_{tot} bits for feedback, and that B_k and $B_{k,\ell}$ bits are used to quantize $\tilde{\mathbf{h}}_k[n]$ and $\tilde{\mathbf{g}}_{k,\ell}[n]$ respectively, where $B_k + \sum_{\substack{\ell=1 \\ \ell \neq k}}^{K} B_{k,\ell} = B_{\text{tot}}$. This approach of splitting available feedback bits between the desired and interfering channels was used in [9, 99]. The delay

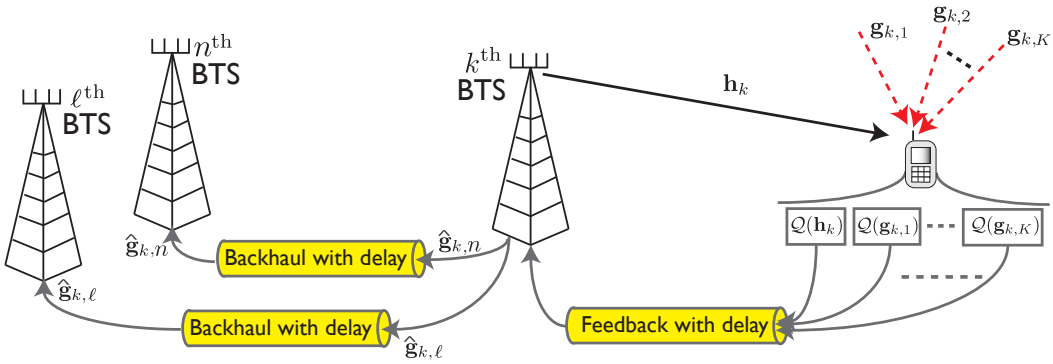

Figure 4.2: The limited feedback model, described in Section 4.2.2, to feedback quantized CSI of the desired and interfering channels. The quantizing operation is denoted by $\mathcal{Q}$.

associated with quantizing $\tilde{\mathbf{h}}_k[n]$ (to $\hat{\mathbf{h}}_k[n]$) and feeding back $\hat{\mathbf{h}}_k[n]$ to the k^{th} base station is denoted by D_k. The k^{th} user also quantizes the interfering channels, $\tilde{\mathbf{g}}_{k,\ell}[n]$ to $\hat{\mathbf{g}}_{k,\ell}[n]$ and feeds back $\hat{\mathbf{g}}_{k,\ell}[n]$ to the k^{th} base station, which then transmits $\hat{\mathbf{g}}_{k,\ell}[n]$ to the ℓ^{th} base station over the backhaul link, incurring a delay of $D_{k,\ell}$, where $\ell = 1, \ldots, K$. Hence, at the time instant n, the k^{th} base station has knowledge of $\tilde{\mathbf{h}}_k[n - D_k]$ and $\tilde{\mathbf{g}}_{\ell,k}[n - D_{\ell,k}]$, for all $\ell \neq k$ [10].

In this chapter, we assume that the delays, D_k and $D_{k,\ell}$, are known at the base station and users. This is reasonable since delays in the feedback and backhaul link can be measured using training signals, assuming perfect synchronization between the transmitter(s) and receiver(s). Note that $D_{k,\ell} \geq D_k$, since $D_{k,\ell}$ includes exchange of CSI over the backhaul link, in addition to limited feedback from the k^{th} user.

4.2.3 Gauss-Markov Model for CSI Delay

The presence of delay in the system leads to a loss in the sum-rate, which can be evaluated by understanding the relation between the current and delayed CSI. In this chapter, the Gauss-Markov block fading autoregressive model is used to characterize the relation between $\mathbf{h}_k[n]$ ($\mathbf{g}_{k,\ell}[n]$) and $\mathbf{h}_k[n-D_k]$ ($\mathbf{g}_{k,\ell}[n-D_{k,\ell}]$). It has been shown in the literature [34, 85, 89] that the Gauss-Markov autoregressive model is reasonably accurate for relatively small delays in the communication links. Hence, it has been widely used in research to model the effect of delay on the performance of wireless systems using limited feedback [39, 45, 64, 101]. Further, as mentioned in [101], the Gauss-Markov model can also be used to model the impact of imperfect CSI at the transmitter due to estimation errors. By assuming that $\mathbf{h}_k[n]$ and $\mathbf{g}_{k,\ell}[n]$ are constant throughout the codeword transmission, the current and delayed CSI are related by

$$\mathbf{h}_k[n] = \eta_k \mathbf{h}_k[n-D_k] + \sqrt{1-\eta_k^2}\mathbf{w}_{\mathbf{h}_k}[n], \quad \text{and} \tag{4.3}$$

$$\mathbf{g}_{k,\ell}[n] = \eta_{k,\ell} \mathbf{g}_{k,\ell}[n-D_{k,\ell}] + \sqrt{1-\eta_{k,\ell}^2}\mathbf{w}_{\mathbf{g}_{k,\ell}}[n], \tag{4.4}$$

where $\mathbf{w}_{\mathbf{h}_k}[n]$ and $\mathbf{w}_{\mathbf{g}_{k,\ell}}[n]$ denote the channel error vectors, and are uncorrelated with $\mathbf{h}_k[n-D_k]$ and $\mathbf{g}_{k,\ell}[n-D_{k,\ell}]$, respectively. The entries of $\mathbf{w}_{\mathbf{h}_k}[n]$ and $\mathbf{w}_{\mathbf{g}_{k,\ell}}[n]$ are distributed by $\mathcal{N}_c(0,1)$. The correlation coefficients for the desired and interfering channels are denoted by η_k and $\eta_{k,\ell}$, respectively. Clarke's

autocorrelation model is used to determine η_k and $\eta_{k,\ell}$ as [19, 39, 45, 64, 101]

$$\begin{aligned} \eta_k &= J_0(2\pi D_k f_d T_s), \quad \text{and} \\ \eta_{k,\ell} &= J_0(2\pi D_{k,\ell} f_d T_s), \end{aligned}$$

where J_0 is the zeroth order Bessel function of the first kind, f_d is the Doppler spread and T_s is the symbol duration. The Doppler spread, $f_d = \nu f_c/c$, where ν is the relative velocity of the transmitter-receiver pair, f_c the carrier frequency, and c, the speed of light.

4.2.4 Inter-Cell Interference Nulling

When full CSI is available at all the base stations and the delay associated with feedback and backhaul is zero, the k^{th} base station has instantaneous knowledge of not only its own desired channel, $\mathbf{h}_k[n]$, but also of the interference caused to neighboring cells, i.e. $\mathbf{g}_{\ell,k}[n], \ell = 1, \ldots, K, \ell \neq k$, made available via the backhaul link. The k^{th} base station then computes the beamforming vector, $\mathbf{f}_k, [n]$, as [51, 62, 99]

$$\mathbf{f}_k[n] = \mathbf{W}_k[n](:, 1), \quad \text{where } \mathbf{W}_\ell[n] = \left(\left[\tilde{\mathbf{h}}_k[n] \; \tilde{\mathbf{g}}_{1,k}[n] \; \ldots \; \tilde{\mathbf{g}}_{K,k}[n] \right] \right)^\dagger. \quad (4.5)$$

Assuming that the channels in $\mathbf{W}_k[n]$ are independent of each other, (4.5) ensures perfect interference nulling, i.e. $\mathbf{g}^*_{k,\ell}[n]\mathbf{f}_\ell[n] = 0$, for $\ell = 1, \ldots, K, \ell \neq k$, when $N_t \geq K$. The sum-rate, assuming full CSI and zero delay, is given by

$$R_s[n] = \sum_{k=1}^{K} \log_2 \left(1 + |\mathbf{h}^*_k[n]\mathbf{f}_k[n]|^2\right),$$

where $\mathbf{f}_k[n]$ is given by (4.5). The denominator is nulled out since the beamforming vector at the ℓ^{th} base station is designed to be lie in the null-space of the $\mathbf{g}_{k,\ell}$.

4.3 Impact of Delayed Limited Feedback

As a result of delay, at the n^{th} time instant, the k^{th} base station has knowledge of its desired channel, $\hat{\mathbf{h}}_k[n-D_k]$ and the interference that it causes to the neighboring $K-1$ cells, $\hat{\mathbf{g}}_{\ell,k}[n-D_{k,\ell}]$ (for $\ell = 1,\ldots,K, \ell \neq k$). Hence, the beamforming vector at the n^{th} time instant, $\hat{\mathbf{f}}_k[n]$, is designed using the delayed and quantized CSI of the desired channels and the interference caused to other cells [10]

$$\hat{\mathbf{f}}_k[n] = \hat{\mathbf{W}}_k[n](:,1), \text{ for } \hat{\mathbf{W}}_k[n] = \left[\hat{\mathbf{h}}_k[n-D_k]\ \hat{\mathbf{g}}_{1,k}[n-D_{1,\ell}]\ \ldots\ \hat{\mathbf{g}}_{K,k}[n-D_{K,k}]\right]^{\dagger}. \tag{4.6}$$

When $N_t \geq K$, the beamforming vector lies in the $N_t-(K-1)$ null-space of the $K-1$ interfering channels. Hence, when $N_t = K$, $\hat{\mathbf{f}}_k[n]$ lies in a one-dimensional subspace, independent of $\hat{\mathbf{h}}_k$. This implies that if $N_t = K$, it is not necessary to feedback the quantized desired channel back to the base station, i.e. $B_k = 0$. In contrast, when $N_t > K$, $\hat{\mathbf{h}}_k$ is desirable at the base station to determine the best $\hat{\mathbf{f}}_k[n]$ in the $N_t-(K-1)$ subspace. This chapter considers the more general $N_t > K$ case. Note that the $N_t \geq K$ case can be imposed by clustering cooperative cells into groups of sizes $\leq N_t$ [40, 100].

The sum-rate, assuming limited feedback and delay, is given by

$$\hat{R}_s[n] = \sum_{k=1}^{K} \log_2 \left(1 + \frac{\rho_k |\mathbf{h}_k^*[n]\hat{\mathbf{f}}_k[n]|^2}{1 + \sum_{\substack{\ell=1 \\ \ell \neq k}}^{K} \alpha_{k,\ell}\rho_k |\mathbf{g}_{k,\ell}^*[n]\hat{\mathbf{f}}_\ell[n]|^2} \right), \tag{4.7}$$

where $\hat{\mathbf{f}}_k[n]$ is given by (4.6). Due to limited feedback, interfering signals in the denominator of (4.2) are not nulled out, i.e. $|\mathbf{g}_{k,\ell}^*[n]\hat{\mathbf{f}}_\ell[n]|^2 \neq 0$. Note, however, that $|\hat{\mathbf{g}}_{k,\ell}^*[n - D_{k,\ell}]\hat{\mathbf{f}}_\ell[n]|^2 = 0$. Hence, the non-zero denominator of (4.7) reduces the sum-rate of the overall system. We define the mean loss in sum-rate due to delay and limited feedback, using ICIN as

$$\mathbb{E}\{\Delta R_s[n]\} := \mathbb{E}\{R_s[n]\} - \mathbb{E}\{\hat{R}_s[n]\}. \tag{4.8}$$

To simplify analysis, we derive an upper bound on the mean loss in sum-rate by deriving first a lower bound on $\mathbb{E}\{\hat{R}_s[n]\}$ given by

$$\mathbb{E}\{\hat{R}_s[n]\} \geq \sum_{k=1}^{K} \log_2 \left(\frac{\rho_k |\mathbf{h}_k^*[n]\hat{\mathbf{f}}_k[n]|^2}{1 + \sum_{\substack{\ell=1 \\ \ell \neq k}}^{K} \alpha_{k,\ell}\rho_k |\hat{\mathbf{g}}_{k,\ell}^*[n]\hat{\mathbf{f}}_\ell[n]|^2} \right), \tag{4.9}$$

$$= \sum_{k=1}^{K} \underbrace{\mathbb{E}\left\{ \log_2 \left(\rho_k |\mathbf{h}_k^*[n]\hat{\mathbf{f}}_k[n]|^2 \right) \right\}}_{R_{k,(\text{des})}} - \underbrace{\mathbb{E}\left\{ \log_2 \left(1 + \sum_{\substack{\ell=1 \\ \ell \neq k}}^{K} \alpha_{k,\ell}\rho_k |\mathbf{g}_{k,\ell}^*[n]\hat{\mathbf{f}}_\ell[n]|^2 \right) \right\}}_{R_{k,(\text{int})}}. \tag{4.10}$$

We label the first term on the right-hand side of (4.10) as $R_{k,(\text{des})}$ and the second term as $R_{k,(\text{int})}$. We obtain a lower bound on the mean sum-rate by deriving a lower-bound on $R_{k,(\text{des})}$ and an upper bound on $R_{k,(\text{int})}$ [10]. To derive closed-form bounds on $R_{k,(\text{des})}$ and $R_{k,(\text{int})}$, using RVQ [49, 75, 76].

Proposition 4.3.1. *The lower bound on* $\mathbb{E}\left\{\log_2\left(\rho_k|\mathbf{h}_k^*[n]\hat{\mathbf{f}}_k[n]|^2\right)\right\}$ *using RVQ approximated as*

$$\log_2(\rho_k\eta_k^2) + \frac{\log_2(e)}{N_t-1}\sum_{i=1}^{N_t-1}\beta\left(2^{B_k}, \frac{i}{N_t-1}\right) + \mathbb{E}\left\{\log_2\left(\|\mathbf{h}_k[n-D_k]\|^2\left|\hat{\mathbf{h}}_k[n-D_k]\hat{\mathbf{f}}_k[n]\right|^2\right)\right\}.$$

Proof. The proof is given in Appendix 4.7.1. □

Now, $\mathbb{E}\{R_s[n]\} \approx \sum_k \mathbb{E}\left\{\log_2\left(\rho_k\|\mathbf{h}_k[n]\|^2|\tilde{\mathbf{h}}_k^*[n]\mathbf{f}_k[n]|^2\right)\right\}$ at large SNR. Note that this is the same approximation used in Section 3.2.2. Using (4.8) and (4.10), Proposition 4.3.1 relates the error from quantizing the desired channel using B_k bits to the mean loss in sum-rate, $\mathbb{E}\{\Delta R_s[n]\}$,

$$\mathbb{E}\{\Delta R_s[n]\} \leq \sum_{k=1}^{K}\log_2(\eta_k^2) + \frac{\log_2(e)}{N_t-1}\sum_{i=1}^{N_t-1}\beta\left(2^{B_k}, \frac{i}{N_t-1}\right) + R_{k,(\text{int})}, \quad (4.11)$$

due to the fact that $\mathbb{E}\left\{\log_2\left(\|\tilde{\mathbf{h}}_k^*[n]\mathbf{f}_k[n]|^2\right)\right\} = \mathbb{E}\left\{\log_2\left(|\hat{\mathbf{h}}_k[n-D_k]\hat{\mathbf{f}}_k[n]|^2\right)\right\}$ and $\mathbb{E}\left\{\log_2\left(\|\mathbf{h}_k[n]\|^2\right)\right\} = \mathbb{E}\left\{\log_2\left(\|\mathbf{h}_k[n-D_k]\|^2\right)\right\}$.

Using Lemma 3.4.3, (4.11) is rewritten as

$$\mathbb{E}\{\Delta R_s[n]\} \leq \sum_{k=1}^{K}\log_2(\eta_k^2) + \frac{\log_2(e)}{N_t-1}\sum_{i=1}^{N_t-1}\beta\left(2^{B_k}, \frac{i}{N_t-1}\right) + R_{k,(\text{int})}. \quad (4.12)$$

Intuitively, as B_k increases, the contribution of the desired channel quantization towards the mean loss in sum-rate reduces. By definition, we have that $\beta(2^{B_1}, x) > \beta(2^{B_2}, x)$ for $B_1 < B_2$. Hence, Proposition 4.3.1 and Lemma 3.4.3 verify that increasing B_k leading to a smaller value of $R_{k,(\text{des})}$.

Using Jensen's inequality, $R_{k,(\text{int})}$ can be upper bounded by

$$R_{k,(\text{int})} \leq \log_2\left(1+\rho_k\sum_{\substack{\ell=1\\ \ell\neq k}}^{K}\alpha_{k,\ell}\mathbb{E}\left\{|\mathbf{g}_{k,\ell}^*[n]\hat{\mathbf{f}}_\ell[n]|^2\right\}\right).$$

We evaluate $\mathbb{E}\left\{|\mathbf{g}_{k,\ell}{}^*[n]\hat{\mathbf{f}}_\ell[n]|^2\right\}$ to derive an upper bound on $R_{k,(\text{int})}$.

Proposition 4.3.2. *The upper bound on* $\mathbb{E}\left\{|\mathbf{g}_{k,\ell}{}^*[n]\hat{\mathbf{f}}_\ell[n]|^2\right\}$ *using RVQ can be approximated as*

$$1-\eta_{k,\ell}^2+\eta_{k,\ell}^2 2^{B_{k,\ell}}\beta\left(2^{B_{k,\ell}},\frac{N_t}{N_t-1}\right)\frac{N_t}{N_t-1}.$$

Proof. The proof is given in Appendix 4.7.2. □

Proposition 4.3.2 relates the mean loss in sum-rate to the number of bits assigned to quantize the interfering channels, $B_{k,\ell}$. Intuitively, increasing N_t for fixed $B_{k,\ell}$ increases the quantization error, which increases the mean loss in sum-rate. This is verified using Proposition 4.3.2, where it is seen that for large N_t, $N_t/(N_t-1)\to 1$, causing $\beta\left(2^{B_{k,\ell}},\frac{N_t}{N_t-1}\right)\frac{N_t}{N_t-1}$ to become larger [10]. Using (4.12) and Proposition 4.3.2, $\mathbb{E}\{\Delta R_s[n]\}$ is upper bounded as

$$\begin{aligned}\mathbb{E}\{\Delta R_s[n]\} \leq{}& \sum_{k=1}^{K}\log_2(\eta_k^2)+\frac{\log_2(e)}{N_t-1}\sum_{n=1}^{N_t-1}\beta\left(2^{B_k},\frac{n}{N_t-1}\right)\\ &+\log_2\left(1+\rho_k\sum_{\substack{\ell=1\\ \ell\neq k}}^{K}\alpha_{k,\ell}\left(1-\eta_{k,\ell}^2+\eta_{k,\ell}^2 2^{B_{k,\ell}}\beta\left(2^{B_{k,\ell}},\frac{N_t}{N_t-1}\right)\frac{N_t}{N_t-1}\right)\right).\end{aligned} \tag{4.13}$$

It is clear from (4.13) that for a given $\{\rho_k,\eta_k\}_{k=1}^K$ and $\{\eta_{k,\ell},\alpha_{k,\ell}\}_{\substack{k=1\\ k\neq\ell}}^K$, the (upper bound on) mean loss in sum-rate will depend on B_k and $B_{k,\ell}$, for all k and ℓ.

For $N_t > K$ ($B_k \neq 0$), one solution for B_k and $B_{k,\ell}$ is to choose $B_k = B_{k,\ell} = B_{\text{tot}}/K$. This simple solution does not account for the different weights associated with each interferer. For example, for a given user k, if $\alpha_{k,\ell} \approx 0$ for all ℓ, it implies that the interfering signals to the user are too weak to degrade the mean loss in sum-rate and can be ignored. Equal-bit partitioning, however, will assign $B_{k,\ell} = B_{\text{tot}}/K$ to each interferer and waste $(K-1)B_{\text{tot}}/K$ bits, while assigning only B_{tot}/K to quantize the desired channel. An *adaptive* feedback bit partitioning strategy will efficiently allocate bits to the different channels depending on the respective delays and signal strengths.

4.4 Feedback-Bit Partitioning

This section minimizes the upper bound on the mean loss in sum-rate in (4.13), with respect to the number of feedback bits assigned to the desired and interfering channels at each user. We simplify (4.13) using approximations for the beta functions to ensure analytical tractability and then derive closed-form expressions for the bit-partitioning.

As described in Chapter 3, we use the approximation $\beta(a,b) \approx \Gamma(b)a^{-b}$, when a is large and b is fixed. Since we are optimizing over B_k and $B_{k,\ell}$ in (4.13), b is always fixed while $a = 2^{B_k}$ (or $2^{B_{k,\ell}}$) is at least equal to 1. Hence,

we approximate the right hand side of the expression in (4.13) as

$$\sum_{k=1}^{K}\log_2(\eta_k^2)+\frac{\log_2(e)}{N_t-1}\sum_{n=1}^{N_t-1}\Gamma\left(\frac{n}{N_t-1}\right)\left(2^{B_k}\right)^{-\frac{n}{N_t-1}}+$$
$$\log_2\left(1+\rho_k\sum_{\substack{\ell=1\\ \ell\neq k}}^{K}\alpha_{k,\ell}\left(1-\eta_{k,\ell}^2+\eta_{k,\ell}^2 2^{B_{k,\ell}}\Gamma\left(\frac{N_t}{N_t-1}\right)\left(2^{B_{k,\ell}}\right)^{-\frac{N_t}{N_t-1}}\frac{N_t}{N_t-1}\right)\right). \tag{4.14}$$

For a large N_t, $\left(2^{B_k}\right)^{-\frac{n}{N_t-1}}$ will be relatively much smaller than $\left(2^{B_k}\right)^{-\frac{1}{N_t-1}}$. It is reasonable to coordinate the first tier of interferers (seven cells for the theorertical hexagonal system), in which case the dimensionality constraint of ICIN requires that $N_t \geq K(=7)$. This ensures that N_t is large enough that N_t, $\left(2^{B_k}\right)^{-\frac{n}{N_t-1}}$ can be ignored. By neglecting the higher order terms $(n=2,\ldots,(N_t-1))$ in the summation

$$\frac{\log_2(e)}{N_t-1}\sum_{n=1}^{N_t-1}\Gamma\left(\frac{n}{N_t-1}\right)\left(2^{B_k}\right)^{-\frac{n}{N_t-1}}\approx\frac{\log_2(e)}{N_t-1}\Gamma\left(\frac{1}{N_t-1}\right)\left(2^{B_k}\right)^{-\frac{1}{N_t-1}}. \tag{4.15}$$

Substituting (4.15) in (4.14) yields

$$\sum_{k=1}^{K}\log_2(\eta_k^2)+\log_2(e)\Gamma\left(\frac{N_t}{N_t-1}\right)2^{-\frac{B_k}{N_t-1}}$$
$$+\log_2\left(1+\rho_k\sum_{\substack{\ell=1\\ \ell\neq k}}^{K}\alpha_{k,\ell}\left(1-\eta_{k,\ell}^2\right)+\Gamma\left(\frac{2N_t-1}{N_t-1}\right)N_t\rho_k\sum_{\substack{\ell=1\\ \ell\neq k}}^{K}\alpha_{k,\ell}\eta_{k,\ell}^2 2^{-\frac{B_{k,\ell}}{N_t-1}}\right),$$

using the identity $N\Gamma(N) = \Gamma(N+1)$. We denote

$$\Delta_{R,k}(B_k, \{B_{k,\ell}\}_\ell) := \log_2(e)\Gamma\left(\frac{N_t}{N_t-1}\right)2^{-\frac{B_k}{N_t-1}}$$
$$+\log_2\left(1+N_t\rho_k\sum_{\substack{\ell=1\\\ell\neq k}}^{K}\alpha_{k,\ell}\left(1-\eta_{k,\ell}^2\right)+\Gamma\left(\frac{2N_t-1}{N_t-1}\right)N_t\rho_k\sum_{\substack{\ell=1\\\ell\neq k}}^{K}\alpha_{k,\ell}\eta_{k,\ell}^2 2^{-\frac{B_{k,\ell}}{N_t-1}}\right)$$

Thus, (4.14) can finally be approximated as

$$\sum_{k=1}^{K}\log_2\left(\eta_k^2\right)+\sum_{k=1}^{K}\Delta_{R,k}(B_k,\{B_{k,\ell}\}_{\substack{\ell=1\\\ell\neq k}}^{K}). \tag{4.16}$$

From (4.16), minimizing each $\Delta_{R,k}(B_k, \{B_{k,\ell}\}_{\substack{\ell=1\\\ell\neq k}}^{K})$ individually for a fixed η_k is equivalent to minimizing (4.16) due to the independence of each term in the summation. Note that this eliminates the need for joint optimization. The k^{th} user's contribution to the mean loss in sum-rate, $\Delta_{R,k}(B_k, \{B_{k,\ell}\}_{\substack{\ell=1\\\ell\neq k}}^{K})$ (and hence, the expression in (4.16)) is minimized as

$$\begin{aligned}&\min_{B_k,\{B_{k,\ell}\}_{\substack{\ell=1\\\ell\neq k}}^{K}}\Delta_{R,k}(B_k,\{B_{k,\ell}\}_{\substack{\ell=1\\\ell\neq k}}^{K})\\ &\text{s.t. } B_k+\sum_{\substack{\ell=1\\\ell\neq k}}^{K}B_{k,\ell}=B_{\text{tot}},\ \text{and } B_k,B_{k,\ell}\geq 0.\end{aligned} \tag{4.17}$$

We denote the total number of bits allocated to quantize interfering channels by $B_{k,(\text{i})} = \sum_{\substack{\ell=1\\\ell\neq k}}^{K} B_{k,\ell}$, where $B_k + B_{k,(\text{i})} = B_{\text{tot}}$. Given $B_{k,(\text{i})}$, we first derive $B_{k,\ell}$ to minimize the contribution of the interfering channels towards the mean loss in sum-rate, i.e., we minimize

$$\log_2\left(1+\rho_k\sum_{\substack{\ell=1\\\ell\neq k}}^{K}\alpha_{k,\ell}\left(1-\eta_{k,\ell}^2\right)+\Gamma\left(\frac{2N_t-1}{N_t-1}\right)\rho_k N_t\sum_{\substack{\ell=1\\\ell\neq k}}^{K}\alpha_{k,\ell}\eta_{k,\ell}^2 2^{-\frac{B_{k,\ell}}{N_t-1}}\right) \tag{4.18}$$

such that $\sum_{\substack{\ell=1 \\ \ell \neq k}}^{K} B_{k,\ell} = B_{k,(\mathrm{i})}$ [10]. Since the log function is monotonic in nature and $\{B_{k,\ell}\}_{\substack{\ell=1 \\ \ell \neq k}}^{K}$ are the only variables in (4.18), the optimization problem in (4.18) is reduced to

$$\begin{aligned} \min_{\{B_{k,\ell}\}_{\substack{\ell=1 \\ \ell \neq k}}^{K}} \quad & \sum_{\substack{\ell=1 \\ \ell \neq k}}^{K} \alpha_{k,\ell} \eta_{k,\ell}^2 2^{-\frac{B_{k,\ell}}{N_t - 1}} \\ \text{s.t.} \quad & \sum_{\substack{\ell=1 \\ \ell \neq k}}^{K} B_{k,\ell} = B_{k,(\mathrm{i})}, \text{ and } B_{k,\ell} \geq 0. \end{aligned} \tag{4.19}$$

The solution to (4.19) and the contribution of each of the terms inside the summation in the objective function of (4.19) is given by Theorem 4.4.1 using the arithmetic-geometric mean inequality. We consider first continuous relaxed optimization, where B_k and $B_{k,\ell}$ can be real numbers and not necessarily integers.

Theorem 4.4.1. *The optimum number of bits assigned to the ℓ^{th} interferer, ${B_{k,\ell}}^*$, that minimizes* (4.19) *is given by*

$${B_{k,\ell}}^* = \frac{B_{k,(\mathrm{i})}}{|\mathcal{K}|} + (N_t - 1) \log_2 \left(\frac{\alpha_{k,\ell} \eta_{k,\ell}^2}{\prod_{\ell \in \mathcal{K}} (\alpha_{k,\ell} \eta_{k,\ell}^2)^{\frac{1}{|\mathcal{K}|}}} \right),$$

for $\ell \in \mathcal{K}$, and $B_{k,\ell} = 0$ for $\ell \notin \mathcal{K}$, where $\mathcal{K}$ is the largest set of interferers that satisfies

$$\log_2 \left(\frac{\prod_{\ell \in \mathcal{K}} (\alpha_{k,\ell} \eta_{k,\ell}^2)^{\frac{1}{|\mathcal{K}|}}}{\alpha_{k,\ell} \eta_{k,\ell}^2} \right) < \frac{B_{k,(\mathrm{i})}}{|\mathcal{K}|(N_t - 1)}.$$

Proof. The proof is given in Appendix 4.7.3. □

In Theorem 4.4.1, $\mathcal{K}$ denotes the *effective* set of interferers. Feedback resources are only allocated to the interferers that belong to the effective set.

The idea is that the limited number of feedback bits are best utilized by allocating them to strong interferers, which can affect the sum-rate drastically or/and to the interferers with small delays, since nulling out outdated CSI will not improve sum-rates. Hence, only the effective interfering channels are quantized using the proposed bit-partitioning algorithm. Feedback bits are assigned to the channels in proportion to their signal strengths and delays [10]. If all the interferers have the same delay and strength, then it is seen from Theorem 4.4.1 that all the channels are assigned the same number of feedback bits. Note that when beamforming is performing to null out only the effective interferers, the degrees of freedom are increased from $N_t - K + 1$ to $N_t - |\mathcal{K}| + 1$.

Using the bit allocation strategy for interfering channels proposed in Theorem 4.4.1, the minimum value of the objective function in (4.19) is

$$\min_{\substack{\{B_{k,\ell}\}_{\ell=1 \\ \ell\neq k}^{K}}} \sum_{\substack{\ell=1 \\ \ell\neq k}}^{K} \alpha_{k,\ell}\eta_{k,\ell}^2 2^{-\frac{B_{k,\ell}}{N_t-1}} = |\mathcal{K}| 2^{-\frac{B_{k,(\mathrm{i})}}{|\mathcal{K}|(N_t-1)}} \prod_{\ell\in\mathcal{K}} (\alpha_{k,\ell}\eta_{k,\ell}^2)^{\frac{1}{|\mathcal{K}|}}.$$

The objective function of (4.17), $\Delta_{R,k}(B_k, \{B_{k,\ell}\}_{\substack{\ell=1 \\ \ell\neq k}}^{K})$, is given by

$$\begin{aligned}
\Delta_{R,k}(B_k, \{B_{k,\ell}\}_{\substack{\ell=1 \\ \ell\neq k}}^{K}) &= \log_2(e)\Gamma\left(\frac{N_t}{N_t-1}\right) 2^{-\frac{B_k}{N_t-1}} \\
&\quad + \log_2\left(1 + N_t\rho_k \sum_{\substack{\ell=1 \\ \ell\neq k}}^{K} \alpha_{k,\ell}\left(1-\eta_{k,\ell}^2\right)\right. \\
&\qquad \left. + |\mathcal{K}|\rho_k N_t \Gamma\left(\frac{2N_t-1}{N_t-1}\right) 2^{-\frac{B_{\mathrm{tot}}-B_k}{|\mathcal{K}|(N_t-1)}} \prod_{\ell\in\mathcal{K}} (\alpha_{k,\ell}\eta_{k,\ell}^2)^{\frac{1}{|\mathcal{K}|}}\right) \\
&= \Delta_{R,k}(B_k).
\end{aligned} \tag{4.20}$$

Hence, the objective function of (4.17) is now reduced to an expression in a single variable. To simplify the function in (4.20), we consider different solutions for the high and low SNR regimes.

Case 1: Low SNR Regime

For $|x| < 1$, $\ln(1+x) = x + o(1)$. Thus, $\ln(1+x) \approx x$ for $x \approx 0$. In this section, we use this approximation to define $\Delta_{R,k}^{\mathrm{LS}}(B_k)$ as

$$\begin{aligned}\Delta_{R,k}^{\mathrm{LS}}(B_k) :=& \log_2(e)\Gamma\left(\frac{N_t}{N_t-1}\right)2^{-\frac{B_k}{N_t-1}} + \log_2(e)\rho_k N_t \sum_{\substack{\ell=1\\ \ell\neq k}}^{K} \alpha_{k,\ell}\left(1-\eta_{k,\ell}^2\right) \\ &+ \log_2(e)|\mathcal{K}|N_t\rho_k\Gamma\left(\frac{2N_t-1}{N_t-1}\right)2^{-\frac{B_{\mathrm{tot}}-B_k}{|\mathcal{K}|(N_t-1)}}\prod_{\ell\in\mathcal{K}}(\alpha_{k,\ell}\eta_{k,\ell}^2)^{\frac{1}{|\mathcal{K}|}}.\end{aligned} \tag{4.21}$$

We use the arithmetic mean-geometric mean inequality to minimize the expression in (4.21), as given in Theorem 4.4.2.

Theorem 4.4.2. *Given the total number of bits allocated to quantize* all *the channels, B_{tot}, the optimum number of bits assigned to the desired channel at the k^{th} user, B_k, to minimize* (4.21) *is given by*

$$B_k = \frac{B_{\mathrm{tot}}}{|\mathcal{K}|+1} - \frac{(N_t-1)|\mathcal{K}|}{|\mathcal{K}|+1}\log_2\left(\rho_k\frac{N_t}{N_t-1}\prod_{\ell\in\mathcal{K}}(\alpha_{k,\ell}\eta_{k,\ell}^2)^{\frac{1}{|\mathcal{K}|}}\right),$$

for $N_t > K$ and $B_k = 0$ for $N_t = K$. The optimum number of bits assigned to all the interfering channels at the k^{th} user is computed as $B_{k,(\mathrm{i})} = B_{\mathrm{tot}} - B_k$.

Proof. The proof is given in Appendix 4.7.4. □

From Theorem 4.4.2, it is seen that as $\rho_k \prod_{\ell \in \mathcal{K}} \alpha_{k,\ell} \eta_{k,\ell}^2$ increases (or as interferers become stronger/ have smaller delays) B_k is reduced. In the presence of strong interference, reducing the interfering signal power will increase the sum-rate more than further improving the already strong desired signal strength. In contrast, when the interfering signals are weak, i.e. $\rho_k \prod_{\ell \in \mathcal{K}} \alpha_{k,\ell} \eta_{k,\ell}^2$ is small, most bits will be assigned to quantize the desired channel more finely in an attempt to improve the desired signal power. Hence, the theorem makes intuitive sense [10].

Case 2: High SNR Regime

In the high SNR regime, $\ln(1+x) = \ln(x) + \mathcal{O}(1/x)$. Using $\ln(1+x) \approx \ln(x)$ for $x >> 1$, we can approximate $\Delta_{R,k}(B_k)$ in (4.20) by $\Delta_{R,k}^{\text{HS}}(B_k)$ given as

$$\begin{aligned}\Delta_{R,k}^{\text{HS}}(B_k) := \log_2(e)\Gamma\left(\frac{N_t}{N_t-1}\right)2^{-\frac{B_k}{N_t-1}} + \log_2\Bigg(\rho_k \sum_{\substack{\ell=1 \\ \ell\neq k}}^{K} \alpha_{k,\ell}\left(1-\eta_{k,\ell}^2\right) \\ +\rho_k\Gamma\left(\frac{2N_t-1}{N_t-1}\right)2^{-\frac{B_{\text{tot}}-B_k}{(N_t-1)(K-1)}} \prod_{\ell=1}^{K}(\alpha_{k,\ell}\eta_{k,\ell}^2)^{\frac{1}{K-1}}\Bigg).\end{aligned} \tag{4.22}$$

The approximate mean loss in sum-rate in (4.22) can be rewritten as

$$\begin{aligned}-\log_2\left(\rho_k \sum_{\substack{\ell=1 \\ \ell\neq k}}^{K} \alpha_{k,\ell}\left(1-\eta_{k,\ell}^2\right)\right) + \log_2(e)\Gamma\left(\frac{N_t}{N_t-1}\right)2^{-\frac{B_k}{N_t-1}} \\ +\log_2\left(1+\frac{\Gamma\left(\frac{2N_t-1}{N_t-1}\right)2^{\frac{-B_{\text{tot}}}{(N_t-1)(K-1)}}\prod_{\ell=1}^{K}(\alpha_{k,\ell}\eta_{k,\ell}^2)^{\frac{1}{K-1}}}{\sum_{\substack{\ell=1 \\ \ell\neq k}}^{K}\alpha_{k,\ell}\left(1-\eta_{k,\ell}^2\right)}2^{\frac{B_k}{(N_t-1)(K-1)}}\right).\end{aligned} \tag{4.23}$$

The first term can be ignored in the optimization problem since it is independent of B_k. Denoting the ratio before $2^{\frac{B_k}{(N_t-1)(K-1)}}$ inside the logarithm by C_i,

the objective function in (4.23) can be simplified as

$$\log_2(e)\Gamma\left(\frac{N_t}{N_t-1}\right)2^{-\frac{B_k}{N_t-1}}+\log_2\left(1+C_i2^{\frac{B_k}{(N_t-1)(K-1)}}\right). \tag{4.24}$$

Note that C_i will typically be large since the denominator of $\sum_{\substack{\ell=1\\ \ell\neq k}}^{K}\alpha_{k,\ell}\left(1-\eta_{k,\ell}^2\right)$ is very small. For large C_i, $\log_2\left(1+C_i2^{\frac{B_k}{(N_t-1)(K-1)}}\right)\approx\log_2(C_i)+\frac{B_k}{(N_t-1)(K-1)}$, which is a linear (hence, convex) function in B_k. Thus, (4.24) is rewritten as

$$\log_2(e)\Gamma\left(\frac{N_t}{N_t-1}\right)2^{-\frac{B_k}{N_t-1}}+C_i2^{\frac{B_k}{(N_t-1)(K-1)}}. \tag{4.25}$$

The optimal number of bits to minimize (4.25) are given in Theorem 4.4.3.

Theorem 4.4.3. *Given the total number of bits allocated to quantize* all *the channels, B_{tot}, the optimum number of bits assigned to the desired channel at the k^{th} user, B_k, to minimize* (4.25) *is given by*

$$B_k=(N_t-1)\log_2\left((|\mathcal{K}|-1)\Gamma\left(\frac{N_t}{N_t-1}\right)\right).$$

The optimum number of bits assigned to all the interfering channels at the k^{th} user, $B_{k,(\text{i})}=B_{\text{tot}}-B_k$.

Proof. The proof is given in Appendix 4.7.5. □

It is seen from Theorem 4.4.3 that B_k and $B_{k,(\text{i})}$ are independent of the SNR, in the high SNR regime. Further, B_k is also independent of the received signal strengths and delays of the interferers. This makes intuitive sense if we take into account that the sum-rate saturates as SNR $\to\infty$. Hence,

minimizing the mean loss in sum-rate at high SNR will be independent of the SNR of the desired (and interfering) channels [10].

The feedback bit assignments in Theorems 4.4.1, 4.4.2, and 4.4.3 are not necessarily integers. One way of getting integer solutions is to check for the ceiling and floor of B_k and $B_{k,\ell}$ due to the convexity of the objective functions in (4.21), (4.25) and (4.19). In (4.21), the objective function is the sum of two non-negatively weighted convex functions, $2^{-\frac{B_k}{N_t-1}}$ and $2^{\frac{B_k}{|\mathcal{K}|(N_t-1)}}$ and hence, is convex. By the same argument, (4.19) is also convex. This is similar to the approach in Chapter 3.

Note that we do not claim an optimal solution for B_k and $B_{k,\ell}$ that will minimize the mean loss in sum-rate in (4.8) (or even (4.17)). Instead, we derive closed-form expressions for feedback-bit partitioning that *reduce* the mean-loss in sum-rate, as shown in Section 4.5.

4.5 Simulation Results

In this section, we present simulation results to demonstrate the gain in the mean per-cell data rate obtained using the proposed adaptive feedback-bit partitioning algorithm, over equal-bit allocation. We consider a seven-cell system with a single active user per cell. Each base station has eight antennas ($N_t = 8$) and each user has a single antenna. For simulation purposes we focus on a target user located in the cell at the center of the seven-cell grid, which receives the desired signal from its own base station and interference from the six neighboring cells as shown in Fig. 4.3 and from base stations out of the

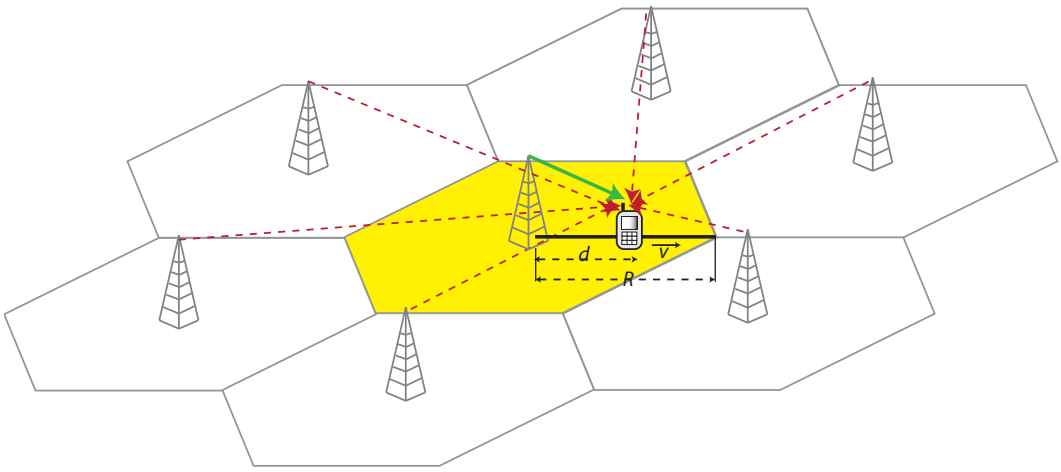

Figure 4.3: The simulation setup in Section 4.5. The base stations are numbered in a clockwise fashion.

seven-cell system. The mobile terminal is assumed to travel in a straight line from the cell center to the cell edge with a velocity v. The distance between the user and the desired base station is given by $d \leq R$. The system setup is based on the urban microcell propagation scenario in the 3GPP spatial channel model [1]. The radius of each cell, R, is assumed to be 400 m. The path loss between the base stations and the mobile user is modeled using the COST 231 Walfish-Ikegami NLOS model [1], adopted for urban microcells. Using a carrier frequency of 1.9 GHz, base station antenna height of 12.5 m, mobile terminal height of 1.5 m, building height 12 m, building to building distance 50 m and street width 25 m, the path-loss in dB, $PL[dB]$, is given by [1] MS antenna height 1.5m

$$PL[dB] = 34.53 + 38 \log_{10}(d) \tag{4.26}$$

Table 4.1: Simulation parameters, based on the 3GPP LTE's urban microcell.

Parameter	**Value**
Number of interferers	6
Carrier frequency, f_c	1.9 GHz
Base station height	12.5 m
Mobile terminal height	1.5 m
Cell radius	400 m
Transmit power, E_s	3 dBW
Noise power, N_0	-144 dBW
Normalized feedback and quantization delay	1
Normalized backhaul delay	1

The transmit power, $E_s = 3$ dBW for all the base stations and the noise power is given by -144 dBW. We also model the delay associated with the feedback of CSI to the desired base station by one frame duration and that with the exchange of CSI over the backhaul link connecting the desired and interfering base stations by two frame durations. The parameters used for simulations are tabulated in Table 4.1.

In Fig. 4.4, we illustrate the concept of effective number of interferers, averaged across 10,000 users located uniformly in the cell with the simulation parameters described in Table 4.1. It is seen that when the number of feedback bits is small, most of the users have a single effective interferer. In contrast, as B_{tot} increases, the percentage of users with a larger number of effective interferers increases. This can be intuitively understood by considering the limiting case of $B_{\text{tot}} \to \infty$, where all the interferers will be allocated feedback bits, implying that the plot will be skewed towards the right hand side.

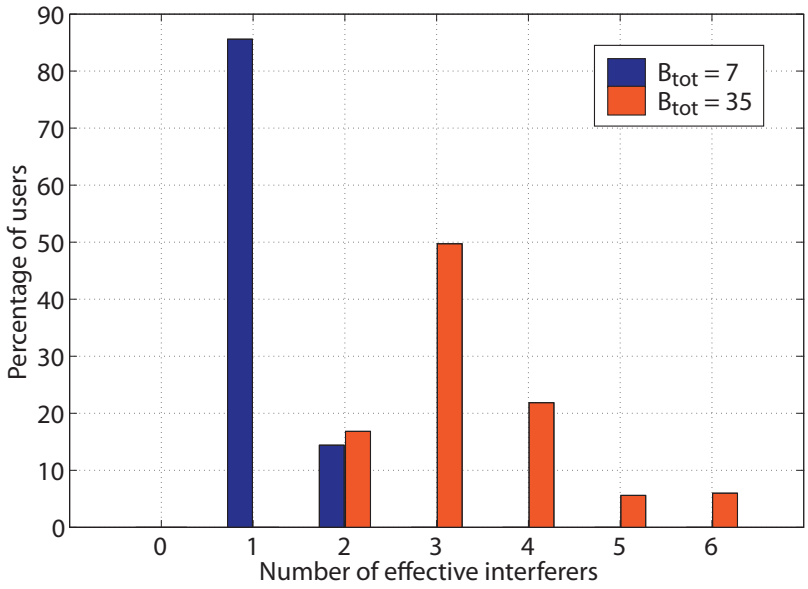

Figure 4.4: Average number of effective number of interferers seen by a user for $B_{\text{tot}} = 7, 35$ and $v = 3$ mph.

In Fig. 4.5, we compare the performance of equi-bit partitioning and the proposed adaptive strategy as a function of the distance from the desired base station. In the figure, we normalize the data rates from the two limited feedback techniques by the full CSI data rate for $B_{\text{tot}} = 7$ and $B_{\text{tot}} = 35$ with $v = 10$ mph. It is seen that the feedback-bit assignment presented in this chapter outperforms equal-bit allocation irrespective of where the user is located. At the cell-edge, adaptive bit assignment achieves about 45% more of the full CSI data rate as compared to uniform allocation.

The bit partitioning corresponding to $B_{\text{tot}} = 35$ are plotted in Figs. 4.6(a) and 4.6(b) as a function of distance for the simulation setup described in Fig. 4.3 and Table 4.1. We consider both the high SNR and low SNR parti-

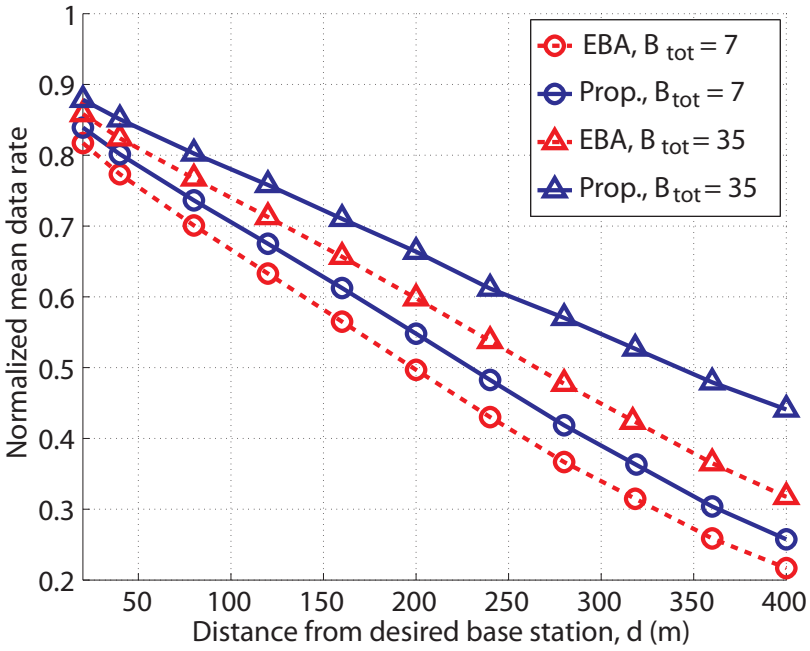

Figure 4.5: Comparison of the normalized data-rate as a function of the distance, d, of the user from the desired base station for $B_{\text{tot}} = 7, 35$ and $v = 10$ mph.

tions by setting $E_s = 3$ dBW and -3 dBW, respectively. The channel from base station j to the user '0' (as shown in Fig. 4.3) is quantized using $B_{0,j}$ bits. In Fig. 4.6(a), it is seen that more bits are assigned to quantize the desired channel towards the cell edge as compared to the low SNR case in Fig. 4.6(b). This makes intuitive sense because at high SNR, the quantization error associated with the desired channel is larger than that at low SNR. Hence, more bits need to be assigned to quantize the desired channel at high SNR. Another interesting point from Figs. 4.6(a) and 4.6(b) is the decrease in the number of bits allocated to the interfering channels from base stations 1, 4, 5 and 6 as the

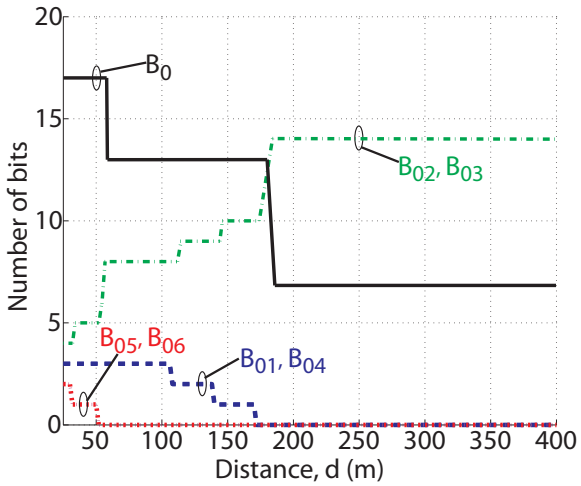

(a) High SNR partitioning, for $E_s = 3$ dBW.

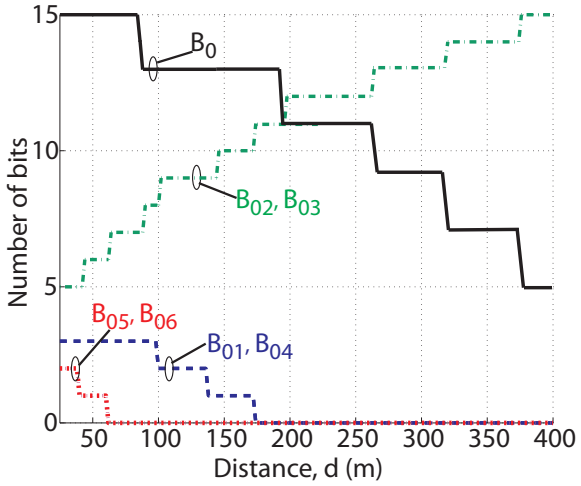

(b) Low SNR partitioning, for $E_s = -3$ dBW.

Figure 4.6: Adaptive feedback-bit partitioning as a function of the distance, d, the user from the desired base station for $B_{\text{tot}} = 35$ and $v = 10$ mph for (a) $E_s = 3dBW$ and (b) $E_s = -3dBW$.

user moves to the cell edge towards cells 2 and 3. This clearly illustrates the adaptive nature of the proposed algorithm, which allocates bits as a function

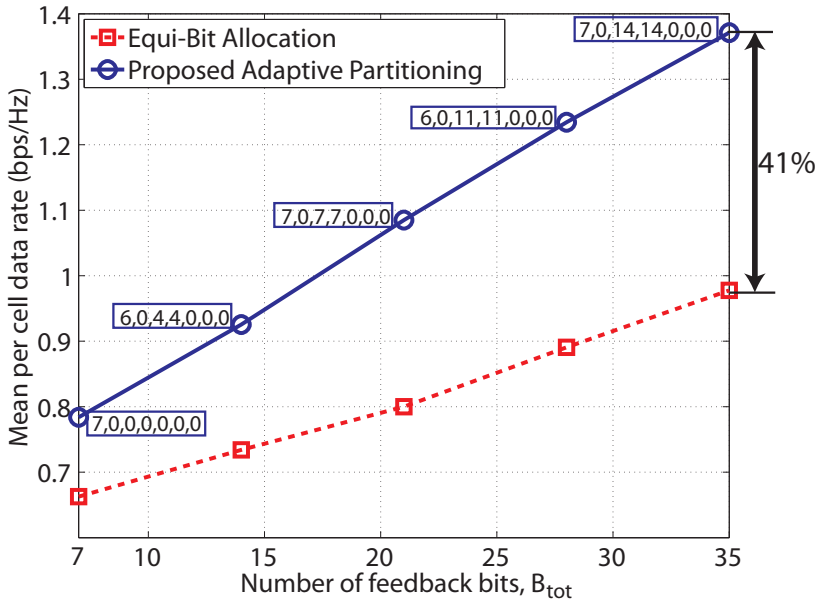

Figure 4.7: Comparison of the mean data-rate at the cell-edge for different values of B_{tot}. Bit assignments are shown corresponding to each B_{tot}.

of the received signal strength and the delays.

We plot the cell-edge data rates using both, equi-bit allocation and the proposed adaptive partitioning, in Fig. 4.7 for the system setup described in this section. Note that at the cell edge, the strongest interference is from BTS 2 and BTS 3, as shown in Fig. 4.3. The corresponding bit assignments, $(B_0, B_{0,1}, B_{0,2}, B_{0,3},\ B_{0,4}, B_{0,5}, B_{0,6})$, are also given in the figure for each B_{tot}. Finally, the effect of delay in the backhaul link is plotted in Fig. 4.8 for a user at cell-edge with $B_{\text{tot}} = 7$ and $B_{\text{tot}} = 35$. We fix the feedback delay, D_k to one frame interval and vary the backhaul delay between $[0, 5]$ frame durations, i.e. $D_{k,\ell} \in [1, 6]$. Similar to Fig. 4.7, it is seen that while the proposed algorithm outperforms equal bit allocation for all the delays and B_{tot} values.

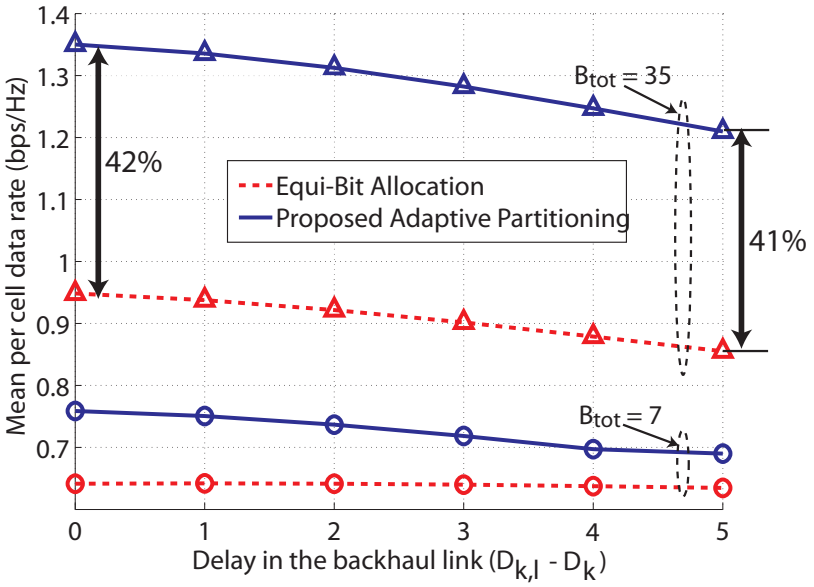

Figure 4.8: Comparison of the mean data-rate at the cell-edge for different values of delay in the backhaul link.

It is seen from both Fig. 4.7 and Fig. 4.8 that while the limited feedback technique in this chapter outperforms EBA for all B_{tot}, the improvement in data rate is larger for higher B_{tot}. The new strategy yields about 40 % higher sum-rates than the equal-bit approach at $B_{\text{tot}} = 35$ in both Fig. 4.7 and Fig. 4.8. This can be explained as follows. At $B_{\text{tot}} = 7$, the desired channel is given all the 7 bits, implying 0 bits for each of the strong interfering channels. For $B_{\text{tot}} = 35$, the strong interfering channels are assigned 14 bits for each of two strong interfering channels. EBA, in contrast, sees an increase in the feedback bits for the strong interfering channels from 1 to 5 bits per channel. Quantizing the strong interferers more finely at the cost of allocating zero bits to the weak channels leads to the significant improvement in data rate using

the proposed algorithm. This leads to a better quantization of the strong interfering channels, leading to a significantly better performance. We can also see from Fig. 4.7 that all the bits are assigned to the desired channel at $B_{\text{tot}} = 7$. The reason is that when the received signal strength for the desired signal is low, the proposed algorithm will first concentrate on improving the desired signal strength through finer quantization, rather than reducing the strength of the interfering signals, which can only be as strong as the desired signal.

4.6 Conclusion

We considered a multicell cooperative MISO system using ICIN. We assumed a single active user per cell, which estimates and feeds back the desired and interfering CSI to its own base station. Backhaul links are used to ensure that each base station has knowledge of the interference that it is causing to neighboring cells. The feedback and backhaul links are assumed to have delays associated with them. In this chapter, we quantified the mean loss in sum-rate due to delayed limited feedback of the desired and interfering CSI, using ICIN. We derived a closed-form expression for allocating feedback bits to quantize the multiple channels. We showed, using simulations, that the proposed algorithm yields higher mean sum-rates as compared to the equal-bit partitioning approach.

4.7 Appendix

4.7.1 Proof of Proposition 4.3.1

To evaluate the sum-rate in (4.7), the relation between $\mathbf{h}_k[n]$ and $\hat{\mathbf{f}}_k[n]$ needs to be known. Since the k^{th} base station uses the delayed quantized desired channel, $\hat{\mathbf{h}}_k[n-D_k]$, to design $\hat{\mathbf{f}}_k[n]$, we first determine the dependence of $\mathbf{h}_k[n]$ and $\hat{\mathbf{h}}_k[n-D_k]$. While the Gauss-Markov model in (4.3) is used to relate $\mathbf{h}_k[n]$ and $\mathbf{h}_k[n-D_k]$, the relationship between $\tilde{\mathbf{h}}_k[n-D_k]$ and $\hat{\mathbf{h}}_k[n-D_k]$ is given by[1][49]

$$\tilde{\mathbf{h}}_k[n-D_k] = \cos(\theta_{\tilde{\mathbf{h}}_k,\hat{\mathbf{h}}_k})\hat{\mathbf{h}}_k[n-D_k] + \sin(\theta_{\tilde{\mathbf{h}}_k,\hat{\mathbf{h}}_k})\mathbf{s}_k[n], \tag{4.27}$$

where $\mathbf{s}_k[n]$ is an isotropically distributed vector in the null-space of $\hat{\mathbf{h}}_k[n-D_k]$, and is independent of $\cos(\theta_{\tilde{\mathbf{h}}_k,\hat{\mathbf{h}}_k})$ (or $\sin(\theta_{\tilde{\mathbf{h}}_k,\hat{\mathbf{h}}_k})$). Substituting (4.27) in (4.3) yields

$$\mathbf{h}_k[n] = \eta_k\|\mathbf{h}_k[n-D_k]\|\left(\cos(\theta_{\tilde{\mathbf{h}}_k,\hat{\mathbf{h}}_k})\hat{\mathbf{h}}_k[n-D_k] + \sin(\theta_{\tilde{\mathbf{h}}_k,\hat{\mathbf{h}}_k})\mathbf{s}_k[n]\right) + \sqrt{1-\eta_k^2}\mathbf{w}_k[n]. \tag{4.28}$$

Computing $|\mathbf{h}_k{}^*[n]\hat{\mathbf{f}}_k[n]|^2$, we have

$$\begin{aligned}|\mathbf{h}_k{}^*[n]\hat{\mathbf{f}}_k[n]|^2 = \Big|\eta_k\|\mathbf{h}_k[n-D_k]\|\Big(&\cos(\theta_{\tilde{\mathbf{h}}_k,\hat{\mathbf{h}}_k})\hat{\mathbf{h}}_k[n-D_k]\hat{\mathbf{f}}_k[n] \\ &+ \sin(\theta_{\tilde{\mathbf{h}}_k,\hat{\mathbf{h}}_k})\mathbf{s}_k[n]\hat{\mathbf{f}}_k[n]\Big) + \sqrt{1-\eta_k^2}\mathbf{w}_k[n]\hat{\mathbf{f}}_k[n]\Big|^2.\end{aligned}$$

Now, $\sin(\theta_{\tilde{\mathbf{h}}_k,\hat{\mathbf{h}}_k}) = \mathcal{O}(\theta_{\tilde{\mathbf{h}}_k,\hat{\mathbf{h}}_k}) \to 0$ when there are a sufficient number of bits for quantization. Further, $\sqrt{1-\eta_k^2} = o(\eta_k) \to 0$ for $\eta_k \to 1$, implying that we can

[1] In the remainder of this proof, we refer to $\cos(\theta_{\tilde{\mathbf{h}}_k[n-D_k],\hat{\mathbf{h}}_k[n-D_k]})$ as $\cos(\theta_{\tilde{\mathbf{h}}_k,\hat{\mathbf{h}}_k})$, and $\sin(\theta_{\tilde{\mathbf{h}}_k[n-D_k],\hat{\mathbf{h}}_k[n-D_k]})$ as $\sin(\theta_{\tilde{\mathbf{h}}_k,\hat{\mathbf{h}}_k})$ for the sake of notational brevity.

neglect $\left|\sqrt{1-\eta_k^2}\mathbf{w}_k[n]\hat{\mathbf{f}}_k[n]\right|^2$. This approximation of neglecting the error term for slowly-varying channels is also used in [102]. Thus, we can approximate $|\mathbf{h}_k{}^*[n]\hat{\mathbf{f}}_k[n]|^2$ by

$$|\mathbf{h}_k{}^*[n]\hat{\mathbf{f}}_k[n]|^2 \approx \eta_k^2\|\mathbf{h}_k[n-D_k]\|^2\cos^2(\theta_{\tilde{\mathbf{h}}_k,\hat{\mathbf{h}}_k})\left|\hat{\mathbf{h}}_k[n-D_k]\hat{\mathbf{f}}_k[n]\right|^2.$$

Hence, the upper bound on $\mathbb{E}\{\log_2(|\mathbf{h}_k{}^*[n]\hat{\mathbf{f}}_k[n]|^2)\}$ can be approximated as

$$\begin{aligned}
&\mathbb{E}\left\{\log_2\left(\eta_k^2\|\mathbf{h}_k[n-D_k]\|^2\cos^2(\theta_{\tilde{\mathbf{h}}_k,\hat{\mathbf{h}}_k})\left|\hat{\mathbf{h}}_k[n-D_k]\hat{\mathbf{f}}_k[n]\right|^2\right)\right\}\\
&=\log_2(\eta_k^2)+\log_2(e)\frac{1}{N_t-1}\sum_{i=1}^{N_t-1}\beta\left(2^{B_k},\frac{i}{N_t-1}\right) \qquad (4.29)\\
&+\mathbb{E}\left\{\log_2\left(\|\mathbf{h}_k[n-D_k]\|^2\left|\hat{\mathbf{h}}_k[n-D_k]\hat{\mathbf{f}}_k[n]\right|^2\right)\right\},
\end{aligned}$$

where (4.29) is obtained using Lemmas 3.4.2 and 3.4.3.

4.7.2 Proof of Proposition 4.3.2

Using (4.4) and similar to (4.28), $\mathbf{g}_{k,\ell}[n]$ is expressed as a function of $\hat{\mathbf{g}}_{k,\ell}[n-D_{k,\ell}]$ as

$$\begin{aligned}
\mathbf{g}_{k,\ell}[n] =&\eta_{k,\ell}\|\mathbf{g}_{k,\ell}[n-D_{k,\ell}]\|\left(\cos(\theta_{\tilde{\mathbf{g}}_{k,\ell},\hat{\mathbf{g}}_{k,\ell}})\hat{\mathbf{g}}_{k,\ell}[n-D_{k,\ell}]\right.\\
&\left.+\sin(\theta_{\tilde{\mathbf{g}}_{k,\ell},\hat{\mathbf{g}}_{k,\ell}})\mathbf{s}_{k,\ell}[n]\right)+\sqrt{1-\eta_{k,\ell}^2}\mathbf{w}_{k,\ell}[n].
\end{aligned}$$

Since $\hat{\mathbf{f}}_\ell[n]$ lies in the null-space of $\hat{\mathbf{g}}_{k,\ell}[n-D_{k,\ell}]$,

$$\begin{aligned}
|\mathbf{g}_{k,\ell}{}^*[n]\hat{\mathbf{f}}_\ell[n]|^2 = &\left|\eta_{k,\ell}\|\mathbf{g}_{k,\ell}[n-D_{k,\ell}]\|\sin(\theta_{\tilde{\mathbf{g}}_{k,\ell},\hat{\mathbf{g}}_{k,\ell}})\mathbf{s}_{k,\ell}[n]\hat{\mathbf{f}}_\ell[n]\right.\\
&\left.+\sqrt{1-\eta_{k,\ell}^2}\mathbf{w}_{k,\ell}[n]\hat{\mathbf{f}}_\ell[n]\right|^2.
\end{aligned}$$

Using the triangle inequality,

$$
\begin{aligned}
|\mathbf{g}_{k,\ell}{}^{*}[n]\hat{\mathbf{f}}_{\ell}[n]|^2 \leq & \Big(\Big|\eta_{k,\ell}\|\mathbf{g}_{k,\ell}[n-D_{k,\ell}]\|\sin(\theta_{\tilde{\mathbf{g}}_{k,\ell},\hat{\mathbf{g}}_{k,\ell}})\mathbf{s}_{k,\ell}[n]\hat{\mathbf{f}}_{\ell}[n]\Big| \\
& + \Big|\sqrt{1-\eta_{k,\ell}^2}\mathbf{w}_{k,\ell}[n]\hat{\mathbf{f}}_{\ell}[n]\Big|\Big)^2 \\
& = \eta_{k,\ell}^2\|\mathbf{g}_{k,\ell}[n-D_{k,\ell}]\|^2\sin^2(\theta_{\tilde{\mathbf{g}}_{k,\ell},\hat{\mathbf{g}}_{k,\ell}})\Big|\mathbf{s}_{k,\ell}[n]\hat{\mathbf{f}}_{\ell}[n]\Big|^2 + \\
& (1-\eta_{k,\ell}^2)\|\mathbf{w}_{k,\ell}[n-D_{k,\ell}]\|^2\Big|\tilde{\mathbf{w}}_{k,\ell}[n]\hat{\mathbf{f}}_{\ell}[n]\Big|^2 + 2\eta_{k,\ell}\|\mathbf{g}_{k,\ell}[n-D_{k,\ell}]\|\cdot \\
& \sin(\theta_{\tilde{\mathbf{g}}_{k,\ell},\hat{\mathbf{g}}_{k,\ell}})\sqrt{1-\eta_{k,\ell}^2}\|\mathbf{w}_{k,\ell}[n-D_{k,\ell}]\|\Big|\mathbf{s}_{k,\ell}[n]\hat{\mathbf{f}}_{\ell}[n]\Big|.\Big|\mathbf{w}_{k,\ell}[n]\hat{\mathbf{f}}_{\ell}[n]\Big|.
\end{aligned}
$$

Evaluating $\mathbb{E}\{|\mathbf{g}_{k,\ell}{}^{*}[n]\hat{\mathbf{f}}_{\ell}[n]|^2\}$ using the relations that $\Big|\mathbf{s}_{k,\ell}[n]\hat{\mathbf{f}}_{\ell}[n]\Big| \leq 1$ and $\Big|\mathbf{w}_{k,\ell}[n]\hat{\mathbf{f}}_{\ell}[n]\Big| \leq 1$,

$$
\begin{aligned}
\mathbb{E}\{|\mathbf{g}_{k,\ell}{}^{*}[n]\hat{\mathbf{f}}_{\ell}[n]|^2\} \leq & \eta_{k,\ell}^2\mathbb{E}\{\|\mathbf{g}_{k,\ell}[n-D_{k,\ell}]\|^2\}\mathbb{E}\{\sin^2(\theta_{\tilde{\mathbf{g}}_{k,\ell},\hat{\mathbf{g}}_{k,\ell}})\}\mathbb{E}\{\Big|\mathbf{s}_{k,\ell}[n]\hat{\mathbf{f}}_{\ell}[n]\Big|^2\} \\
& + (1-\eta_{k,\ell}^2)\mathbb{E}\{\|\mathbf{w}_{k,\ell}[n-D_{k,\ell}]\|^2\}\mathbb{E}\{\Big|\tilde{\mathbf{w}}_{k,\ell}[n]\hat{\mathbf{f}}_{\ell}[n]\Big|^2\} \\
& + 2\eta_{k,\ell}\sqrt{1-\eta_{k,\ell}^2}\mathbb{E}\{\sin(\theta_{\tilde{\mathbf{g}}_{k,\ell},\hat{\mathbf{g}}_{k,\ell}})\}\mathbb{E}\{\|\mathbf{g}_{k,\ell}[n-D_{k,\ell}]\|\}\mathbb{E}\{\|\mathbf{w}_{k,\ell}[n-D_{k,\ell}]\|\}.
\end{aligned} \tag{4.30}
$$

Now, $\mathbb{E}\{\|\mathbf{g}_{k,\ell}[n-D_{k,\ell}]\|^2\} = \mathbb{E}\{\|\mathbf{w}_{k,\ell}[n-D_{k,\ell}]\|^2\} = N_t$. Further, since $\mathbf{s}_{k,\ell}[n]$ and $\hat{\mathbf{f}}_{\ell}[n]$ are both isotropically and independently distributed in the $N_t - 1$ null-space of $\hat{\mathbf{g}}_{k,\ell}[n-D_{k,\ell}]$, $\Big|\mathbf{s}_{k,\ell}[n]\hat{\mathbf{f}}_{\ell}[n]\Big|^2$ is beta distributed as $\beta(1, N_t-2)$ [49]. Similarly, $\tilde{\mathbf{w}}_{k,\ell}[n]$ and and $\hat{\mathbf{f}}_{\ell}[n]$ are both isotropically and independently distributed in the N_t dimensions, implying that $\Big|\tilde{\mathbf{w}}_{k,\ell}[n]\hat{\mathbf{f}}_{\ell}[n]\Big|^2$ is beta distributed as $\beta(1, N_t-1)$. The mean of a beta distribution $\beta(a,b)$ is $\frac{a}{a+b}$. Since $\|\mathbf{g}_{k,\ell}[n-D_{k,\ell}]\|$ and $\|\mathbf{w}_{k,\ell}[n-D_{k,\ell}]\|$ are χ distributed with $2N_t$ degrees of freedom, $\mathbb{E}\{\|\mathbf{g}_{k,\ell}[n-D_{k,\ell}]\|\} = \mathbb{E}\{\|\mathbf{w}_{k,\ell}[n-D_{k,\ell}]\|\} = \frac{\Gamma(N_t+1/2)}{\sqrt{2}\Gamma N_t}$. Using these

results, (4.30) is rewritten as

$$\mathbb{E}\{|\mathbf{g}_{k,\ell}{}^{*}[n]\hat{\mathbf{f}}_{\ell}[n]|^{2}\} \leq \eta_{k,\ell}^{2} 2^{B_{k,\ell}} \beta\left(2^{B_{k,\ell}}, \frac{N_t}{N_t-1}\right)\frac{N_t}{N_t-1} + (1-\eta_{k,\ell}^{2}) + \eta_{k,\ell}\sqrt{1-\eta_{k,\ell}^{2}}\,\mathbb{E}\{\sin(\theta_{\tilde{\mathbf{g}}_{k,\ell},\hat{\mathbf{g}}_{k,\ell}})\}\left(\frac{\Gamma(N_t+1/2)}{\Gamma(N_t)}\right)^{2}. \quad (4.31)$$

The last term in the upper bound of $\mathbb{E}\left\{|\mathbf{g}_{k,\ell}{}^{*}[n]\hat{\mathbf{f}}_{\ell}[n]|^{2}\right\}$ in (4.31) includes the product of $\eta_{k,\ell}(<1)$, $\sqrt{1-\eta_{k,\ell}^{2}}(<<1)$ and $\mathbb{E}\{\sin(\theta_{\tilde{\mathbf{g}}_{k,\ell},\hat{\mathbf{g}}_{k,\ell}})\}(\leq 1)$. Further, as N_t increases, $\frac{\Gamma(N_t+1/2)}{\Gamma(N_t)} \rightarrow 1$. For this reason, the product in (4.31) is small and ignored. The lower-bound in (4.31) is then rewritten as

$$\mathbb{E}\{|\mathbf{g}_{k,\ell}{}^{*}[n]\hat{\mathbf{f}}_{\ell}[n]|^{2}\} \leq \log_2\left(1+\rho_k\sum_{\substack{\ell=1\\ \ell\neq k}}^{K}\alpha_{k,\ell}\left(1-\eta_{k,\ell}^{2}+\eta_{k,\ell}^{2}2^{B_{k,\ell}}\beta\left(2^{B_{k,\ell}},\frac{N_t}{N_t-1}\right)\frac{N_t}{N_t-1}\right)\right).$$

4.7.3 Proof of Theorem 4.7.3

Applying the arithmetic mean - geometric mean inequality to the objective function in (4.19), we get

$$\sum_{\substack{\ell=1\\ \ell\neq k}}^{K}\alpha_{k,\ell}\eta_{k,\ell}^{2}2^{-\frac{B_{k,\ell}}{N_t-1}} \geq (K-1)\left(\prod_{\substack{\ell=1\\ \ell\neq k}}^{K}\alpha_{k,\ell}\eta_{k,\ell}^{2}2^{-\frac{B_{k,\ell}}{N_t-1}}\right)^{\frac{1}{K-1}}, \quad (4.32)$$

where the equality holds for $\alpha_{k,\ell}\eta_{k,\ell}^{2}2^{-\frac{B_{k,\ell}}{N_t-1}} = \alpha_{k,n}\eta_{k,n}^{2}2^{-\frac{B_{k,n}}{N_t-1}}, \ell \neq n$. The minimum value of (4.32) is

$$(K-1)\alpha_{k,\ell}\eta_{k,\ell}^{2}2^{-\frac{B_{k,\ell}}{N_t-1}} = (K-1)\left(2^{\frac{-B_{k,(\mathrm{i})}}{N_t-1}}\prod_{\substack{\ell=1\\ \ell\neq k}}^{K}\alpha_{k,\ell}\eta_{k,\ell}^{2}\right)^{\frac{1}{K-1}}.$$

Solving for $B_{k,\ell}$ gives us

$$B_{k,\ell}{}^{*} = \frac{B_{k,(\mathrm{i})}}{K-1} + (N_t - 1)\log_2\left(\frac{\alpha_{k,\ell}\eta_{k,\ell}^2}{\prod_{\ell=1}^{K}(\alpha_{k,\ell}\eta_{k,\ell}^2)^{\frac{1}{K-1}}}\right). \tag{4.33}$$

Note that (4.33) can be negative when $\alpha_{k,\ell}\eta_{k,\ell}^2$ is sufficiently small. Since $B_{k,\ell}$ can only be non-negative, we set the $B_{k,\ell} = 0$ for all ℓ which cause (4.33) to become negative. This implies that we partition bits among only the effective set of interferers $\mathcal{K}$ that will result in a non-negative value of $B_{k,\ell}$ for all $\ell \in \mathcal{K}$.

4.7.4 Proof of Theorem 4.4.2

By ignoring the terms in (4.21) that do not depend on B_k, the new objective function is given by

$$\begin{aligned}&\log_2(e)\Gamma\left(\frac{N_t}{N_t-1}\right)2^{-\frac{B_k}{N_t-1}}\\ &+\log_2(e)\rho_k(K-1)\Gamma\left(\frac{2N_t-1}{N_t-1}\right)2^{-\frac{B_{\mathrm{tot}}-B_k}{(N_t-1)(K-1)}}\prod_{\substack{\ell=1\\ \ell\neq k}}^{K}(\alpha_{k,\ell}\eta_{k,\ell}^2)^{\frac{1}{K-1}}.\end{aligned} \tag{4.34}$$

The expression in (4.34) can be further simplified by dividing the expression by the constant $\log_2(e)\Gamma\left(\frac{N_t}{N_t-1}\right)$ and denoting

$$C_i = \rho_k\frac{(K-1)N_t}{N_t-1}2^{\frac{-B_{\mathrm{tot}}}{(N_t-1)(K-1)}}\prod_{\substack{\ell=1\\ \ell\neq k}}^{K}(\alpha_{k,\ell}\eta_{k,\ell}^2)^{\frac{1}{K-1}}.$$

This results in the expression

$$2^{-\frac{B_k}{N_t-1}} + C_i 2^{\frac{B_k}{(N_t-1)(K-1)}}.$$

Using the arithmetic mean-geometric mean inequality, we get

$$2^{-\frac{B_k}{N_t-1}} + C_i 2^{\frac{B_k}{(N_t-1)(K-1)}} \geq 2\sqrt{2^{-\frac{B_k}{N_t-1}}\cdot C_i 2^{\frac{B_k}{(N_t-1)(K-1)}}}$$

We can minimize (4.34) (and hence, (4.21)) by solving for B_k that satisfies the equality $2^{-\frac{B_k}{N_t-1}} = C_i 2^{\frac{B_k}{(N_t-1)(K-1)}}$. Hence, the approximate mean loss in sum-rate at low SNR can be minimized by setting B_k as

$$B_k{}^{\mathrm{LS}} = \frac{B_{\mathrm{tot}}}{K} - \frac{(N_t-1)(K-1)}{K}\log_2\left(\rho_k \frac{N_t}{N_t-1}\prod_{\substack{\ell=1\\ \ell\neq k}}^{K}(\alpha_{k,\ell}\eta_{k,\ell}^2)^{\frac{1}{K-1}}\right).$$

4.7.5 Proof of Theorem 4.4.3

From (4.25), we have

$$\log_2(e)\Gamma\left(\frac{N_t}{N_t-1}\right)2^{-\frac{B_k}{N_t-1}} + C_i 2^{\frac{B_k}{(N_t-1)(K-1)}}.$$

Now, $2^{-\frac{B_k}{N_t-1}}$ is a convex functions in B_k. As the sum of non-negatively weighted convex functions is convex, the expression in (4.25) is convex. Hence, there exists a global minimizer for (4.25), $B_k \in [0, B_{\mathrm{tot}}]$. Finding the derivative of the objective function in (4.25) with respect to B_k, we get

$$\frac{-1}{N_t-1}\Gamma\left(\frac{N_t}{N_t-1}\right)2^{-\frac{B_k}{N_t-1}} + \frac{C_i 2^{\frac{B_k}{(N_t-1)(K-1)}}}{1+C_i 2^{\frac{B_k}{(N_t-1)(K-1)}}}\frac{1}{(N_t-1)(K-1)}. \tag{4.35}$$

In (4.25), $\frac{C_i 2^{\frac{B_k}{(N_t-1)(K-1)}}}{1+C_i 2^{\frac{B_k}{(N_t-1)(K-1)}}} \to 1$, as C_i increases. Setting (4.35) to zero, we get,

$$B_k{}^{\mathrm{HS}} = (N_t-1)\log_2\left((K-1)\Gamma\left(\frac{N_t}{N_t-1}\right)\right).$$

Chapter 5

Joint CSI Quantization

This chapter presents joint CSI quantization for multicell cooperative limited feedback, assuming zero-delay communication links. A selection criterion is developed using RVQ [49, 75, 76] to show that joint quantization yields higher sum-rates than those obtained using separate codebooks. Simulations are used to show that the proposed joint quantization approach performs almost as well as the full CSI case.

5.1 Overview and Contributions

Chapters 3 and 4 develop multicell limited feedback strategies that are based on individually quantizing channels with separate codebooks. It was shown in Fig. 4.5 that the proposed adaptive bit partitioning algorithm, while yielding higher data rates as compared to equal-bit allocation, achieves only about 45% of the full CSI data rate with $B_{\text{tot}} = 35$. In this chapter, joint CSI quantization is proposed to reduce the large feedback requirements of multicell cooperative systems and improve data rates [12]. The idea of quantizing the CSI of multiple channels as a *net channel vector* comes from the well known result in vector quantization that jointly quantizing separate components as

a vector can lead to a smaller distortion than individually quantizing each component, even when the entries are independent [27].

The performance of any limited feedback approach is strongly dependent on the *selection criterion*, which determines how codewords are selected from a codebook. In single-CSI quantization, minimizing the angular separation between the measured channel and the quantization vectors is a popular selection criterion [63]. This, however, is not very suitable for selecting codewords for a vector formed by concatenating the CSI of multiple channels. Selecting a codeword with a minimum angular separation from the net channel vector does not guarantee that individual portions of the codeword are well aligned with the corresponding measured channels. Further, as stronger channels are quantized with the same resolution as the weaker ones, feedback resources are not utilized efficiently. A more fitting selection criterion would choose codewords in a way that the portion of the quantization vector corresponding to a stronger channels is more closely aligned than the other channels, as shown in Fig. 5.1 for a single-interferer system. This chapter derives a selection criterion to quantize channels that impact the data rate more significantly with greater resolution as compared to the other channels.

The contributions of this chapter are as follows.

1. A limited feedback model is presented for jointly quantizing the CSI of the desired and (multiple) interfering channels, assuming zero-delay in the communication links. The model requires each user to concatenate

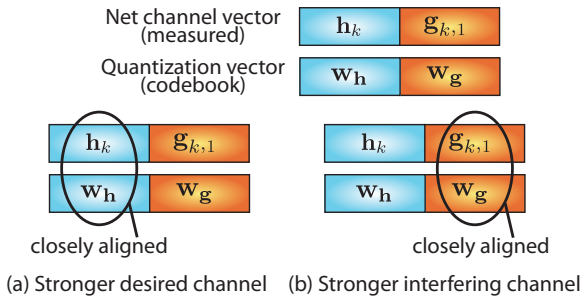

Figure 5.1: Illustration of the selection criterion for joint CSI quantization when (a) the desired channel is stronger and (b) the interfering channel is stronger.

the CSI of multiple channels into a *net channel vector*, which is fed back to its own base station. Portions of the net channel vector, which represent different channels, are fed back to the respective neighboring base stations through backhaul links [12].

2. Joint quantization of CSI raises the question of how codewords are selected from a codebook, since single-CSI criteria like minimum angular separation do not account for varying signal strengths of the different channels. This chapter derives a new selection criterion that can be used for joint quantization of multiple CSI to reduce the loss in sum-rate [12]. The proposed expression chooses codewords that are well aligned to stronger channels, thus quantizing them with higher resolution, as compared to weaker signals. This enables efficient utilization of the available feedback resources.

3. Simulation results are presented to show that the proposed adaptive joint

CSI feedback algorithm yields higher mean sum-rates using ICIN than separate quantization approaches.

5.2 System Description

This chapter uses the system model described in Chapter 4, with zero-delay. This section briefly summarizes the system model and the cooperative strategy, ICIN, before presenting the limited feedback model.

5.2.1 System Model

The multicell system used in this chapter is shown in Fig. 4.1, with the exception that the feedback and backhaul links are assumed to be zero-delay. A single user is considered in each cell, using intra-cell TDMA or a comparable orthogonal strategy. The base stations in each cell have N_t antennas each, while users have a single antenna. Each user faces interference from $K-1$ cells and the ISR of the ℓ^{th} base station to the k^{th} user is given by $\alpha_{k,\ell}$. Similar to the notation in Chapter 4, the desired channel at the n^{th} time instant from the k^{th} base station to the k^{th} user is denoted by $\mathbf{h}_k[n]$ and the interfering channel from the ℓ^{th} base station to the k^{th} user is denoted by $\mathbf{g}_{k,\ell}[n]$.

Since we assume that all the channels have zero-delay associated with them, we ignore the time-index n in this chapter. For the input-output relation in (4.1), the SINR of the k^{th} user at the n^{th} instant is given by

$$\mathsf{SINR}_k = \frac{\rho_k |\mathbf{h}_k^* \mathbf{f}_k|^2}{1 + \sum_{\substack{\ell=1 \\ \ell \neq k}}^{K} \alpha_{k,\ell} \rho_k |\mathbf{g}_{k,\ell}^* \mathbf{f}_\ell|^2},$$

where ρ_k represents the received desired SNR. As in Chapters 3 and 4, base stations are assumed to have perfect knowledge of ρ_k [18, 41, 78]. The sum-rate of all the users within the system is

$$R_s = \sum_k \log_2 \left(1 + \mathsf{SINR}_k\right).$$

The beamforming vectors $\{\mathbf{f}_k\}_{k=1}^K$ are designed using ICIN, described in Chapter 4. The sum-rate, assuming full CSI and zero delay, is given by

$$R_s = \sum_{k=1}^{K} \log_2 \left(1 + |\mathbf{h}_k^* \mathbf{f}_k|^2\right), \tag{5.1}$$

where $\mathbf{f}_k$ is given by (4.5). The denominator is nulled out since the beamforming vector at the ℓ^{th} base station is designed to be lie in the null-space of the $\mathbf{g}_{k,\ell}$.

5.2.2 Limited Feedback Model

Channel directions, denoted by $\tilde{\mathbf{h}}_k := \mathbf{h}_k/\|\mathbf{h}_k\|$ and $\tilde{\mathbf{g}}_{k,\ell} := \mathbf{g}_{k,\ell}/\|\mathbf{g}_{k,\ell}\|$, are concatenated to form a net channel vector, $\mathbf{h}^{\text{net}} = [\tilde{\mathbf{h}}_k^* \ \tilde{\mathbf{g}}_{k,1}^* \ \ldots \ \tilde{\mathbf{g}}_{k,K}^*]$, which is then quantized using a single codebook, $\mathcal{W}$, of size 2^B, where B is the total number of feedback bits available. Note that this is in contrast to the approaches in Chapters 3 and 4, where each channel was quantized individually using a separate codebook. This feedback model is illustrated in Fig. 5.2. The idea is that different portions of each codeword, $\mathbf{w}_n \in \mathcal{W}, n = 1, \ldots, 2^B$, correspond to each of the different channels. Thus, $\mathbf{w}_n(1 : N_t)$ and $\mathbf{w}_n((Nt \cdot i + 1 : N_t \cdot (i+1)), i = 1, \ldots, (K-1)$ are the quantized versions of $\tilde{\mathbf{h}}_k$

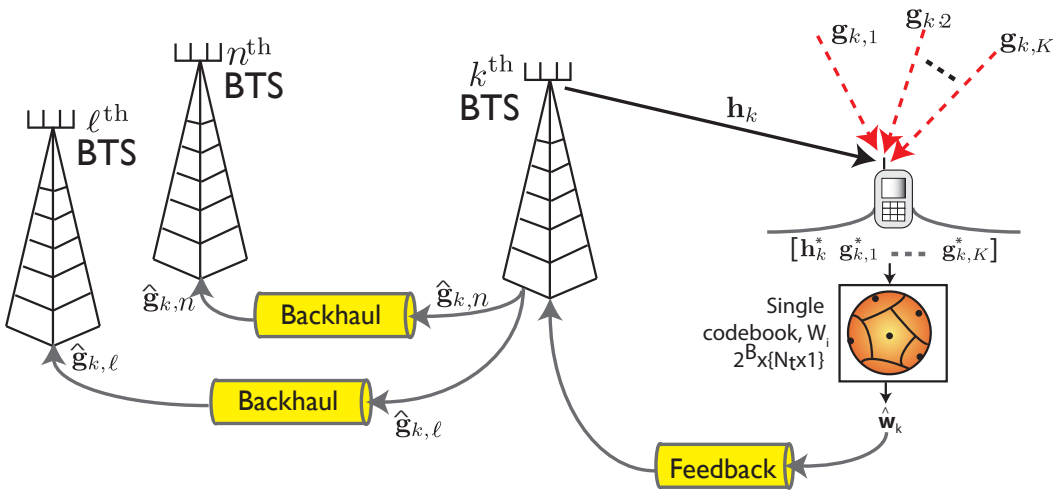

Figure 5.2: The limited feedback model for joint quantization, described in Section 5.2.2.

and $\tilde{\mathbf{g}}_{k,i}$, respectively. The k^{th} base station extracts $\hat{\mathbf{g}}_{k,\ell}$ from the quantized composite channel vector, $\hat{\mathbf{h}}^{\text{net}}$ and uses the backhaul to inform the ℓ^{th} base station of the interference it is causing to the k^{th} user [12].

In separate quantization, stronger channels were quantized using more feedback bits as compared to weaker channels. This enabled an efficient use of feedback bandwidth by diverting resources toward the stronger channels, which affected data rates most drastically. In joint quantization, it is desirable to introduce a bias in quantization, so that stronger channels are quantized more finely, even if the weaker channels have a smaller resolution. This can be accomplished using the selection criterion, which is used to select codewords from a given codebook. The selection criterion in Chapters 3 and 4 chooses codewords to minimize the angular separation between the channel and quantization vectors. This, however, will not introduce the bias towards stronger

channels. This chapter derives a new selection criterion for jointly quantizing the CSI of multiple channels, to reduce the loss in data-rate from limited feedback.

5.3 Impact of Delayed Limited Feedback

Assuming zero-delay feedback and backhaul links, the beamforming vector at the k^{th} base station, $\hat{\mathbf{f}}_k$, is designed using the quantized CSI of the desired channels and the interference caused to other cells

$$\hat{\mathbf{f}}_k = \hat{\mathbf{W}}_k(:,1), \text{ where } \hat{\mathbf{W}}_{\text{k}} = \left[\hat{\mathbf{h}}_{\text{k}}\ \hat{\mathbf{g}}_{1,\text{k}}\ \ldots\ \hat{\mathbf{g}}_{\text{K,k}}\right]^{\dagger}.$$

When $N_t \geq K$, the beamforming vector lies in the $N_t-(K-1)$ null-space of the $K-1$ interfering channels. Hence, when $N_t = K$, $\hat{\mathbf{f}}_k$ lies in a one-dimensional subspace, independent of $\hat{\mathbf{h}}_k$, making it unnecessary to feedback $\hat{\mathbf{h}}_k$. This chapter considers the more general case of $N_t > K$, where $\hat{\mathbf{h}}_k$ is required at the base station using the clustering argument mentioned in Chapter 4. The sum-rate, assuming limited feedback, is given by

$$\hat{R}_s = \sum_{k=1}^{K} \log_2 \left(1 + \frac{\rho_k |\mathbf{h}_k^* \hat{\mathbf{f}}_k|^2}{1 + \sum_{\substack{\ell=1 \\ \ell \neq k}}^{K} \alpha_{k,\ell} \rho_k |\mathbf{g}_{k,\ell}^* \hat{\mathbf{f}}_\ell|^2} \right), \tag{5.2}$$

where the denominator is non-zero since the beamforming vector is orthogonal to $\hat{\mathbf{g}}_{k,\ell}$ and not $\tilde{\mathbf{g}}_{k,\ell}$. This results in a loss in the sum-rate.

5.3.1 Selection Criterion

In this section, a selection criterion is derived to choose codewords that will reduce the loss in sum-rate, using RVQ. Each of the 2^B codeword vectors

in the codebook is independently chosen from the isotropic distribution on the N_t dimensional unit hypersphere [76]. RVQ is used for analytical tractability. We denote $\mathbf{w}(1:N_t) = \mathbf{w}_{\mathbf{h}_k}$ and $\mathbf{w}_n(N_t \cdot i + 1 : N_t \cdot (i+1)) = \mathbf{w}_{\mathbf{g}_{k,i}}$.

The *instantaneous* loss in data-rate arising due to quantization of CSI is given by

$$\Delta R_s := R_s - \hat{R}_s, \tag{5.3}$$

where R_s and $\hat{R}_s$ are given by (5.1) and (5.2), respectively. The expression in (5.3) can be approximated, using the high SINR approximation, as

$$\begin{aligned}\Delta R_s &\approx \sum_{k=1}^{K} \log_2\left(\rho_k |\mathbf{h}_k^* \mathbf{f}_k|^2\right) - \log_2\left(\frac{\rho_k |\mathbf{h}_k^* \hat{\mathbf{f}}_k|^2}{1 + \sum_{\substack{\ell=1 \\ \ell \neq k}}^{K} \alpha_{k,\ell} \rho_k |\mathbf{g}_{k,\ell}^* \hat{\mathbf{f}}_\ell|^2}\right) \\ &= \sum_{k=1}^{K} \log_2\left(\frac{|\tilde{\mathbf{h}}_k^* \mathbf{f}_k|^2}{|\tilde{\mathbf{h}}_k^* \hat{\mathbf{f}}_k|^2}\right) + \log_2\left(1 + \sum_{\substack{\ell=1 \\ \ell \neq k}}^{K} \alpha_{k,\ell} \rho_k |\mathbf{g}_{k,\ell}^* \hat{\mathbf{f}}_\ell|^2\right), \end{aligned} \tag{5.4}$$

where (5.4) is obtained by interchanging terms and using $\mathbf{h}_k = \|\mathbf{h}_k\| \tilde{\mathbf{h}}_k$ [12]. From (3.17), it can be shown that

$$\begin{aligned}\log_2\left(\frac{|\tilde{\mathbf{h}}_k^* \mathbf{f}_k|^2}{|\tilde{\mathbf{h}}_k^* \hat{\mathbf{f}}_k|^2}\right) &\leq \log_2\left(\frac{|\tilde{\mathbf{h}}_k^* \mathbf{f}_k|^2}{|\tilde{\mathbf{h}}_k^* \mathbf{w}_{\mathbf{h}_k}|^2 |\hat{\mathbf{h}}^* \hat{\mathbf{f}}|^2}\right), \\ &= \log_2\left(\frac{|\tilde{\mathbf{h}}_k^* \mathbf{f}_k|^2}{|\hat{\mathbf{h}}^* \hat{\mathbf{f}}|^2}\right) - \log_2\left(|\tilde{\mathbf{h}}_k^* \mathbf{w}_{\mathbf{h}_k}|^2\right). \end{aligned} \tag{5.5}$$

The loss in sum-rate due to the quantization of interfering CSI in (5.4) is upper

bounded by

$$\log_2\left(1+\sum_{\substack{\ell=1\\ \ell\neq k}}^{K}\alpha_{k,\ell}\rho_k\|\mathbf{g}_{k,\ell}{}^*\hat{\mathbf{f}}_\ell|^2\right)=\log_2\left(1+\sum_{\substack{\ell=1\\ \ell\neq k}}^{K}\alpha_{k,\ell}\rho_k\|\mathbf{g}_{k,\ell}\|^2|\tilde{\mathbf{g}}_{k,\ell}^*\hat{\mathbf{f}}_\ell|^2\right)$$

$$\leq\log_2\left(1+\sum_{\substack{\ell=1\\ \ell\neq k}}^{K}\alpha_{k,\ell}\rho_k\|\mathbf{g}_{k,\ell}\|^2(1-|\tilde{\mathbf{g}}_{k,\ell}^*\mathbf{w}_{\mathbf{g}_{k,\ell}}|^2)\right), \tag{5.6}$$

where (5.6) is obtained using the upper bound derived in (3.33). Now, from (3.18), it is also known that $\mathbb{E}\left\{\log_2(|\tilde{\mathbf{h}}^*\mathbf{f}_{\text{full}}|^2)\right\}=\mathbb{E}\left\{\log_2(|\hat{\mathbf{h}}^*\hat{\mathbf{f}}|^2)\right\}$, implying that the first term in (5.5) can be ignored when the selection criterion is used for reducing the mean loss in sum-rate [12]. Thus, codewords can be chosen to minimize

$$\log_2\left(1+\sum_{\substack{\ell=1\\ \ell\neq k}}^{K}\alpha_{k,\ell}\rho_k\|\mathbf{g}_{k,\ell}\|^2(1-|\tilde{\mathbf{g}}_{k,\ell}^*\mathbf{w}_{\mathbf{g}_{k,\ell}}|^2)\right)-\log_2\left(|\tilde{\mathbf{h}}_k^*\mathbf{w}_{\mathbf{h}_k}|^2\right).$$

Using the monotonicity of the logarithm and fact that minimizing an expression is equivalent to maximizing its negative, the selection criterion is written as

$$\hat{\mathbf{w}}_k=\arg\max_{\mathbf{w}\in\mathcal{W}}\frac{|\tilde{\mathbf{h}}_k^*\mathbf{w}_{\mathbf{h}_k}|^2}{1+\sum_{\substack{\ell=1\\ \ell\neq k}}^{K}\alpha_{k,\ell}\rho_k\|\mathbf{g}_{k,\ell}\|^2(1-|\tilde{\mathbf{g}}_{k,\ell}^*\mathbf{w}_{\mathbf{g}_{k,\ell}}|^2)}. \tag{5.7}$$

Note that in the case where $\alpha_{k,\ell}=0$ for all $\ell\neq k$, the expression in (5.7) boils down to choosing the codeword that is at the smallest angular separation with respect to the desired channel, $\mathbf{h}_k$. Thus, the derived selection criterion ensures that codewords are selected to be closely aligned to the stronger channels, thereby quantizing them with a finer resolution as compared the weaker

channels [12]. This makes intuitive sense. Simulation results show that biasing the selection criterion towards stronger channels yields higher data rates than separate quantization approaches.

A disadvantage of joint quantization is that it requires the design of special codebooks, which are a function of the signal strengths of the various interfering channels, to obtain maximum performance gains. This poses not only a design problem, but also implies that a large number of codebooks need to be stored at the mobile and the base station for obtaining the gains of joint quantization. This is one of the reasons why separate quantization is better suited for the current state-of-art, even though it yields smaller data rates.

5.4 Simulation Results

In this section, it is shown that joint quantization, used in conjunction with the proposed selection criterion, reduces the mean loss in data rate due to quantization. The simulation setup in Section 4.5 is adopted in this chapter. A seven-cell system is assumed with a single active user per cell. Each base station has $N_t = 8$ antennas while each user has a single antenna. The mobile terminal is assumed to move from the cell center towards the cell-edge with a velocity v. In particular, three different velocities, $v = \{3, 10, 30\}$ mph are used for simulation purposes. The cell at the center of the grid is considered, whose user receives the desired signal from its own base station and interference from the six neighboring cells as shown in Fig. 4.3. The radius of each cell, R, is assumed to be 500 m (Chapter 4 considered a radius of 400 m). The path loss

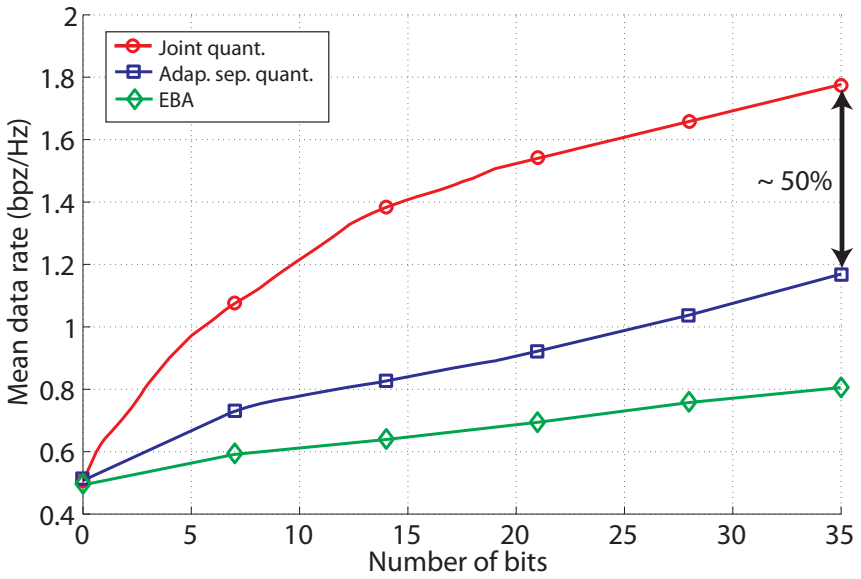

Figure 5.3: Comparison of the mean data rates joint and separate quantization approaches as a function of the total number of bits.

between the base stations and the mobile user is modeled using the COST 231 Walfish-Ikegami NLOS model [1], adopted for urban microcells, and is given in (4.26). The transmit power is $E_s = 3$ dBW for all the base stations and the noise power is given by -144 dBW. The delay associated with the feedback of CSI to the desired base station is modeled by one frame duration and that with the exchange of CSI over the backhaul link connecting the desired and interfering base stations by two frame durations. The simulation parameters are summarized in Table 4.1, except for the delay, which is set to zero.

The data rates obtained using joint quantization with the proposed selection criterion are compared to that of the adaptive bit partitioning approach in Chapter 4 and equal bit allocation (EBA) in Fig. 5.3 for a cell-edge

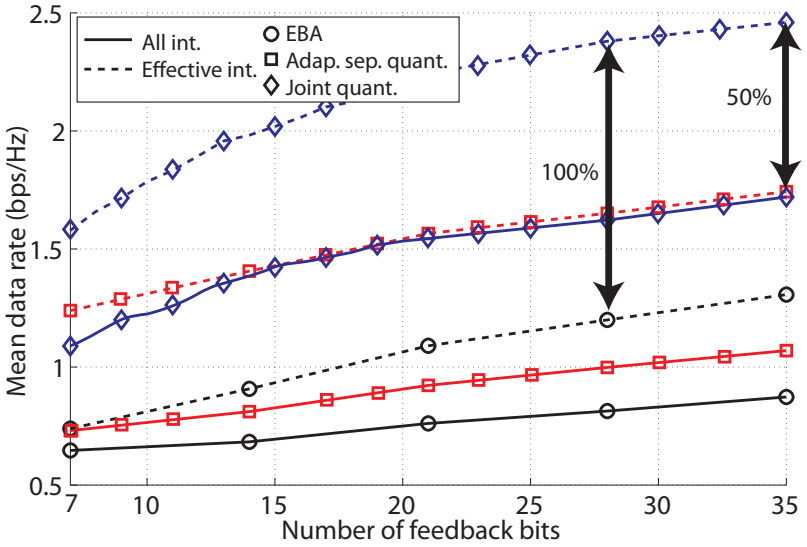

Figure 5.4: Comparison of the mean data-rate at the cell-edge when beamforming using only effective interferers.

user moving at a velocity $v = 3$ mph. Joint quantization is shown to perform about 50% better than separate quantization, which outperforms EBA considerably. This figure illustrates the potential gains that can be obtained using joint quantization.

Finally, in Fig. 5.4, we show that significant gains in the data rates can be obtained by mitigating only the effective interferers, as defined in Theorem 4.4.1. The user is assumed to be located close to the cell-edge. Since the total number of interferers in the system is greater than or equal to the number of effective interferers, i.e. $K \geq |\mathcal{K}|$, beamforming to mitigate only the effective set of interferers will increase the degrees of freedom from $N_t - K + 1$ to $N_t - |\mathcal{K}| + 1$. This improves the data rates that can be obtained using ICIN.

This effect is especially evident for joint quantization, which yields a gain of about 50% compared to adaptive separate quantization (proposed in Chapter 4). When beamforming is done with just the effective interferers, joint quantization results double the data rates obtained using EBA.

5.5 Conclusion

In this chapter, we considered limited feedback for multicell MISO systems using joint quantization. We proposed jointly quantizing the desired and interfering channels [12] as a composite vector to yield sum-rates higher than the separate quantization approaches in previous c . We derived a new selection criterion to minimize the loss in sum-rate of a multicell system. Using simulations, we showed that joint quantization of the desired and interfering channels using RVQ yields sum-rates that are not only higher than the separate codebook approach, but also reasonably close to the full-CSI case with sufficient number of feedback bits. This is a strong motivation for joint quantization of the desired and interfering channels.

Chapter 6

Joint Predictive Vector Quantization

Chapters 3 and 4 present separate quantization as a solution for limited CSI feedback in multicell cooperative systems, while joint CSI quantization is introduced in Chapter 5. While the proposed algorithms outperform equal-bit allocation, they suffer from large feedback requirements. This chapter presents joint predictive vector quantization (PVQ) as a solution for reducing the feedback requirements associated with multicell systems in slowly fading environments by exploiting the temporal correlation in channels. Note that previous chapters were based on memoryless quantization approaches. Simulation results are used to verify that substantial gains in the data rates can be obtained with low feedback requirements using the proposed technique. The drawbacks of joint PVQ strategy, however, are that it is of very high complexity and requires special codebook designs to achieve performance gains.

6.1 Overview and Contributions

PVQ is used for data compression in speech and image processing, where signal correlation can be exploited to reduce distortion in the quantization process [27, 31, 32]. PVQ can also offer a solution for limited feedback

in wireless communication systems. In slow fading propagation environments, channels exhibit temporal correlation, which can be utilized to decrease the feedback requirements and improve data rates [43, 44, 57, 81, 86, 93]. In multicell cooperative systems where high resolution CSI of multiple channels is essential to realizing performance gains, predictive CSI quantization offers an attractive solution to decrease the large feedback requirements. Grassmann predictive coding is an attractive solution for limited CSI feedback. In the presence of temporal correlation, the unit-norm and phase-invariant (channel) vectors form a correlated sequence on the manifold [43, 44, 63, 71]. Existing literature on PVQ is applicable to single-cell non-cooperative systems.

This dissertation proposes a novel approach to employ PVQ for limited CSI feedback in a multicell cooperative system with multiple interferers and non-zero delays. Extending existing single-CSI predictive quantization to multicell limited feedback poses the question of how to feedback the error vectors generated from the predictive CSI quantization of each of the multiple channels. Joint quantization is employed in this chapter to feedback the error vectors generated for each channel. Since realistic cellular networks are associated with delays, it is not clear how available feedback resources should be shared among the different error vectors in a predictive setting. The selection criterion derived for the joint CSI feedback technique in Chapter 5 chooses codewords using instantaneous CSI. In prediction-based systems with delay, however, the error vector will reach the base station after a delay and will impact the prediction of future channel realizations. Hence, the selection cri-

terion derived in Chapter 5 is not applicable to joint PVQ. This chapter derives a new selection criterion that can be used for practical systems with delays and multiple interferers. This chapter presents an approach to predict CSI on the Grassmann manifold using the mathematical tools derived in [43], [71], and [23]. While GPC in [43, 44] feeds back the norm and direction of the tangent vector, the proposed strategy feeds back only the unit-norm direction of the error vector between the tangent vectors. By eliminating the overhead associated with feeding back the norm of the error vectors, the presented algorithm reduces feedback requirements.

The contributions of this chapter are as follows.

1. A limited feedback model is presented for predictive vector quantization in a multicell cooperative scenario, with multiple interferers and delay in feedback and backhaul links [11]. Prediction and quantization operations are described at the receiver and transmitter sides for the proposed framework.

2. The error vectors resulting from predicting the multiple channels are proposed to be jointly fed back as a net error vector. This is known as *joint error quantization* and is shown to result in smaller feedback requirements in the multicell cooperative case.

3. A selection criterion is derived to choose appropriate codewords from a given codebook to quantize the concatenated error vector, such that

stronger channels are quantized with higher resolution than the weaker channels [11].

4. A predictor is proposed for subspace tracking on the Grassmann manifold, which quantizes only the unit-norm direction of the error between the predicted and actual tangent vectors. A linear predictor is also given for comparison purposes. An approach to quantize only the unit-norm channel direction is also presented in this chapter [11]. This is shown to reduce the considerable feedback requirements associated with feeding back norms of multiple error vectors.

5. It is shown using simulations that the proposed predictive quantization approach can yield an improvement in the sum-rate as compared to the separate and joint quantization approaches in [12] and [10], respectively.

6.2 System Description

This section briefly summarizes the notation introduced in Section 3.2.1 (and Table 3.1) and presents some chapter-specific terminology. ICIN with prediction is then described. The limited feedback setup is also presented.

6.2.1 System Model

The K-cell setup used in Section 4.2 (and Fig. 4.1) is adopted in this chapter as well. A single active user is assumed per cell, which faces interference from $K-1$ neighboring cells. Each base station is assumed to have

N_t antennas, while each user has a single antenna. The desired channel at the k^{th} user at the n^{th} time instant is given by $\mathbf{h}_k[n]$. The interfering channel from the ℓ^{th} base station to the k^{th} user is denoted as $\mathbf{g}_{k,\ell}[n]$. The unit-norm channel directions of the desired and interfering channels are denoted as $\tilde{\mathbf{h}}_k[n]$ and $\tilde{\mathbf{g}}_{k,\ell}[n]$, respectively. The delays corresponding to the k^{th} user's feedback link is given by D_k and the delay associated with the ℓ^{th} interfering channel is denoted by $D_{k,\ell}$. In this chapter we assume that $D_{k,\ell} = \overline{D}_k$, $\forall \ell \neq k$, i.e, that the delays corresponding to the interference channels faced by the k^{th} receiver are all equal. This is a reasonable assumption since it implies that the delays over the backhaul links connecting neighboring base stations are equal.

Each user faces interference from $K-1$ cells and the ISR of the ℓ^{th} base station to the k^{th} user is given by $\alpha_{k,\ell}$, where $\ell = 1, \ldots, K$, $\ell \neq k$. For the input-output relation in (4.1), the SINR of the k^{th} user at the n^{th} instant is given by

$$\mathsf{SINR}_k[n] = \frac{\rho_k |\mathbf{h}_k^*[n]\mathbf{f}_k[n]|^2}{1 + \sum_{\substack{\ell=1 \\ \ell \neq k}}^{K} \alpha_{k,\ell}\rho_k |\mathbf{g}_{k,\ell}^*[n]\mathbf{f}_\ell[n]|^2}.$$

The sum-rate of all the users within the system is

$$R_s[n] = \sum_k \log_2 \left(1 + \mathsf{SINR}_k[n]\right).$$

The beamforming vectors $\{\mathbf{f}_k\}_{k=1}^K$ are designed using ICIN, as will be described in Section 6.2.2.

6.2.2 Limited Feedback Model

At time instant n, the k^{th} receiver has knowledge of its own desired channel, $\mathbf{h}_k[m], m \leq n$, and of the interference seen from neighboring cells, i.e. $\mathbf{g}_{k,\ell}[n], m \leq n$. These *previous full CSI* estimates can be used to predict the channels $\mathbf{h}_k^{\text{p,full}}[n + D_k]$ and $\mathbf{g}_{k,\ell}^{\text{p,full}}[n + \overline{D}_k]$, as

$$\mathbf{h}_k^{\text{p,full}}[n + D_k] = \mathsf{P}\left(\mathbf{h}_k[n + D_k] \middle| \{\mathbf{h}_k[n - m]\}_{m=0}^{r-1}\right) \tag{6.1}$$

$$\mathbf{g}_{k,\ell}^{\text{p,full}}[n + \overline{D}_\ell] = \mathsf{P}\left(\mathbf{g}_{k,\ell}[n + \overline{D}_\ell] \middle| \{\mathbf{g}_{k,\ell}[n - m]\}_{m=0}^{r-1}\right), \tag{6.2}$$

where $\mathsf{P}\left(\mathbf{x}[n] \middle| \{\mathbf{x}[n - m]\}_{m=0}^{r-1}\right)$ refers to the predictor used to predict $\mathbf{x}$ at time instant n given the previous samples, $\mathbf{x}[n - D], \ldots, \mathbf{x}[n - D - r + 1]$ and r is prediction order. The base station, however, does not have access to full CSI and has knowledge of only the previous reconstructed (quantized) channels. Hence, the base station predicts CSI using reconstructed in place of full CSI as

$$\mathbf{h}_k^{\text{p}}[n] = \mathsf{P}\left(\mathbf{h}_k[n + D_k] \middle| \{\mathbf{h}_k^{\text{r}}[n - m]\}_{m=0}^{r-1}\right) \tag{6.3}$$

$$\mathbf{g}_{k,\ell}^{\text{p}}[n] = \mathsf{P}\left(\mathbf{g}_{k,\ell}[n + \overline{D}_\ell] \middle| \left\{\mathbf{g}_{k,\ell}^{\text{r}}[n - m]\right\}_{m=0}^{r-1}\right), \tag{6.4}$$

where where $\mathbf{h}_k^{\text{r}}$ and $\mathbf{g}_{k,\ell}^{\text{r}}$ refer to the *reconstructed channels* that are generated using the quantized error information. Note the difference between ${\mathbf{h}_k}^{\text{p}}[n]$ (${\mathbf{g}_{k,\ell}}^{\text{p}}[n]$) and $\mathbf{h}_k^{\text{p,full}}[n]$ ($\mathbf{g}_{k,\ell}^{\text{p,full}}[n]$), which refers to the CSI predicted at time n *using past full CSI*. The receiver generates predicted channels using reconstructed vectors and informs the base station of the error between ${\mathbf{h}_k}^{\text{p}}[n]$ (${\mathbf{g}_{k,\ell}}^{\text{p}}[n]$) and $\mathbf{h}_k^{\text{p,full}}[n]$ ($\mathbf{g}_{k,\ell}^{\text{p,full}}[n]$) in an attempt to drive the transmitter towards

the full CSI prediction. The error vectors between the actual and predicted channels are generated as

$$\mathbf{e}_{\mathbf{h}_k}[n] = \mathsf{E}(\mathbf{h}_k^{\mathrm{p,full}}[n], \mathbf{h}_k^{\mathrm{p}}[n]), \text{ and}$$
$$\mathbf{e}_{\mathbf{g}_{k,\ell}}[n] = \mathsf{E}(\mathbf{g}_{k,\ell}^{\mathrm{p,full}}[n], \mathbf{g}_{k,\ell}^{\mathrm{p}}[n]).$$

Since $\mathbf{e}_{\mathbf{h}_k}[n]$ and $\mathbf{e}_{\mathbf{g}_{k,\ell}}[n]$ are propagated over a finite-bandwidth feedback link, they are quantized to unit-norm quantization vectors, $\hat{\mathbf{e}}_{\mathbf{h}_k}[n]$ and $\hat{\mathbf{e}}_{\mathbf{g}_{k,\ell}}[n]$, respectively. The reconstructed channels, $\mathbf{h}_k^{\mathrm{r}}[n]$ and $\mathbf{g}_{k,\ell}^{\mathrm{r}}[n]$, are generated using $\hat{\mathbf{e}}_{\mathbf{h}_k}[n]$ and $\hat{\mathbf{e}}_{\mathbf{g}_{k,\ell}}[n]$, respectively, as

$$\mathbf{h}_k^{\mathrm{r}}[n] = \mathsf{R}(\mathbf{h}_k^{\mathrm{p}}[n], \hat{\mathbf{e}}_{\mathbf{h}_k}[n]), \text{ and} \tag{6.5}$$
$$\mathbf{g}_{k,\ell}^{\mathrm{r}}[n] = \mathsf{R}(\mathbf{g}_{k,\ell}^{\mathrm{p}}[n], \hat{\mathbf{e}}_{\mathbf{g}_{k,\ell}}[n]), \tag{6.6}$$

where R refers to the reconstruction operation. At time instant n, the k^{th} base station receives the quantized error vectors, $\hat{\mathbf{e}}_{\mathbf{h}_k}[n - D_k]$ transmitted by the k^{th} user at time instant $n - D_k$ and $\hat{\mathbf{e}}_{\mathbf{g}_{\ell,k}}[n - \overline{D}_\ell]$ from the ℓ^{th} base station.

To summarize, at time n, the base station has knowledge of the reconstructed deisred channels $\mathbf{h}_k^{\mathrm{r}}[n - i]$, for $i < D_k$, which is used to predict $\mathbf{h}_k^{\mathrm{p}}[n - D_k]$, using (6.3). The regenerated channel vector at the $n - D_k$ instant, $\mathbf{h}_k^{\mathrm{r}}[n - D_k]$, is obtained at the k^{th} base station using $\mathbf{h}_k^{\mathrm{p}}[n - D_k]$ and $\hat{\mathbf{e}}_{\mathbf{h}_k}[n - D_k]$ (refer to (6.5)). The predicted desired channel vector at the n^{th} instant, $\mathbf{h}_k^{\mathrm{p}}[n]$, is then generated using $\mathbf{h}_k^{\mathrm{r}}[n - i]$, for $i \leq D_k$ using (6.3). In a similar fashion, the k^{th} base station uses $\mathbf{g}_{\ell,k}^{\mathrm{r}}[n - \overline{D}_\ell]$, for $\ell = 1, \ldots, K, \ell \neq K$ to generate $\mathbf{g}_{\ell,k}^{\mathrm{p}}[n]$ [11].

6.2.2.1 Predictive ICIN

In Chapter 4, outdated CSI, $\tilde{\mathbf{h}}_k[n-D_k]$ and $\tilde{\mathbf{g}}_{k,\ell}[n-D_{k,\ell}]$, was used to generate ICIN beamforming vectors [10]. In *predictive ICIN*, the beamforming vector at the k^{th} base station at the n^{th} time instant designed to null out the predicted interference caused to users in other base stations, $\mathbf{f}_k^{\text{p}}[n]$, is given by [51, 62, 99]

$$\mathbf{f}_k^{\text{p}}[n] = \frac{\mathbf{W}_k^p[n](:,1)}{||\mathbf{W}_k^p[n](:,1)||}, \text{ where } \mathbf{W}_{\text{k}}^{\text{p}}[\text{n}] = \left(\left[\mathbf{h}_{\text{k}}^{\text{p}}[\text{n}]\ \mathbf{g}_{1,\text{k}}^{\text{p}}[\text{n}]\ \ldots\ \mathbf{g}_{\text{C,k}}^{\text{p}}[\text{n}]\right]\right)^{\dagger}. \quad (6.7)$$

When full (but delayed) CSI is available at the base stations, $\mathbf{h}_k^{\text{p,full}}[n]$ and $\mathbf{g}_{k,\ell}^{\text{p,full}}[n]$, are used to design beamformers. This best-case scenario beamforming vector, $\mathbf{f}_k[n]$ is obtained as

$$\mathbf{f}_k[n] = \frac{\mathbf{W}_k[n](:,1)}{||\mathbf{W}_k[n](:,1)||}, \text{ where } \mathbf{W}_{\ell}[\text{n}] = \left(\left[\mathbf{h}_{\text{k}}^{\text{p,full}}[\text{n}]\ \mathbf{g}_{1,\text{k}}^{\text{p,full}}[\text{n}]\ \ldots\ \mathbf{g}_{\text{C,k}}^{\text{p,full}}[\text{n}]\right]\right)^{\dagger}. \quad (6.8)$$

The users' objective is to help steer the base station towards $\mathbf{f}_k[n]$ by quantizing the error between $\mathbf{h}_k{}^{\text{p}}[n]$ ($\mathbf{g}_{k,\ell}{}^{\text{p}}[n]$) and $\mathbf{h}_k^{\text{p,full}}[n]$ ($\mathbf{g}_{k,\ell}^{\text{p,full}}[n]$).

6.3 Impact of Delayed Limited Feedback with PVQ

At high SINR, $\log(1+\mathsf{SINR}) = \log(\mathsf{SINR}) + \mathcal{O}(1/\mathsf{SINR})$. At high SINR, $\mathcal{O}(1/\mathsf{SINR}) \to 0$, and can be ignored, thus $\log(1+\mathsf{SINR}) \approx \log(\mathsf{SINR})$. In the remainder of the chapter, we deal with the first term, i.e. $\log(\mathsf{SINR})$. Assuming *instantaneous full CSI*, the sum-rate across all users averaged over

n time instances is approximated as

$$\bar{R} = \frac{1}{n} \sum_{n} \sum_{k=1}^{C} \log_2 \left(\frac{\rho_k |\mathbf{h}_k^*[n] \mathbf{f}_k[n]|^2}{1 + \sum_{\substack{\ell=1 \\ \ell \neq k}}^{C} \alpha_{k,\ell} \rho_k |\mathbf{g}_{k,\ell}^*[n] \mathbf{f}_\ell[n]|^2} \right), \tag{6.9}$$

$$= \frac{1}{n} \sum_{k=1}^{C} \sum_{n} \log_2 \left(\frac{\rho_k |\mathbf{h}_k^*[n] \mathbf{f}_k[n]|^2}{1 + \sum_{\substack{\ell=1 \\ \ell \neq k}}^{C} \alpha_{k,\ell} \rho_k |\mathbf{g}_{k,\ell}^*[n] \mathbf{f}_\ell[n]|^2} \right), \tag{6.10}$$

where (6.10) is obtained by interchanging the finite summations in (6.9). This allows (6.10) to be represented as the sum of each user's *average data-rate over time*.

At time instant n, each receiver ideally chooses a codeword that maximizes the sum-rate in systems with zero-delay. In practical systems, however, the error vectors fed back at time n reach the base station at a future time instant due to delayed limited feedback. Hence, a reasonable alternative is for the user to estimate the *predicted sum-rate*, $R^{\mathrm{p}}[n]$, using the expected future channels (predicted channel vectors) as

$$R^{\mathrm{p}}[n] = \sum_{k=1}^{C} \log_2 \left(\frac{\rho_k |(\mathbf{h}_k^{\mathrm{p,full}}[n])^* \mathbf{f}_k^{\mathrm{p}}[n]|^2}{1 + \sum_{\substack{\ell=1 \\ \ell \neq k}}^{C} \alpha_{k,\ell} \rho_k |(\mathbf{g}_{k,\ell}^{\mathrm{p,full}}[n])^* \mathbf{f}_\ell^{\mathrm{p}}[n]|^2} \right). \tag{6.11}$$

and choose codewords that will maximizes $R^{\mathrm{p}}[n]$. Note that $\mathbf{h}_k^{\mathrm{p,full}}[n]$ and $\mathbf{g}_{k,\ell}^{\mathrm{p,full}}[n]$ are given by (6.1) and (6.2), respectively and $\mathbf{f}_k^{\mathrm{p}}[n]$ is given in (6.7). The sum-rate obtained when prediction is assumed to be perfect (full CSI), $R^{\mathrm{p,full}}[n]$ is defined as

$$R^{\mathrm{p,full}}[n] := \sum_{k=1}^{C} \log_2 \left(\frac{\rho_k |(\mathbf{h}_k^{\mathrm{p,full}}[n])^* \mathbf{f}_k[n]|^2}{1 + \sum_{\substack{\ell=1 \\ \ell \neq k}}^{C} \alpha_{k,\ell} \rho_k |(\mathbf{g}_{k,\ell}^{\mathrm{p,full}}[n])^* \mathbf{f}_\ell[n]|^2} \right),$$

where $\mathbf{f}_k[n]$ is given by (6.8). Delayed PVQ results in a loss in the sum-rate (across all users and times). It is desirable to maximize the predicted sum-rates with limited feedback (in (6.11)). Maximizing R^{p} is equivalent to minimizing the loss in the sum-rate arising due to quantization,

$$\Delta R^{\mathrm{p}} := \frac{1}{n}\sum_{n} R^{\mathrm{p,full}}[n] - R^{\mathrm{p}}[n]. \tag{6.12}$$

By realigning the terms in $R^{\mathrm{p,full}}[n]$, the loss in sum-rate in (6.12) can be expressed as

$$\begin{aligned}\Delta R^{\mathrm{p}} =& \frac{1}{n}\sum_{k=1}^{C}\sum_{n}\log_2\left(\frac{\rho_k|(\mathbf{h}_k^{\mathrm{p,full}}[n+D_k])^*\mathbf{f}_k[n+D_k]|^2}{1+\sum_{\substack{\ell=1\\ \ell\neq k}}^{C}\alpha_{k,\ell}\rho_k|(\mathbf{g}_{k,\ell}^{\mathrm{p,full}}[n+\overline{D}_k])^*\mathbf{f}_\ell[n+\overline{D}_k]|^2}\right)\\ &-\sum_{n}\log_2\left(\frac{\rho_k|(\mathbf{h}_k^{\mathrm{p,full}}[n+D_k])^*\mathbf{f}_k^{\mathrm{p}}[n+D_k]|^2}{1+\sum_{\substack{\ell=1\\ \ell\neq k}}^{C}\alpha_{k,\ell}\rho_k|(\mathbf{g}_{k,\ell}^{\mathrm{p,full}}[n+\overline{D}_k])^*\mathbf{f}_\ell^{\mathrm{p}}[n+\overline{D}_k]|^2}\right).\end{aligned} \tag{6.13}$$

The first and second logarithm terms in (6.13) correspond to the loss in the data-rate corresponding to the predictive quantization of the desired and interfering channels, respectively.

6.4 Joint Error Quantization

At time instant n, the k^{th} receiver minimizes the expression in (6.13) by minimizing the loss in sum-rate, $\Delta R_k^{\text{p}}[n]$ as

$$\Delta R_k^{\text{p}}[n] = \underbrace{\log_2\left(\frac{|(\mathbf{h}_k^{\text{p,full}}[n+D_k])^*\mathbf{f}_k[n+D_k]|^2}{|(\mathbf{h}_k^{\text{p,full}}[n+D_k])^*\mathbf{f}_k^{\text{p}}[n+D_k]|^2}\right)}_{R_{k,(\text{d})}[n]} + \underbrace{\log_2\left(\frac{1+\sum_{\substack{\ell=1\\ \ell\neq k}}^{C}\alpha_{k,\ell}\rho_k|(\mathbf{g}_{k,\ell}^{\text{p,full}}[n+\overline{D}_k])^*\mathbf{f}_\ell^{\text{p}}[n+\overline{D}_k]|^2}{1+\sum_{\substack{\ell=1\\ \ell\neq k}}^{C}\alpha_{k,\ell}\rho_k|(\mathbf{g}_{k,\ell}^{\text{p,full}}[n+\overline{D}_k])^*\mathbf{f}_\ell[n+\overline{D}_k]|^2}\right)}_{R_{k,(\text{i})}[n]}. \quad (6.14)$$

The first and second logarithm terms in (6.14) are denoted by $R_{k,(\text{d})}[n]$ and $R_{k,(\text{i})}[n]$, respectively. Note that $R_{k,(\text{d})}[n]$ and $R_{k,(\text{i})}[n]$ correspond to the loss in the data-rate corresponding to the predictive quantization of the desired and interfering channels, respectively.

It is seen from (6.14) that $R_{k,(\text{d})}[n] \to 0$ ($R_{k,(\text{i})}[n] \to 0$), if $\mathbf{f}_k^{\text{p}}[n] \to \mathbf{f}_k[n]$ ($\mathbf{f}_\ell^{\text{p}}[n] \to \mathbf{f}_\ell[n]$). Hence, the loss in sum-rate is a function of the prediction; the closer the predicted channel is to the actual channel, the closer the beamforming vectors obtained from PVQ will be to $\mathbf{f}_k[n]$ ($\mathbf{f}_\ell[n]$) and smaller the loss in sum-rate. Hence, error quantization plays an important role in minimizing the expression in (6.14). Error vectors can be quantized separately or as a composite *net error vector*, using joint quantization [12].

Joint error quantization involves concatenating error vectors at user k as $[\mathbf{e}_{\mathbf{h}_k}[n]\ \mathbf{e}_{\mathbf{g}_{k,1}}[n]\ldots\ \mathbf{e}_{\mathbf{g}_{k,C}}[n]]$. The idea is to use codebooks, $\mathcal{W}$, of size 2^B with codewords, $\mathbf{w}_n(n=1,\ldots,2^B)$, such that $\mathbf{w}_n(1:N_t)$ and $\mathbf{w}_n(N_t+1:$

$N_t(i+1)$) correspond to $\hat{\mathbf{e}}_{\mathbf{h}_k}$ and $\hat{\mathbf{e}}_{\mathbf{g}_{k,i}}$, respectively, where $i = 1, \ldots, (C-1)$. Due to the joint quantization of all the channels using a single representative vector, selecting an appropriate codeword is very important to determine the performance of the joint error quantization approach [12]. The derivation of the selection criterion involves first upper bounding $R_{k,(\mathrm{d})}[n]$ and $R_{k,(\mathrm{i})}[n]$ in (6.14), as presented in Propositions 6.4.1 and 6.4.2 .

Proposition 6.4.1. *The upper bound on the mean loss in sum-rate due to quantizing the desired channel of the k^{th} user, $R_{k,(\mathrm{d})}[n]$ in (6.14) is approximated by*

$$\log_2\left(\frac{|(\mathbf{h}_k^{\mathrm{p,full}}[n+D_k])^*\mathbf{f}_k[n+D_k]|^2}{|(\mathbf{h}_k^{\mathrm{p}}[n+D_k])^*\mathbf{f}_k^{\mathrm{p}}[n+D_k]|^2}\right) - \log_2\left(|(\tilde{\mathbf{h}}_k^{\mathrm{p,full}}[n+D_k])^*\tilde{\mathbf{h}}_k^{\mathrm{p}}[n+D_k]|^2\right) .$$

Proof. The proof is given in Appendix 6.8.1. □

Proposition 6.4.2. *The upper bound on the mean loss in sum-rate due to quantizing the interfering channels at the k^{th} user, $R_{k,(\mathrm{i})}[n]$ in (6.14) is approximated by*

$$\log_2\left(1 + \sum_{\substack{\ell=1 \\ \ell\neq k}}^{C} \alpha_{k,\ell}\rho_k|\mathbf{g}_{k,\ell}^{\mathrm{p,full}}[n+\overline{D}_k]|^2(1-|(\tilde{\mathbf{g}}_{k,\ell}^{\mathrm{p,full}}[n+\overline{D}_k])^*\tilde{\mathbf{g}}_{k,\ell}^{\mathrm{p}}[n+\overline{D}_k]|^2)\right) .$$

Proof. The proof is given in Appendix 6.8.2. □

Note that the $n+D_k$ and $n+\overline{D}_k$ indices are omitted in the remainder of the section, for notational brevity. Using propositions 6.4.1 and 6.4.2, the

loss in sum-rate due to delayed predictive quantization in (6.14) is bounded as

$$\Delta R_k^{\mathrm{p}}[n] \leq \log_2\left(\frac{|(\mathbf{h}_k^{\mathrm{p,full}})^*\mathbf{f}_k|^2}{|\mathbf{h}_k^{\mathrm{p}*}\mathbf{f}_k^{\mathrm{p}}|^2}\right) - \log_2\left(|(\tilde{\mathbf{h}}_k^{\mathrm{p,full}})^*\tilde{\mathbf{h}}_k^{\mathrm{p}}|^2\right) + \log_2\left(1+\sum_{\substack{\ell=1\\ \ell\neq k}}^{C}\alpha_{k,\ell}\rho_k|\mathbf{g}_{k,\ell}^{\mathrm{p,full}}|^2(1-|(\tilde{\mathbf{g}}_{k,\ell}^{\mathrm{p,full}})^*\tilde{\mathbf{g}}_{k,\ell}^{\mathrm{p}}|^2)\right). \quad (6.15)$$

For a quantization scheme where the distribution of $\mathbf{h}_k^{\mathrm{p,full}}$ is the same as that of $\mathbf{h}_k^{\mathrm{p}}$, $\mathbb{E}(|\mathbf{h}_k^{\mathrm{p,full}^*}\mathbf{f}_k|^2) = \mathbb{E}(|\mathbf{h}_k^{\mathrm{p}*}\mathbf{f}_k^{\mathrm{p}}|^2)$. Hence, the term $\log_2\left(|(\mathbf{h}_k^{\mathrm{p,full}})^*\mathbf{f}_k|^2/|\mathbf{h}_k^{\mathrm{p}*}\mathbf{f}_k^{\mathrm{p}}|^2\right)$ is ignored. This implies that minimizing the *mean loss in sum-rate* is equivalent to minimizing

$$-\log_2\left(|(\tilde{\mathbf{h}}_k^{\mathrm{p,full}})^*\tilde{\mathbf{h}}_k^{\mathrm{p}}|^2\right) + \log_2\left(1+\sum_{\substack{\ell=1\\ \ell\neq k}}^{C}\alpha_{k,\ell}\rho_k|\mathbf{g}_{k,\ell}^{\mathrm{p,full}}|^2(1-|(\tilde{\mathbf{g}}_{k,\ell}^{\mathrm{p,full}})^*\tilde{\mathbf{g}}_{k,\ell}^{\mathrm{p}}|^2)\right). \quad (6.16)$$

Thus, given a codebook $\mathcal{W}$ where each codeword $\mathbf{w} \in \mathcal{W}$ is formed by concatenating error vectors, the quantization vector is chosen as the codeword that will minimize (6.16). Using the monotonic nature of the logarithm and the fact that minimizing (6.16) is equivalent to maximizing its negative, the selection criterion can be written as

$$\hat{\mathbf{w}} = \arg\max_{\mathbf{w}\in\mathcal{W}} \frac{|(\tilde{\mathbf{h}}_k^{\mathrm{p,full}})^*\tilde{\mathbf{h}}_k^{\mathrm{p}}(\mathbf{w})|^2}{1+\sum_{\substack{\ell=1\\ \ell\neq k}}^{C}\alpha_{k,\ell}\rho_k|\mathbf{g}_{k,\ell}^{\mathrm{p,full}}|^2(1-|(\tilde{\mathbf{g}}_{k,\ell}^{\mathrm{p,full}})^*\tilde{\mathbf{g}}_{k,\ell}^{\mathrm{p}}(\mathbf{w})|^2)}, \quad (6.17)$$

where $\tilde{\mathbf{h}}_k^{\mathrm{p}}$ and $\tilde{\mathbf{g}}_{k,\ell}^{\mathrm{p}}$ are replaced by $\tilde{\mathbf{h}}_k^{\mathrm{p}}(\mathbf{w})$ and $\tilde{\mathbf{g}}_{k,\ell}^{\mathrm{p}}(\mathbf{w})$, respectively, to illustrate the dependence of the predicted codewords on error quantization vectors. Note that if $\alpha_{k,\ell} = 0$ for all $\ell \neq k$, then the selection criterion in (6.17) simplifies to

the minimum angular separation criterion that is used popularly in single-CSI limited feedback [63]. This serves as an intuitive check for the expression in (6.17) .

The selection criterion in (6.17) does not use assumptions about the channel statistics, predictor or the transmission strategy, as long as the beamforming vector can reduce the predicted interference. This makes the derived criterion versatile enough that it can be used for most types of multicell cooperation-based strategies, with limited CSI feedback quantization.

Predictive quantization suffers from *error propagation* since the quantized error is added to the predicted channel to obtain the reconstructed channel at every time instant. This can result in errors adding up at every instance of prediction. Hence, to keep the errors from dominating the performance gains obtained, high resolution CSI needs to be made available at the base stations periodically, referred to as *reinitialization* in this chapter. The frequency of reinitialization is a function of the delays in the system, user velocity, and the predictor used for quantization, as shown using simulations [11]. Another significant disadvantage of joint predictive quantization is that it requires the design of special codebooks, which are a function of the signal strengths of the various interfering channels.

6.5 Predictive CSI Quantization

This section presents an approach to predict CSI on the Grassmann manifold using the mathematical tools derived in [43],[71], and [23]. While

GPC in [43, 44] feeds back the norm and direction of the *tangent vector*, the proposed strategy feeds back only the unit-norm direction of the error between the tangent vectors. A simple technique is proposed for base stations to evaluate channel norms using predicted channels and error direction vector. By eliminating the overhead associated with feeding back the norm of error vectors, the presented algorithm reduces feedback requirements. A linear predictor is also discussed in this section for comparison purposes.

6.5.1 Proposed Prediction on Grassmann Manifold

Denoting the space of all unit-norm $N_t \times 1$ dimensional channel vectors by $\mathcal{H}_{N_t}$, an *equivalence relation* between two vectors, $\mathbf{h}_1, \mathbf{h}_2 \in \mathcal{H}_{N_t}$ is defined as $\mathbf{h}_1 \equiv \mathbf{h}_2$ if for some $\theta \in [0, 2\pi)$, $\mathbf{h}_1 = \mathsf{e}^{j\theta}\mathbf{h}_2$. This implies that vectors, $\mathbf{h}_1$ and $\mathbf{h}_2$ are equivalent if they are on the same line in $\mathbb{C}^{N_t \times 1}$. The Grassmann manifold, $\mathcal{G}_{N_t,1}$, which is the set of all one-dimensional subspaces in $\mathbb{C}^{N_t \times 1}$, is the quotient space corresponding to this equivalence relation. It is thus seen how the problem of predicting channel directions relates to that of subspace tracking.

While the Grassmann manifold is topologically smooth, it has only a locally Euclidean structure [43, 44, 63]. Subspace tracking can be done using state space models describing the evolution of the correlated signal sequence on the non-Euclidean Grassmann manifold [20, 21, 23, 71, 84]. This chapter utilizes the state space model in [23, 71] to predict tangent vectors. While the GPC algorithm in [43] quantizes the norm and direction of the *tangent*

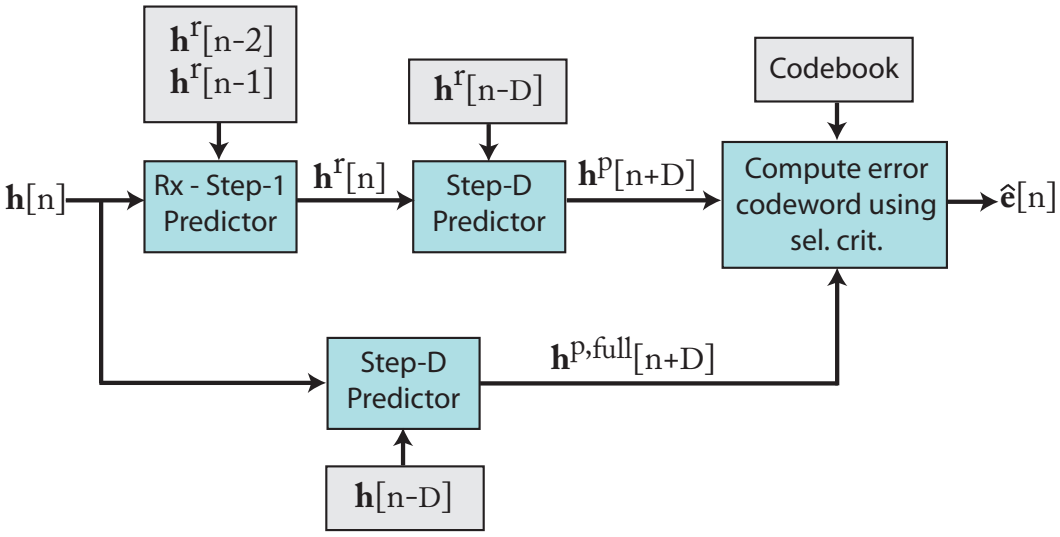

Figure 6.1: Receiver structure for proposed predictive algorithm.

vector between two prior normalized channel vectors, the subspace-tracking technique presented in this chapter feeds back the change in the tangent vector, which is then used to predict the unit-norm channel directions that lie on the Grassmann manifold. Further, a novel technique is also developed to avoid feeding back the norms of error vectors generated using the proposed predictor.

In this section, we describie the prediction algorithm for only the desired CSI for brevity, since interfering channel directions are predicted in a similar manner. The receiver structure is outlined in Fig. 6.1. The basic idea is as follows. At time instant n, the user terminal has knowledge of the full desired CSI $\tilde{\mathbf{h}}_k[n]$, along with the reconstructed channels, $\mathbf{h}_k^{\mathrm{r}}[i]$ for $i < n$, which are used to obtain $\mathbf{h}_k^{\mathrm{p}}[n+D]$. We propose a *step-1* predictor to first obtain $\mathbf{h}_k^{\mathrm{r}}[n]$ from $\mathbf{h}_k^{\mathrm{r}}[n-1]$ and $\mathbf{h}_k^{\mathrm{r}}[n-2]$. Then, $\mathbf{h}_k^{\mathrm{r}}[n-D]$ and $\mathbf{h}_k^{\mathrm{r}}[n]$ are used to obtain

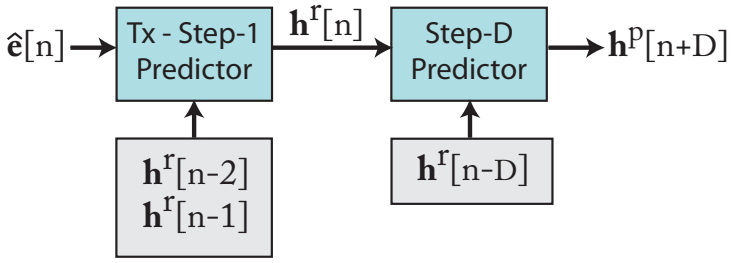

Figure 6.2: Transmitter structure for proposed predictive algorithm.

$\mathbf{h}_k^{\mathrm{p}}[n+D]$ from the proposed *step-D* predictor. A similar step-D predictor is used to obtain $\mathbf{h}_k^{\mathrm{p,full}}[n+D]$ [11]. The receiver computes the error between $\mathbf{h}_k^{\mathrm{p,full}}[n+D]$ and $\mathbf{h}_k^{\mathrm{p}}[n+D]$ for *each* channel.

The transmitter structure is illustrated in Fig 6.2 for time instant $n+D$. The goal of the transmitter is to predict the channel at time-instant $n+D$ for designing the beamforming vectors (using (6.7)). A step-1 predictor, similar to the one in Fig. 6.1, is used to generate $\mathbf{h}_k^{\mathrm{r}}[n]$. A step-D predictor then uses $\mathbf{h}_k^{\mathrm{r}}[n]$ and $\mathbf{h}_k^{\mathrm{r}}[n-D]$ as inputs to obtain $\mathbf{h}_k^{\mathrm{p}}[n+D]$ [11].

It is seen from Figs. 6.1 and 6.2 that the step-1 and step-D predictors form the basis of the proposed predictive algorithm. The step-1 predictor at the receiver uses $\mathbf{h}_k^{\mathrm{r}}[n-2], \mathbf{h}_k^{\mathrm{r}}[n-1]$, and $\tilde{\mathbf{h}}_k[n]$ as inputs to generate $\mathbf{h}_k^{\mathrm{r}}[n]$. At the transmitter side, $\mathbf{h}_k^{\mathrm{r}}[n]$ is obtained using $\mathbf{h}_k^{\mathrm{r}}[n-2], \mathbf{h}_k^{\mathrm{r}}[n-1]$, and $\hat{\mathbf{e}}[n]$ as inputs. The step-1 predictor at the base station uses a subset of operations of that at the user terminal.

The receiver has knowledge of $\mathbf{h}_k^{\mathrm{r}}[n-2], \mathbf{h}_k^{\mathrm{r}}[n-1]$ and $\tilde{\mathbf{h}}_k[n]$, which is used to *steer* the base station towards a reconstructed value of $\tilde{\mathbf{h}}_k[n]$. The

tangent vector between $\mathbf{h}_k^{\mathrm{r}}[n-2]$ and $\mathbf{h}_k^{\mathrm{r}}[n-1]$, denoted by $\mathbf{v}(\mathbf{h}_k^{\mathrm{r}}[n-2], \mathbf{h}_k^{\mathrm{r}}[n-1])$, is obtained at the user terminal using [43] as

$$\mathbf{v}(\mathbf{h}_k^{\mathrm{r}}[n-2], \mathbf{h}_k^{\mathrm{r}}[n-1]) = \tan^{-1}\left(\frac{d_o}{|\rho_o|}\right) \frac{\mathbf{h}_k^{\mathrm{r}}[n-1]/\rho_o - \mathbf{h}_k^{\mathrm{r}}[n-2]}{d_o/\rho_o}, \qquad (6.18)$$

where $\rho_o = (\mathbf{h}_k^{\mathrm{r}}[n-2])^* \mathbf{h}_k^{\mathrm{r}}[n-1]$ and $d_o = \sqrt{1-|\rho_o|^2}$. Now, $\mathbf{v}(\mathbf{h}_k^{\mathrm{r}}[n-2], \mathbf{h}_k^{\mathrm{r}}[n-1])$ is used to predict the tangent vector between $\mathbf{h}_k^{\mathrm{r}}[n-1]$ and $\mathbf{h}_k^{\mathrm{r}}[n]$. Using the state-space model in [71], the *predicted* (or mean) tangent vector, $\mathbf{v}^{\mathrm{p}}(\mathbf{h}_k^{\mathrm{r}}[n-1], \mathbf{h}_k^{\mathrm{r}}[n])$ is given by Proposition 6.5.1 [11].

Proposition 6.5.1. *The predicted (or mean) tangent vector between* $\mathbf{h}_k^{\mathrm{r}}[n-1]$ *and* $\mathbf{h}_k^{\mathrm{r}}[n]$, $\mathbf{v}^{\mathrm{p}}(\mathbf{h}_k^{\mathrm{r}}[n-1], \mathbf{h}_k^{\mathrm{r}}[n])$, *is computed at the receiver as*

$$\mathbf{v}^{\mathrm{p}}(\mathbf{h}_k^{\mathrm{r}}[n-1], \mathbf{h}_k^{\mathrm{r}}[n]) = \mathbf{h}_k^{\mathrm{r}}[n-1]\frac{\cos(|\rho_1|)}{\rho_1} - \mathbf{h}_k^{\mathrm{r}}[n-2]\left(\sin(d_1)\frac{d_1}{|\rho_1|} + \cos(|\rho_1|)\right),$$

where $\rho_0 = (\mathbf{h}_k^{\mathrm{r}}[n-2])^* \mathbf{h}_k^{\mathrm{r}}[n-1]$ *and* $d_0 = \sqrt{1-|\rho_0|^2}$.

Proof. The proof is given in Appendix 6.8.3. □

Now, the actual tangent vector between $\mathbf{h}_k^{\mathrm{r}}[n-1]$ and $\tilde{\mathbf{h}}_k[n]$ is generated at the receiver, along the lines of (6.18) as [43]

$$\mathbf{v}^{\mathrm{act}}(\mathbf{h}_k^{\mathrm{r}}[n-1], \tilde{\mathbf{h}}_k[n]) = \tan^{-1}\left(\frac{d_1}{|\rho_1|}\right) \frac{\tilde{\mathbf{h}}_k[n]/\rho_2 - \mathbf{h}_k^{\mathrm{r}}[n-1]}{d_1/\rho_1},$$

where $\rho_1 = (\tilde{\mathbf{h}}_k[n-1])^* \mathbf{h}_k^{\mathrm{r}}[n]$ and $d_1 = \sqrt{1-|\rho_1|^2}$. Since the transmitter can generate $\mathbf{v}^{\mathrm{p}}(\mathbf{h}_k^{\mathrm{r}}[n-1], \mathbf{h}_k^{\mathrm{r}}[n])$ using $\mathbf{h}_k^{\mathrm{r}}[n-1]$ and $\mathbf{h}_k^{\mathrm{r}}[n-2]$, the receiver feeds back the *error vector* between $\mathbf{v}^{\mathrm{act}}(\mathbf{h}_k^{\mathrm{r}}[n-2], \tilde{\mathbf{h}}_k[n])$ and $\mathbf{v}^{\mathrm{p}}(\mathbf{h}_k^{\mathrm{r}}[n-1], \mathbf{h}_k^{\mathrm{r}}[n])$ as

$$\mathbf{e}[n-1] = \mathbf{v}^{\mathrm{act}}(\mathbf{h}_k^{\mathrm{r}}[n-2], \tilde{\mathbf{h}}_k[n]) - \mathbf{v}^{\mathrm{p}}(\mathbf{h}_k^{\mathrm{r}}[n-1], \mathbf{h}_k^{\mathrm{r}}[n]).$$

The unit-norm direction of error vector, $\tilde{\mathbf{e}}[n-1] = \mathbf{e}[n-1]/\|\mathbf{e}[n-1]\|$ is quantized to $\hat{\mathbf{e}}[n-1]$ to transmit over the finite-bandwidth feedback channel. Either separate or joint quantization approaches can be used at this point. Codewords are selected using the minimum angular distance criterion for separate quantization, whereas (6.17) is used to choose an error vector codeword using joint quantization. The *reconstructed tangent vector* is now generated at both the transmitter and receiver as

$$\mathbf{v}^{\mathrm{r}}(\mathbf{h}_k^{\mathrm{r}}[n-1], \tilde{\mathbf{h}}_k[n]) = \mathbf{v}^{\mathrm{p}}(\mathbf{h}_k^{\mathrm{r}}[n-1], \mathbf{h}_k^{\mathrm{r}}[n]) + \alpha\hat{\mathbf{e}}[n-1], \tag{6.19}$$

where $\alpha = \|\mathbf{e}[n-1]\|$ is the norm of the error vector. The reconstructed channel, $\mathbf{h}_k^{\mathrm{r}}[n]$ is then obtained at the user terminal and the base station as the geodesic path from $\mathbf{h}_k^{\mathrm{r}}[n-1]$, lying on the Grassmann manifold along the direction of $\mathbf{v}^{\mathrm{r}}(\mathbf{h}_k^{\mathrm{r}}[n-1], \mathbf{h}_k^{\mathrm{r}}[n])/\|\mathbf{v}^{\mathrm{r}}(\mathbf{h}_k^{\mathrm{r}}[n-1], \mathbf{h}_k^{\mathrm{r}}[n])\|$ at a distance of $\|\mathbf{v}^{\mathrm{r}}(\mathbf{h}_k^{\mathrm{r}}[n-1], \mathbf{h}_k^{\mathrm{r}}[n])\|$ [43, 71]

$$\begin{aligned}\mathbf{h}_k^{\mathrm{r}}[n] = \mathbf{h}_k^{\mathrm{r}}[n-1]\cos(\|\mathbf{v}^{\mathrm{r}}(\mathbf{h}_k^{\mathrm{r}}[n-2], \tilde{\mathbf{h}}_k[n])\|) \\ + \frac{\mathbf{v}^{\mathrm{r}}(\mathbf{h}_k^{\mathrm{r}}[n-1], \mathbf{h}_k^{\mathrm{r}}[n])}{\|\mathbf{v}^{\mathrm{r}}(\mathbf{h}_k^{\mathrm{r}}[n-2], \tilde{\mathbf{h}}_k[n])\|}\sin(\|\mathbf{v}^{\mathrm{r}}(\mathbf{h}_k^{\mathrm{r}}[n-2], \tilde{\mathbf{h}}_k[n])\|).\end{aligned} \tag{6.20}$$

It is seen from (6.19) and (6.20) that $\alpha = \|\mathbf{e}[n-1]\|$ plays an important role in generating $\mathbf{h}_k^{\mathrm{r}}[n]$ at the base station. Feeding back the norm of each of the multiple error vectors, however, could impose a substantial feedback overhead in the case of the multicell cooperative system. In this section, a technique is proposed for base stations to compute $\alpha = \|\mathbf{e}[n-1]\|$, making feedback of the error vector norm unnecessary. For slow fading channels, it

can be assumed that $\|\mathbf{v}^{\mathrm{r}}(\mathbf{h}_k^{\mathrm{r}}[n-2], \tilde{\mathbf{h}}_k[n])\| = \|\mathbf{v}^{\mathrm{p}}(\mathbf{h}_k^{\mathrm{r}}[n-1], \mathbf{h}_k^{\mathrm{r}}[n])\|$. The base station can then evaluate α as

$$\begin{aligned}
&\|\mathbf{v}^{\mathrm{r}}(\mathbf{h}_k^{\mathrm{r}}[n-2], \tilde{\mathbf{h}}_k[n])\|^2 = \|\mathbf{v}^{\mathrm{p}}(\mathbf{h}_k^{\mathrm{r}}[n-1], \mathbf{h}_k^{\mathrm{r}}[n]) + \alpha\hat{\mathbf{e}}[n-1]\|^2 \\
&= \|\mathbf{v}^{\mathrm{p}}(\mathbf{h}_k^{\mathrm{r}}[n-2], \tilde{\mathbf{h}}_k[n])\|^2 + \|\alpha\hat{\mathbf{e}}[n-1]\|^2 + 2\alpha\mathbb{R}\{(\mathbf{v}^{\mathrm{p}}(\mathbf{h}_k^{\mathrm{r}}[n-1], \mathbf{h}_k^{\mathrm{r}}[n]))^*\hat{\mathbf{e}}[n-1] \\
&= \|\mathbf{v}^{\mathrm{r}}(\mathbf{h}_k^{\mathrm{r}}[n-2], \tilde{\mathbf{h}}_k[n])\|^2 + \alpha^2 + 2\alpha\mathbb{R}\left\{(\mathbf{v}^{\mathrm{p}}(\mathbf{h}_k^{\mathrm{r}}[n-1], \mathbf{h}_k^{\mathrm{r}}[n]))^*\hat{\mathbf{e}}[n-1]\right\}
\end{aligned} \tag{6.21}$$

where (6.21) is obtained using $\|\mathbf{v}^{\mathrm{r}}(\mathbf{h}_k^{\mathrm{r}}[n-2], \tilde{\mathbf{h}}_k[n])\| = \|\mathbf{v}^{\mathrm{p}}(\mathbf{h}_k^{\mathrm{r}}[n-1], \mathbf{h}_k^{\mathrm{r}}[n])\|$ and $\|\hat{\mathbf{e}}[n-1]\|^2 = 1$. Solving for α from (6.21) yields

$$\alpha = -2\mathbb{R}\left\{(\mathbf{v}^{\mathrm{p}}(\mathbf{h}_k^{\mathrm{r}}[n-1], \mathbf{h}_k^{\mathrm{r}}[n]))^*\hat{\mathbf{e}}[n-1]\right\},$$

by ignoring the trivial solution $\alpha = 0$. Thus, the base station can compute the norm of the error vector by itself, reducing feedback requirements for multicell cooperation.

The step-D predictor used at both the transmit and receive sides involves essentially the same operations. Note that while the predictor is described here for generating $\mathbf{h}_k^{\mathrm{p}}[n+D]$ using $\mathbf{h}_k^{\mathrm{r}}[n-D]$ and $\mathbf{h}_k^{\mathrm{r}}[n]$, it is applicable to predict $\mathbf{h}_k^{\mathrm{p,full}}[n+D]$ by simply replacing $\mathbf{h}_k^{\mathrm{p}}[n+D]$ with $\mathbf{h}_k^{\mathrm{p,full}}[n+D]$, $\mathbf{h}_k^{\mathrm{r}}[n-D]$ with $\tilde{\mathbf{h}}_k[n-D]$, and $\mathbf{h}_k^{\mathrm{r}}[n]$ with $\tilde{\mathbf{h}}_k[n]$. The tangent vector between $\mathbf{h}_k^{\mathrm{r}}[n-D]$, and $\mathbf{h}_k^{\mathrm{r}}[n]$, $\mathbf{v}(\mathbf{h}_k^{\mathrm{r}}[n-D], \mathbf{h}_k^{\mathrm{r}}[n])$ is obtained using [43] as

$$\mathbf{v}(\mathbf{h}_k^{\mathrm{r}}[n-D], \mathbf{h}_k^{\mathrm{r}}[n]) = \tan^{-1}\left(\frac{d_2}{|\rho_2|}\right)\frac{\mathbf{h}_k^{\mathrm{r}}[n]/\rho_2 - \mathbf{h}_k^{\mathrm{r}}[n-D]}{d_2/\rho_2},$$

where $\rho_2 = (\mathbf{h}_k^{\mathrm{r}}[n-D])^*\mathbf{h}_k^{\mathrm{r}}[n]$ and $d_2 = \sqrt{1-|\rho_2|^2}$. The *predicted* (or mean) tangent vector from $\mathbf{h}_k^{\mathrm{r}}[n]$ to $\mathbf{h}_k^{\mathrm{r}}[n+D]$, $\mathbf{v}^{\mathrm{p}}(\mathbf{h}_k^{\mathrm{r}}[n-1], \mathbf{h}_k^{\mathrm{r}}[n])$ is given by Propo-

sition 6.5.1 as

$$\mathbf{v}^{\mathrm{p}}(\mathbf{h}_k^{\mathrm{r}}[n], \mathbf{h}_k^{\mathrm{r}}[n+D]) = \mathbf{h}_k^{\mathrm{r}}[n]\frac{\cos(|\rho_2|)}{\rho_2} - \mathbf{h}_k^{\mathrm{r}}[n-D]\left(\sin(d_2)\frac{d_2}{|\rho_2|} + \cos(|\rho_2|)\right).$$

The predicted channel at time instant $n+D$, $\mathbf{h}_k^{\mathrm{p}}[n+D]$, is then written as

$$\begin{aligned}\mathbf{h}_k^{\mathrm{p}}[n+D] = \mathbf{h}_k^{\mathrm{r}}[n]\cos(\|\mathbf{v}^{\mathrm{p}}(\mathbf{h}_k^{\mathrm{r}}[n], \mathbf{h}_k^{\mathrm{r}}[n+D])\|) \\ + \frac{\mathbf{v}^{\mathrm{p}}(\mathbf{h}_k^{\mathrm{r}}[n], \mathbf{h}_k^{\mathrm{r}}[n+D])}{\|\mathbf{v}^{\mathrm{p}}(\mathbf{h}_k^{\mathrm{r}}[n], \mathbf{h}_k^{\mathrm{r}}[n+D])\|}\sin(\|\mathbf{v}^{\mathrm{p}}(\mathbf{h}_k^{\mathrm{r}}[n], \mathbf{h}_k^{\mathrm{r}}[n+D])\|).\end{aligned}$$

The proposed Grassmannian predictive framework is shown in Section 6.6 to yield higher sum-rates with smaller feedback requirements as compared to existing multicell limited feedback approaches. The performance gains, however, come at the cost of additional complexity, especially at the receiver side. In the next section, we describe linear prediction, which is relatively low-complexity but results in smaller sum-rates as compared to the proposed approach.

6.5.2 Linear Prediction

Linear prediction, while being low-complexity compared to non-linear techniques, is not very suitable for long-range prediction [15, 25, 35, 94]. In this section, linear prediction uses an AR model of the order r to predict channels [15, 22, 36, 37]. The predicted channel, $\mathbf{h}_k^{\mathrm{p}}[n]$, using a linear MMSE predictor, is given by [34]

$$\mathbf{h}_k^{\mathrm{p}}[n] = \mathsf{P}\left(\mathbf{h}_k[n] | \{\mathbf{h}_k^{\mathrm{r}}[n-D_k]\}_r\right) = \sum_{i=1}^{r} a_i \mathbf{h}_k^{\mathrm{r}}[n-i]$$

$$\mathbf{g}_{k,\ell}^{\mathrm{p}}[n] = \mathsf{P}\left(\mathbf{g}_{k,\ell}[n] | \{\mathbf{g}_{k,\ell}^{\mathrm{r}}[n-\overline{D}_k]\}_r\right) = \sum_{i=1}^{r} b_i \mathbf{g}_{k,\ell}^{\mathrm{r}}[n-i],$$

where $\{a_i\}_{i=1}^r$ and $\{b_i\}_{i=1}^r$ are linear coefficients, which can be obtained using Yule Walker equations [22, 34] as

$$\mathbf{R}_{\mathbf{h}_k}\mathbf{a} = \mathbf{r}_{\mathbf{h}_k}$$

$$\mathbf{R}_{\mathbf{g}_{k,\ell}}\mathbf{b} = \mathbf{r}_{\mathbf{g}_{k,\ell}}$$

such that for $R_{\mathbf{h}_k}[i] = \mathbb{E}\{\mathbf{h}_k[n]^*\mathbf{h}_k[n+i]\}$, and $R_{\mathbf{g}_{k,\ell}}[i] = \mathbb{E}\{\mathbf{g}_{k,\ell}[n]^*\mathbf{g}_{k,\ell}[n+i]\}$, $[\mathbf{R}_{\mathbf{h}_k}]_{(i,m)} = R_{\mathbf{h}_k}[|i-m|]$ and $\mathbf{r}_{\mathbf{h}_k}(i) = R_{\mathbf{h}_k}[i+D_k-1]$. Similarly, $[\mathbf{R}_{\mathbf{g}_{k,\ell}}]_{(i,m)} = R_{\mathbf{g}_{k,\ell}}[|i-m|]$ and $\mathbf{r}_{\mathbf{g}_{k,\ell}}(i) = R_{\mathbf{g}_{k,\ell}}[i+\overline{D}_k-1]$ [22]. In linear prediction, the error vector is evaluated as

$$\mathbf{e}_{\mathbf{h}_k}[n] = \mathbf{h}_k[n] - \mathbf{h}_k^{\mathrm{p}}[n], \text{ and}$$

$$\mathbf{e}_{\mathbf{g}_{k,\ell}}[n] = \mathbf{g}_{k,\ell}[n] - \mathbf{g}_{k,\ell}^{\mathrm{p}}[n].$$

Since it is known that the reconstructed channel vector is unit-norm, it is proposed in this section to quantize only the error direction and determine the error norm adaptively. The desired reconstructed vector is given as

$$\mathbf{h}_k^{\mathrm{r}}[n] = \mathbf{h}_k^{\mathrm{p}}[n] + \beta\hat{\mathbf{e}}_{\mathbf{h}_k}[n],$$

where $\beta = \|\mathbf{e}_{\mathbf{h}_k}[n]\|$ is the norm of the error vector. The base station can evaluate α by solving for $\|\mathbf{h}_k^{\mathrm{r}}[n]\|^2 = 1$ as

$$\begin{aligned}
\|\mathbf{h}_k^{\mathrm{r}}[n]\|^2 =& \|\mathbf{h}_k^{\mathrm{p}}[n] + \alpha\hat{\mathbf{e}}_{\mathbf{h}_k}[n]\|^2 \\
=& (\mathbf{h}_k^{\mathrm{p}}[n] + \alpha\hat{\mathbf{e}}_{\mathbf{h}_k}[n])(\mathbf{h}_k^{\mathrm{p}}[n] + \alpha\hat{\mathbf{e}}_{\mathbf{h}_k}[n])^* \\
=& \|\mathbf{h}_k^{\mathrm{p}}[n]\|^2 + 2\alpha\mathbb{R}\{\mathbf{h}_k^{\mathrm{p}}[n]\hat{\mathbf{e}}_{\mathbf{h}_k}[n]\} + \alpha^2\|\hat{\mathbf{e}}_{\mathbf{h}_k}[n]\|^2 \\
=& 1 + 2\alpha\mathbb{R}\{\mathbf{h}_k^{\mathrm{p}}[n]\hat{\mathbf{e}}_{\mathbf{h}_k}[n]\} + \alpha^2
\end{aligned} \tag{6.22}$$

where (6.22) is obtained using $\|\mathbf{h}_k^{\mathrm{p}}[n]\|^2 = \|\hat{\mathbf{e}}_{\mathbf{h}_k}[n]\|^2 = 1$. Solving for α by setting (6.22) equal to one yields the reconstruction operation as

$$\mathbf{h}_k^{\mathrm{r}}[n] = \mathsf{R}(\mathbf{h}_k^{\mathrm{p}}[n], \hat{\mathbf{e}}_{\mathbf{h}_k}[n]) = \mathbf{h}_k^{\mathrm{p}}[n] - 2\mathbb{R}\{(\mathbf{h}_k^{\mathrm{p}}[n])^* \hat{\mathbf{e}}_{\mathbf{h}_k}[n]\}\hat{\mathbf{e}}_{\mathbf{h}_k}[n], \text{ and}$$

$$\mathbf{g}_{k,\ell}^{\mathrm{r}}[n] = \mathsf{R}(\mathbf{g}_{k,\ell}^{\mathrm{p}}[n], \hat{\mathbf{e}}_{\mathbf{g}_{k,\ell}}[n]) = \mathbf{g}_{k,\ell}^{\mathrm{p}}[n] - 2\mathbb{R}\{(\mathbf{g}_{k,\ell}^{\mathrm{p}}[n])^* \hat{\mathbf{e}}_{\mathbf{g}_{k,\ell}}[n]\}\hat{\mathbf{e}}_{\mathbf{g}_{k,\ell}}[n].$$

It is seen from (6.21) and (6.22) that in both the proposed subspace-tracking approach and linear prediction, base stations can predict the error norm. This implies that available feedback resources can be used for quantizing the error directions, and do not have to be expended on the error norms. In contrast, [43, 44] proposes that both the magnitude and direction be quantized, incurring significant overhead for the feedback of norm.

6.6 Simulation Results

Simulation results demonstrating the performance of predictive joint quantization are presented for a multicell scenario with delayed limited CSI feedback. It is also shown that the proposed approach significantly outperforms separate CSI quantization, which does not exploit the temporal correlation in the wireless channels.

Temporally correlated channels are generated using a modified *sum of sinusoids* approach [103], based on Jakes's classic model [47]. It was shown in [103] that the autocorrelation obtained using this modification to Jakes's model match the simulated and statistical values more closely. Clarke's isotropic scattering model is used to generate the autocorrelation as $R[n] = J_0(2\pi f_d n)$

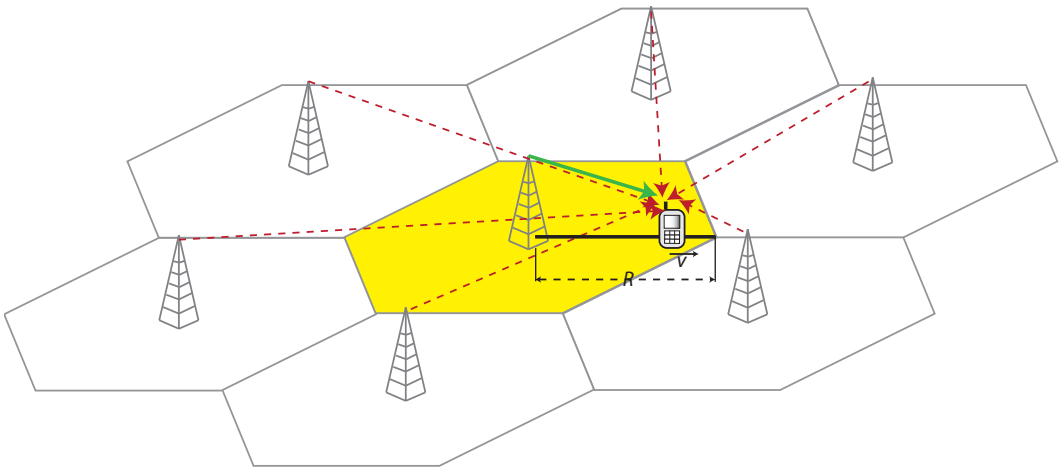

Figure 6.3: The simulation setup in Section 6.6.

where J_0 is the zeroth-order Bessel function and f_d is the maximum Doppler frequency [19].

The simulation setup in Section 4.5 is also adopted in this chapter, and illustrated in Fig. 6.3. A seven-cell system is assumed with a single active user per cell. Each base station has $N_t = 8$ antennas while each user has a single antenna. The mobile terminal is assumed to be located close to the cell edge and travelling with a velocity v. The cell at the center of the grid is considered, whose user receives the desired signal from its own base station and interference from the six neighboring cells as shown in Fig. 6.3. The radius of each cell, R, is assumed to be 500 m (Chapter 4 considered a radius of 400 m). The path loss between the base stations and the mobile user is modeled using the COST 231 Walfish-Ikegami NLOS model [1], adopted for urban microcells, and is given in (4.26). The transmit power is $E_s = 3$ dBW

for all the base stations and the noise power is given by -144 dBW. The delay associated with the feedback of CSI to the desired base station is modeled by one frame duration and that with the exchange of CSI over the backhaul link connecting the desired and interfering base stations by two frame durations. The simulation parameters are summarized in Table 4.1.

The proposed subspace-tracking approach requires the feedback of unit-norm directions of error vectors using joint quantization. The GPC algorithm in [43] involves the feedback of both the directions and norm of the tangent vectors, and GPC with step-size optimization (in [44]) also requires the feedback of the optimized step-size. In this section, codebooks associated with the feedback of unit-norm directions (of either tangent or error vectors) are generated using RVQ. The codebooks for quantizing the magnitude of the tangent vectors are designed along what was done in [43, 44]. Uniform codebooks are generated for the interval $[0, 1]$ using 2 bits per channel norm, implying a total of 14 *additional* bits for the case when all the interferers are mitigated. Note that it is sufficient to consider a quantization interval of $[0, 1]$ since the norm of the tangent vector, $\tan^{-1}(d/|\rho|) = \tan^{-1}(\sqrt{1-|\rho|^2}/|\rho|)$ can be obtained by feeding back $|\rho| \in [0, 1]$. Further, on the lines of [44], we assume that full information of the prediction step-size is available at the base stations.

The data rates obtained for ICIN using the proposed prediction algorithm, linear prediction, GPC with step-size optimization in [44], joint feedback in Chapter 5, the separate CSI quantization in Chapter 4 and equal-bit allocation (EBA) are compared in Fig. 6.4, for $v = 3$ mph and RVQ. For

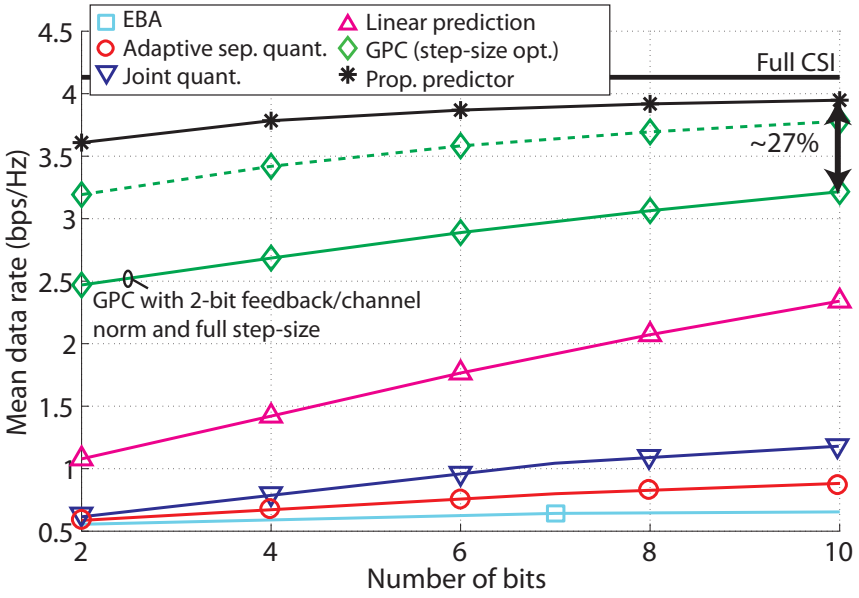

Figure 6.4: Comparison of the data rates obtained using predictive quantization and other multicell limited feedback approaches.

GPC, the prediction step-size is optimized using the approach described in [44]. *Note that the three prediction strategies use the selection criterion derived in this chapter* (refer to (6.17)). The number of times prediction is carried out, i.e., the error is allowed to propagate, before reinitializing the CSI is fixed at 10. It is seen that CSI prediction yields significantly better performance as compared to the joint and separate quantization approaches, over all values of B_{tot}. Further, even $B_{\text{tot}} = 10$ is sufficient to yield data rates reasonably close to the full CSI data rate, using the proposed subspace-tracking approach. Note that GPC with full tangent vector magnitude performs reasonably close to the algorithm presented in this chapter. When the error vector magnitude is quantized using 2 bits per channel (thus, 14 *additional* bits) the performance

of GPC drops and is about 27% away from that of the proposed technique.

Linear prediction yields data rates that are smaller than the other two strategies due to the inherent drawback of not being a good alternative for long-range prediction. It is seen that EBA yields the worst performance of all the strategies compared in Fig. 6.4, as expected. This is followed by the adaptive separate quantization technique in Chapter 4, which requires a higher number of feedback bits to attain data rate comparable that of full CSI. The significant gains in data rate from joint CSI prediction come at the price of much higher complexity, particularly at the user terminal. This is in contrast to adaptive separate quantization, which is relatively low-complexity. The data rates in Fig. 6.4 increase with increased complexity.

Fig. 6.5 illustrates the gains that can be obtained from designing beamforming vectors to null out only the effective interferers, for the similar setup in Fig. 6.4. The three prediction approaches use the selection criterion derived in (6.17)). While the performance of all the three prediction techniques increases considerably, it is seen that the proposed subspace-tracking algorithm approaches the full CSI data rate for as low as $B_{\text{tot}} = 6$ bits. Note that in comparison, separate quantization approaches require a very large amount of feedback to compensate for low complexity.

Finally, the performance of the proposed subspace-tracking prediction is shown in Fig. 6.6 as a function of the number of predictions carried out before reinitialization for $v = 3$ mph and a user at the cell-edge. From Fig. 6.6, it is clear that the data rate falls as the number of predictions increase, due

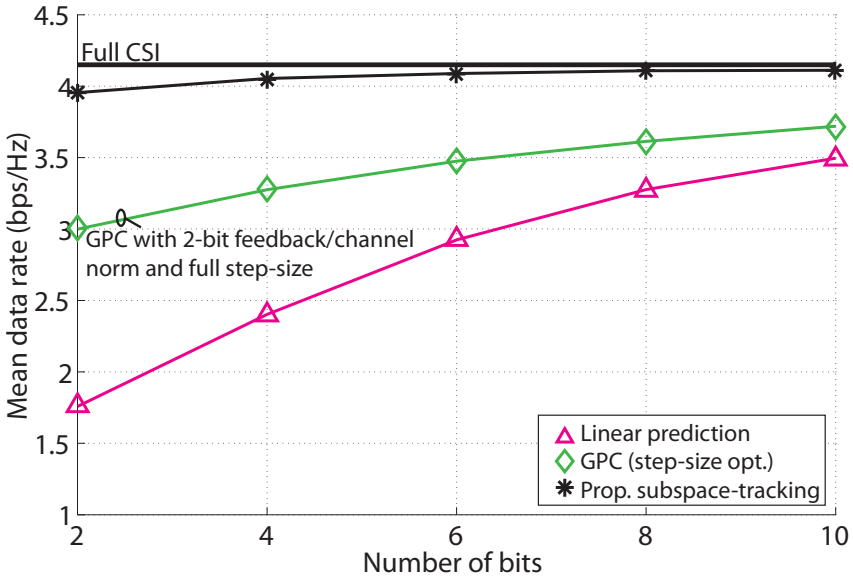

Figure 6.5: Comparison of the data rates obtained using predictive quantization and GPC, when beamforming is performed using only the effective interferers.

to error propagation. As expected, the data rate at higher velocities is more sensitive to the number of predictions. This is because the errors associated with quickly varying channels are larger to begin with, and hence, add up more quickly at every prediction. The data rate floor at $v = 30$ mph occurs due to large quantization error at higher velocities.

6.7 Conclusion

In this chapter, a joint predictive quantization technique was proposed for limited CSI feedback in multicell cooperation. The feedback model was presented, where users transmit only the error vectors between the actual

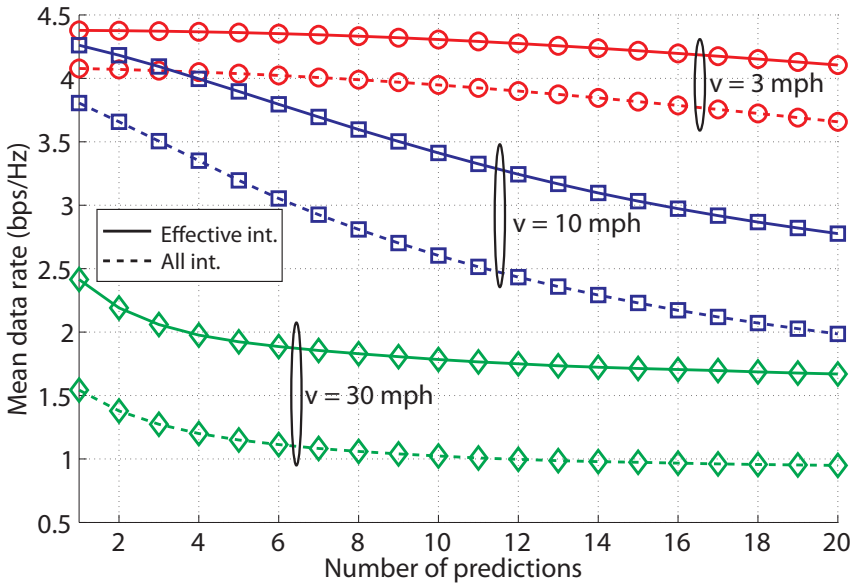

Figure 6.6: Variation of the data rates obtained using the proposed predictive CSI quantization as a function of the number of predictions.

and predicted channels over the uplink. Joint quantization was considered for feeding back the error vectors together. A selection criterion was derived to choose appropriate codewords by introducing an inherent bias, which is a function of the signal strengths and delays of the channels. The idea is that stronger channels are quantized with a higher resolution by ensuring a closer alignment to the codeword as compared to the weaker channels. The selection criterion derived is universal in that it can be used for most multicell cooperative strategies, predictors and channel statistics. A predictor on the Grassmann manifold was also presented. Simulation results showed that joint predictive quantization can yield significant performance gains over separate quantization approaches.

6.8 Appendices

6.8.1 Proof of Proposition 6.4.1

From (6.14), $R_{k,(\mathrm{d})}[n]$ is given as

$$R_{k,(\mathrm{d})}[n] = \log_2 \left(\frac{|(\mathbf{h}_k^{\mathrm{p,full}})^*[n+D_k]\mathbf{f}_k[n+D_k]|^2}{|(\mathbf{h}_k^{\mathrm{p,full}})^*[n+D_k]\mathbf{f}_k^{\mathrm{p}}[n+D_k]|^2} \right).$$

Dropping the time index $n + D_k$ for convenience, $R_{k,(\mathrm{d})}[n]$ can rewritten in terms of the channel directions as

$$\log_2 \left(\frac{|(\mathbf{h}_k^{\mathrm{p,full}})^*\mathbf{f}_k|^2}{|(\mathbf{h}_k^{\mathrm{p,full}})^*\mathbf{f}_k^{\mathrm{p}}|^2} \right) = \log_2(|(\tilde{\mathbf{h}}_k^{\mathrm{p,full}})^*\mathbf{f}_k|^2) - \log_2(|(\tilde{\mathbf{h}}_k^{\mathrm{p,full}})^*\mathbf{f}_k^{\mathrm{p}}|^2) \ . \tag{6.23}$$

By defining the angle $\angle(\mathbf{x}, \mathbf{y}) \in [0, \frac{\pi}{2}]$ between two vectors $\mathbf{x}$ and $\mathbf{y}$ as $\angle(\mathbf{x}, \mathbf{y}) = \cos^{-1} |\mathbf{x}^*\mathbf{y}|$, the triangle inequality for angles [90] yields

$$\angle(\tilde{\mathbf{h}}_k^{\mathrm{p,full}}, \mathbf{f}_k^{\mathrm{p}}) \leq \angle(\tilde{\mathbf{h}}_k^{\mathrm{p,full}}, \tilde{\mathbf{h}}_k^{\mathrm{p}}) + \angle(\tilde{\mathbf{h}}_k^{\mathrm{p}}, \mathbf{f}_k^{\mathrm{p}}). \tag{6.24}$$

If the number of quantization bits is sufficiently large, $\angle(\tilde{\mathbf{h}}_k^{\mathrm{p,full}}, \tilde{\mathbf{h}}_k^{\mathrm{p}}) \approx 0$. Further, for ICIN $\angle(\tilde{\mathbf{h}}_k^{\mathrm{p}}, \mathbf{f}_k^{\mathrm{p}}) << \frac{\pi}{2}$. Hence, it is reasonable to assume that $\angle(\tilde{\mathbf{h}}_k^{\mathrm{p,full}}, \tilde{\mathbf{h}}_k^{\mathrm{p}}) + \angle(\tilde{\mathbf{h}}_k^{\mathrm{p}}, \mathbf{f}_k^{\mathrm{p}}) < \frac{\pi}{2}$. Therefore, $|(\tilde{\mathbf{h}}_k^{\mathrm{p,full}})^*\mathbf{f}_k^{\mathrm{p}}|^2 = \cos^2(\angle(\tilde{\mathbf{h}}_k, \mathbf{f}_k^{\mathrm{p}}))$ is lower bounded by

$$\begin{aligned}
|(\tilde{\mathbf{h}}_k^{\mathrm{p,full}})^*\mathbf{f}_k^{\mathrm{p}}|^2 &= \cos^2(\angle(\tilde{\mathbf{h}}_k^{\mathrm{p,full}}, \mathbf{f}_k^{\mathrm{p}})) \\
&\geq \Big[\cos(\angle(\tilde{\mathbf{h}}_k^{\mathrm{p,full}}, \tilde{\mathbf{h}}_k^{\mathrm{p}}))\cos(\angle(\tilde{\mathbf{h}}_k^{\mathrm{p}}, \mathbf{f}_k^{\mathrm{p}})) \\
&\qquad - \sin(\angle(\tilde{\mathbf{h}}_k^{\mathrm{p,full}}, \tilde{\mathbf{h}}_k^{\mathrm{p}}))\sin(\angle(\tilde{\mathbf{h}}_k^{\mathrm{p}}, \mathbf{f}_k^{\mathrm{p}}))\Big]^2 \qquad (6.25) \\
&\approx \Big[\cos(\angle(\tilde{\mathbf{h}}_k^{\mathrm{p,full}}, \tilde{\mathbf{h}}_k^{\mathrm{p}}))\cos(\angle(\tilde{\mathbf{h}}_k^{\mathrm{p}}, \mathbf{f}_k^{\mathrm{p}}))\Big]^2 \qquad (6.26) \\
&= |(\tilde{\mathbf{h}}_k^{\mathrm{p,full}})^*\tilde{\mathbf{h}}_k^{\mathrm{p}}|^2 |(\tilde{\mathbf{h}}_k^{\mathrm{p}})^*\mathbf{f}_k^{\mathrm{p}}|^2 \qquad (6.27)
\end{aligned}$$

where (6.26) is obtained from (6.25) by ignoring $\sin(\angle(\tilde{\mathbf{h}}_k^{\mathrm{p,full}}, \tilde{\mathbf{h}}_k^{\mathrm{p}}))\sin(\angle(\tilde{\mathbf{h}}_k^{\mathrm{p}}, \mathbf{f}_k^{\mathrm{p}}))$, since $\sin(\angle(\tilde{\mathbf{h}}_k^{\mathrm{p,full}}, \tilde{\mathbf{h}}_k^{\mathrm{p}}))$ will be negligible for a good quantization scheme.

Substituting (6.27) in (6.23), we get

$$\log_2\left(\frac{|(\mathbf{h}_k^{\mathrm{p,full}})^*\mathbf{f}_k|^2}{|(\mathbf{h}_k^{\mathrm{p,full}})^*\mathbf{f}_k^{\mathrm{p}}|^2}\right) \leq \log_2\left(\frac{|\mathbf{h}_k^{\mathrm{p,full}*}\mathbf{f}_k|^2}{|\mathbf{h}_k^{\mathrm{p}*}\mathbf{f}_k^{\mathrm{p}}|^2}\right) - \log_2\left(|(\tilde{\mathbf{h}}_k^{\mathrm{p,full}})^*\tilde{\mathbf{h}}_k^{\mathrm{p}}|^2\right) \tag{6.28}$$

6.8.2 Proof of Proposition 6.4.2

From (6.14), $R_{k,(\mathrm{i})}[n]$ is given as

$$R_{k,(\mathrm{i})}[n] = \log_2\left(\frac{1+\sum_{\substack{\ell=1\\ \ell\neq k}}^{K}\alpha_{k,\ell}\rho_k|(\mathbf{g}_{k,\ell}^{\mathrm{p,full}})^*[n+\overline{D}_k]\mathbf{f}_\ell^{\mathrm{p}}[n+\overline{D}_k]|^2}{1+\sum_{\substack{\ell=1\\ \ell\neq k}}^{K}\alpha_{k,\ell}\rho_k|(\mathbf{g}_{k,\ell}^{\mathrm{p,full}})^*[n+\overline{D}_k]\mathbf{f}_\ell[n+\overline{D}_k]|^2}\right).$$

Dropping the time index $n+\overline{D}_k$ for convenience, $R_{k,(\mathrm{i})}[n]$ can be rewritten as

$$R_{k,(\mathrm{i})}[n] = \log_2\left(\frac{1+\sum_{\substack{\ell=1\\ \ell\neq k}}^{K}\alpha_{k,\ell}\rho_k|(\mathbf{g}_{k,\ell}^{\mathrm{p,full}})^*\mathbf{f}_\ell^{\mathrm{p}}|^2}{1+\sum_{\substack{\ell=1\\ \ell\neq k}}^{K}\alpha_{k,\ell}\rho_k|(\mathbf{g}_{k,\ell}^{\mathrm{p,full}})^*\mathbf{f}_\ell|^2}\right).$$

Using the triangle inequality again [90],

$$\begin{aligned}\angle(\tilde{\mathbf{g}}_{k,\ell}^{\mathrm{p,full}}, \mathbf{f}_k^{\mathrm{p}}) &\geq |\angle(\tilde{\mathbf{g}}_{k,\ell}^{\mathrm{p,full}}, \tilde{\mathbf{g}}_{k,\ell}^{\mathrm{p}}) - \angle(\tilde{\mathbf{g}}_{k,\ell}^{\mathrm{p}}, \mathbf{f}_k^{\mathrm{p}})| \\ &= |\angle(\tilde{\mathbf{g}}_{k,\ell}^{\mathrm{p,full}}, \tilde{\mathbf{g}}_{k,\ell}^{\mathrm{p}}) - \frac{\pi}{2}| \end{aligned} \tag{6.29}$$

where (6.29) follows from the fact that in ICIN, the beamforming vector, $\mathbf{f}_\ell^{\mathrm{p}}$ is designed to be orthogonal to $\tilde{\mathbf{g}}_{k,\ell}^{\mathrm{p}}$, i.e., $\angle(\tilde{\mathbf{g}}_{k,\ell}^{\mathrm{p}}, \mathbf{f}_k^{\mathrm{p}}) = \frac{\pi}{2}$. Therefore,

$$\sin^2(\angle(\tilde{\mathbf{g}}_{k,\ell}^{\mathrm{p,full}}, \mathbf{f}_k^{\mathrm{p}})) \geq \cos^2(\angle(\tilde{\mathbf{g}}_{k,\ell}^{\mathrm{p,full}}, \tilde{\mathbf{g}}_{k,\ell}^{\mathrm{p}})) \tag{6.30}$$

Dropping the time index $n + \overline{D}_k$ we upper bound $R_{k,(\mathrm{i})}$ as

$$R_{k,(\mathrm{i})} = \log_2 \left(\frac{1 + \sum_{\substack{\ell=1 \\ \ell \neq k}}^{K} \alpha_{k,\ell} \rho_k |(\mathbf{g}_{k,\ell}^{\mathrm{p,full}})^* \mathbf{f}_\ell^{\mathrm{p}}|^2}{1 + \sum_{\substack{\ell=1 \\ \ell \neq k}}^{K} \alpha_{k,\ell} \rho_k |(\mathbf{g}_{k,\ell}^{\mathrm{p,full}})^* \mathbf{f}_\ell|^2} \right) \tag{6.31}$$

$$\leq \log_2 \left(1 + \sum_{\substack{\ell=1 \\ \ell \neq k}}^{K} \alpha_{k,\ell} \rho_k |(\mathbf{g}_{k,\ell}^{\mathrm{p,full}})^* \mathbf{f}_\ell^{\mathrm{p}}|^2 \right) \tag{6.32}$$

$$\leq \log_2 \left(1 + \sum_{\substack{\ell=1 \\ \ell \neq k}}^{K} \alpha_{k,\ell} \rho_k |\mathbf{g}_{k,\ell}^{\mathrm{p,full}}|^2 (1 - |(\tilde{\mathbf{g}}_{k,\ell}^{\mathrm{p,full}})^* \tilde{\mathbf{g}}_{k,\ell}^{\mathrm{p}}|^2) \right) \tag{6.33}$$

where (6.33) follows from (6.30).

6.8.3 Proof of Proposition 6.5.1

Using the state-space model in [71], the tangent vector between $\mathbf{h}_k^{\mathrm{r}}[n-1]$ and $\mathbf{h}_k^{\mathrm{r}}[n]$ is defined as

$$\begin{aligned}
\mathbf{v}(\mathbf{h}_k^{\mathrm{r}}[n-1], \mathbf{h}_k^{\mathrm{r}}[n]) &= [-\mathbf{h}_k^{\mathrm{r}}[n-1] \sin(\|\mathbf{v}(\mathbf{h}_k^{\mathrm{r}}[n-2], \mathbf{h}_k^{\mathrm{r}}[n-1])\|) \\
&+ \frac{\mathbf{v}(\mathbf{h}_k^{\mathrm{r}}[n-2], \mathbf{h}_k^{\mathrm{r}}[n-1])}{\|\mathbf{v}(\mathbf{h}_k^{\mathrm{r}}[n-1], \mathbf{h}_k^{\mathrm{r}}[n])\|} \cos(\|\mathbf{v}(\mathbf{h}_k^{\mathrm{r}}[n-1], \mathbf{h}_k^{\mathrm{r}}[n])\|) \Big] \|\mathbf{v}(\mathbf{h}_k^{\mathrm{r}}[n-2], \mathbf{h}_k^{\mathrm{r}}[n-1])\| \\
&+ (\mathbf{I}_{N_t} - \mathbf{h}_k^{\mathrm{r}}[n](\mathbf{h}_k^{\mathrm{r}}[n])^*) \mathbf{w}_k[n],
\end{aligned}$$

where $\mathbf{w}_k[n]$ corresponds to Gaussian noise with zero-mean and unit-variance. Since the MMSE predictor for $\mathbf{v}(\mathbf{h}_k^{\mathrm{r}}[n-1], \mathbf{h}_k^{\mathrm{r}}[n])$, $\mathbf{v}^{\mathrm{p}}(\mathbf{h}_k^{\mathrm{r}}[n-1], \mathbf{h}_k^{\mathrm{r}}[n])$ will be equal to its mean,

$$\begin{aligned}
\mathbf{v}^{\mathrm{p}}(\mathbf{h}_k^{\mathrm{r}}[n-1], \mathbf{h}_k^{\mathrm{r}}[n]) &= [-\mathbf{h}_k^{\mathrm{r}}[n-1] \sin(\|\mathbf{v}(\mathbf{h}_k^{\mathrm{r}}[n-2], \mathbf{h}_k^{\mathrm{r}}[n-1])\|) \\
&+ \frac{\mathbf{v}(\mathbf{h}_k^{\mathrm{r}}[n-2], \mathbf{h}_k^{\mathrm{r}}[n-1])}{\mathbf{v}(\mathbf{h}_k^{\mathrm{r}}[n-1], \mathbf{h}_k^{\mathrm{r}}[n])\|} \cos(\|\mathbf{v}(\mathbf{h}_k^{\mathrm{r}}[n-1], \mathbf{h}_k^{\mathrm{r}}[n])\|) \Big] \|\mathbf{v}(\mathbf{h}_k^{\mathrm{r}}[n-2]. \quad (6.34)
\end{aligned}$$

Now, from [43], $\|\mathbf{v}(\mathbf{h}_k^{\mathrm{r}}[n-2], \mathbf{h}_k^{\mathrm{r}}[n-1])\| = \tan^{-1}(d_o/\rho_o)$ and the unit-norm direction, $\frac{\mathbf{v}(\mathbf{h}_k^{\mathrm{r}}[n-2], \mathbf{h}_k^{\mathrm{r}}[n-1])}{\|\mathbf{v}(\mathbf{h}_k^{\mathrm{r}}[n-2], \mathbf{h}_k^{\mathrm{r}}[n-1])\|} = \frac{\mathbf{h}_k^{\mathrm{r}}[n-1]/\rho_o - \mathbf{h}_k^{\mathrm{r}}[n-2]}{d_o/\rho_o}$. Substituting in (6.34), $\mathbf{v}^{\mathrm{p}}(\mathbf{h}_k^{\mathrm{r}}[n-1], \mathbf{h}_k^{\mathrm{r}}[n])$ is obtained as

$$\mathbf{v}^{\mathrm{p}}(\mathbf{h}_k^{\mathrm{r}}[n-1], \mathbf{h}_k^{\mathrm{r}}[n]) = \mathbf{h}_k^{\mathrm{r}}[n-1]\frac{\cos(|\rho_1|)}{\rho_1} - \mathbf{h}_k^{\mathrm{r}}[n-2]\left(\sin(d_1)\frac{d_1}{|\rho_1|} + \cos(|\rho_1|)\right),$$

using the trigonometric relations that for $d_o, \rho_o \leq 1, \sin(\tan^{-1}(d_o/\rho_o)) = \sin(d_o)$ and $\cos(\tan^{-1}(d_o/\rho_o)) = \cos(\rho_o)$.

Chapter 7

Conclusion

7.1 Summary

In this dissertation, we proposed limited feedback strategies for multicell MISO systems using partial cooperation, known as coordinated beamforming in the 3GPP LTE Advanced literature. We first discussed the challenges associated with limited feedback in multicell cooperative systems, where the CSI of multiple channels is required to be fed back over the a finite-bandwidth link. We then presented three different approaches for feeding back the CSI of multiple channels over the feedback link.

The first approach proposed for multicell cooperative limited feedback is referred to as *separate quantization* as it involves the quantization and feedback of the different channels using individual codebooks. We motivated the problem of partitioning the available feedback bits among different channels using a single-interferer system based on the Wyner model. We derived closed-form expressions to allocate bits adaptively among the desired and interfering channels, based on their respective signal strengths, for generalized eigenvector beamforming. While the single-interferer and zero-delay system was helpful to understand limited feedback in cooperative networks, it does not offer a

realistic depiction of cellular systems.

We considered a more practical scenario where each user faced interference from multiple interferers and communication links were associated with finite non-zero delays. For inter-cell interference nulling, we defined a set of *effective interferers*, which is a function of the number of feedback bits available, relative signal strengths and temporal correlations of each channel. We derived closed-form expressions to partition feedback resources only among the desired channel and effective interferers in a waterfilling fashion. Stronger channels with smaller delays are assigned more bits than weaker channels with larger delays. The idea is to make the most efficient use of the available feedback bits by using them to finely quantize those channels that will affect data rate the most. Using simulations, we showed that the proposed separate quantization algorithms yield higher data rates than equal bit allocation techniques.

The second approach proposed for multicell cooperative limited feedback is *joint quantization*, where the CSI of multiple channels is quantized as a net channel vector, using a single codebook. We derived a *selection criterion* to select codewords that are more closely aligned to stronger channels as compared to the weaker ones. Hence, channels that can impact the data rates significantly are quantized with a finer resolution than those that do not. We used simulations to show that the data rates obtained using the proposed selection criterion with joint quantization are higher than those from separate quantization. We also discussed the disadvantages associated with jointly quantizing CSI, which include the need for specially designed codebooks and

the storage of a large number of codebooks at the user terminal.

The final approach presented in this dissertation is *predictive joint quantization*, where temporal correlation is exploited to reduce the large feedback requirements associated with feeding back multiple channels. We proposed transmitter and receiver structures for predictive limited feedback in systems with multiple interferers and non-zero delays. Since the error vectors from predictive quantization are fed back jointly as a net error vector, we derived a selection criterion to increase the data rates that can be attained. Further, we developed a technique based on subspace tracking of CSI on the Grassmann manifold. Simulations are used to show that the proposed strategy can yield significant improvements in the data rate, at the cost of considerable complexity at the receiver side.

7.2 Future Work

Since multicell limited feedback is a relatively new area, this dissertation establishes the ground for several directions of future work, some of which are listed below.

- **Codebook Design** - Joint and predictive quantization can potentially yield high data rates with small feedback requirements in multicell cooperative systems, if multiple CSI codebooks can be suitably designed. These codebooks should consider the relative strengths of the different channels being fed back, spatial and temporal correlation among the

different channels. This, however, implies that a large number of codebooks should be stored at the receiver terminal corresponding to different combinations of channel strengths and correlations, which leads to implementation issues. Future work could include developing universal codebooks that will yield performance gains for all the ranges of signal strengths.

- **Limited Feedback for MIMO Cooperation** - This dissertation focused on MISO systems and dealt with the feedback of channel vectors. Extending this to multiple antennas will be relevant for the upcoming wireless communication systems. Since precoding matrices will be designed at the base station in cooperative systems, users will not be able to feedback beamforming vectors (or precoding matrices) and will have to rely on CSI (matrix) quantization. Further, high quality CSI will be required at the base stations to avoid interference between the different transmission streams, which could render the entire system to be highly sensitive to delay. This could lead to large feedback requirements for cooperative MIMO systems, which will increase with the number of antennas employed at the base stations and receivers. Future work can include investigating efficient MIMO limited feedback techniques for multicell cooperation.

- **Simultaneous Transmission to Multiple Users** - The assumption of a single user per cell can be relaxed to allow multiple users in each

cell. While it will provide a more practical scenario, developing limited feedback strategies for this scenario will involve the feeding back a larger number of channels, since each user will have to feedback CSI of not only the desired channel and the interference it receives from other base stations, but also the CSI of the interference it sees from the transmissions to other users within its own cell.

Bibliography

[1] 3GPP Technical Specification Group. Spatial channel model, SCM-134 text V6.0. Technical report, Spatial Channel Model AHG (Combined ad-hoc from 3GPP and 3GPP2), Apr. 2003.

[2] 3GPP, TR 36.814. Further advancements for E-UTRA; physical layer aspects. Technical report, 2008.

[3] 3rd Generation Partnership Project (3GPP). UTRA-UTRAN long term evolution (LTE). Technical report, Nov. 2004.

[4] S. Akoum and R. W. Heath, Jr. Limited feedback beamforming for temporally correlated MIMO channels with other cell interference. *Proc. IEEE International Conference on Acoustics, Speech, and Signal Processing*, pages 3054–3057, Mar. 2010.

[5] S. H. Ali and V. C. M. Leung. Dynamic frequency allocation in fractional frequency reused OFDMA networks. *IEEE Transactions on Wireless Communications*, 8(8):4286–4295, Aug. 2009.

[6] C. K. Au-Yeung and D. J. Love. On the performance of random vector quantization limited feedback beamforming in a MISO system. *IEEE Transactions on Wireless Communications*, 6(2):458–462, Feb. 2007.

[7] K. E. Baddour and N. C. Beaulieu. Autoregressive modeling for fading channel simulations. *IEEE Transactions on Wireless Communications*, 4(4):1650–1662, Jul. 2005.

[8] R. Bendlin, Y.-F. Huang, M. T. Ivriac, and J. A. Nossek. Fast distributed multi-cell scheduling with delayed limited-capacity backhaul links. *Proc. IEEE International Conference on Communications*, pages 1–5, Jun. 2009.

[9] R. Bhagavatula and R. W. Heath, Jr. Adaptive limited feedback for sum-rate maximizing beamforming in cooperative multicell systems. *IEEE Transactions on Signal Processing*, accepted, Oct. 2010.

[10] R. Bhagavatula and R. W. Heath, Jr. Adaptive bit partitioning for multicell intercell interference cancellation with delayed limited feedback. *IEEE Transactions on Signal Processing*, submitted, July 2010.

[11] R. Bhagavatula and R. W. Heath, Jr. Joint predictive CSI quantization for intercell interference nulling. In preparation for submission to *IEEE Transactions on Signal Processing*, 2010.

[12] R. Bhagavatula, B. Rao, and R. W. Heath, Jr. Limited feedback with joint CSI quantization for multicell cooperative generalized eigenvector beamforming. *Proc. IEEE International Conference on Acoustics, Speech and Signal Processing*, pages 2838 - 2841, Mar. 2010.

[13] F. Boccardi, H. Huang, and A. Alexiou. Hierarchical quantization and its application to multiuser eigenmode transmissions for MIMO broadcast

channels with limited feedback. *Proc. IEEE International Symposium on Personal, Indoor and Mobile Radio Communications*, pages 1–5, Sept. 2007.

[14] M. Borga. *Learning Multidimensional Signal Processing.* Ph.D. thesis, Linkoping University, Sweden, SE-581 83 Linkoping, Sweden, 1998.

[15] P. J. Brockwell and R. A. Davis. *Introduction to Time Series and Forecasting.* Springer-Verlag New York, Inc., 2000.

[16] V. R. Cadambe and S. A. Jafar. Interference alignment and degrees of freedom of the K-user interference channel. *IEEE Transactions on Information Theory*, 54(8):3425–3441, Aug. 2008.

[17] W. Choi and J. G. Andrews. The capacity gain from intercell scheduling in multi-antenna systems. *IEEE Transactions on Wireless Communications*, 7(2):714–725, Feb. 2008.

[18] W. Choi, A. Forenza, J. G. Andrews, and R. W. Heath, Jr. Opportunistic space-division multiple access with beam selection. *IEEE Transactions on Communications*, 55(12):2371–2380, Dec. 2007.

[19] R. H. Clarke. A statistical theory of mobile-radio reception. *Bell System Technical Journal*, 47:957–1000, 1968.

[20] F. Daum. Nonlinear filters: Beyond the Kalman filter. *IEEE Aerospace and Electronic Systems Magazine*, 20(8):57–69, Aug. 2005.

[21] P. M. Djuric, J. H. Kotecha, J. Zhang, Y. Huang, T. Ghirmai, M. F. Bugallo, and J. Miguez. Particle filtering. *IEEE Signal Processing Magazine*, 20(5):19–38, Sept. 2003.

[22] A. Duel-Hallen, S. Hu, and H. Hallen. Long range prediction of fading signals. *IEEE Signal Processing Magazine*, 17(3):62–75, May 2000.

[23] A. Edelman, T. A. Arias, and S. T. Smith. The geometry of algorithms with orthogonality constraints. *SIAM Journal on Matrix Analysis and Applications*, 20(2):303–353, Apr. 1999.

[24] J. M. Ekbal and A. Cioffi. Distributed transmit beamforming in cellular networks - a convex optimization perspective. *Proc. IEEE International Conference on Communications*, volume 4, pages 2690–2694, May 2005.

[25] T. Ekman, G. Kubin, M. Sternad, and A. Ahlen. Quadratic and linear filters for radio channel propagation. *Proc. IEEE Vehicular Technology Conference*, pages 146–150, Sept. 1999.

[26] G. Nemes. New asymptotic expansion for the Gamma function. *Archiv der Mathematik*, 95(2):161–169, 2010.

[27] A. Gersho and R. M. Gray. *Vector Quantization and Signal Compression*. Kluwer Academic Publishers, 1993.

[28] K. Gokbayrak and C. G. Cassandras. Stochastic discrete optimization using a surrogate problem methodology. *Proc. IEEE Conference on Decision & Control*, pages 1779–1784, Dec. 1999.

[29] M. Grieger, P. Marsch, and G. Fettweis. Ad Hoc Cooperation for the Cellular Uplink with Capacity Constrained Backhaul. *Proc. IEEE International Conference on Communications*, pages 1–5, May 2010.

[30] I. S. Gradshteyn and I. M. Ryzhik. *Tables of Integrals, Series and Products*. Academic Press, 7 edition, 2007.

[31] H.-M. Hang and J. Woods. Predictive vector quantization of images. *IEEE Transactions on Communications*, 33(11):1208–1219, Nov. 1985.

[32] A. Haoui and D. Messerschmitt. Predictive vector quantization. *Proc. IEEE International Conference on Acoustics, Speech and Signal Processing*, pages 420–423, Mar. 1984.

[33] B. Hassibi and B. M. Hochwald. How much training is needed in multiple-antenna wireless links. *IEEE Transactions on Information Theory*, 49(4): 951–963, Apr. 2003.

[34] S. Haykin. *Adaptive Filter Theory*. Prentice-Hall, Englewood Cliffs, NJ, USA, 3rd edition edition, 1996.

[35] A. Heidari, A. K. Khandani, and D. McAvoy. Adaptive modelling and long-range prediction of mobile fading channels. *Institution of Engineering and Technology Communications*, 4(1):39–50, Jan. 2010.

[36] A. Hewitt, W. H. Lau, J. Austin, and E. Vilar. An autoregressive approach to the identification of multipath ray parameters from field mea-

surements. *IEEE Transactions on Communications*, 37(11):1136–1143, Nov. 1989.

[37] S. J. Howard and K. Pahlavan. Autoregressive modeling of wideband indoor radio propagation. *IEEE Transactions on Communications*, 40(9):1540–1552, Sept. 1992.

[38] J. Hoydis, M. Kobayashi, and M. Debbah On the optimal number of cooperative base stations in network MIMO systems. *IEEE Transactions on Signal Processing*, submitted, Mar. 2010.

[39] G. Hu, F. Jiang, Y. Wang, Y. Xu, and P. Zhang. On the performance of a multi-user multi-antenna system with transmit zero-forcing beamforming and feedback delay. *Proc. IEEE Wireless Communications and Networking Conference*, pages 1821–1825, Mar. 2008.

[40] H. Huang and M. Trivellato. Performance of multiuser MIMO and network coordination in downlink cellular networks. *Proc. IEEE International Symposium on Modeling and Optimization in Mobile, Ad Hoc, and Wireless Networks and Workshops*, pages 85–90, Apr. 2008.

[41] K. Huang, J. G. Andrews, and R. W. Heath, Jr. Performance of orthogonal beamforming for SDMA with limited feedback. *IEEE Transactions on Vehicular Technology*, 58(1):152–164, Jan. 2009.

[42] K. Huang, R. W. Heath, Jr., and J. G. Andrews. Limited feedback beamforming over temporally-correlated channels. *IEEE Transactions*

on Signal Processing, 57(5):1959–1975, May 2009.

[43] T. Inoue and R. W. Heath, Jr. Grassmannian predictive coding for delayed limited feedback MIMO systems. *Proc. IEEE Allerton Conference on Signals, Systems, and Computers*, pages 738–788, 2009.

[44] T. Inoue and R. W. Heath, Jr. Predictive coding on the Grassmann manifold. *IEEE Transactions on Signal Processing*, submitted, Aug. 2009.

[45] Y. Isukapalli and B. D. Rao. Finite rate feedback for spatially and temporally correlated MISO channels in the presence of estimation errors and feedback delay. *Proc. IEEE Global Telecommunications Conference*, pages 2791–2795, Nov. 2007.

[46] S. A. Jafar, G. J. Foschini, and A. J. Goldsmith. PhantomNet: Exploring optimal multicellular multiple antenna systems. *EURASIP Journal of Applied Signal Proccessing*, 2004:591–604, 2004.

[47] W. C. Jakes. *Microwave Mobile Communications*. IEEE Press, New York, 1974.

[48] N. Jindal. A high SNR analysis of MIMO broadcast channels. *Proc. IEEE International Symposium on Information Theory*, pages 2310–2314, Sept. 2005.

[49] N. Jindal. MIMO broadcast channels with finite-rate feedback. *IEEE Transactions on Information Theory*, 52(11):5045–5060, Nov. 2006.

[50] S. Jing, D. N. C. Tse, J. B. Soriaga, J. Hou, J. E. Smee, and R. Adovani. Multicell downlink capacity with coordinated processing. *EURASIP Journal of Wireless Communications and Networking*, 2008:19 pages, 2008.

[51] E. Jorswieck, E. G. Larsson, and D. Danev. Complete characterization of the pareto boundary for the MISO interference channel. *IEEE Transactions on Signal Processing*, 56(10):5292–5296, Oct. 2008.

[52] V. Jungnickel, T. Wirth, M. Schellmann, T. Haustein, and W. Zirwas. Synchronization of cooperative base stations. *Proc. IEEE International Symposium on Wireless Communication Systems*, pages 329–334, Oct. 2008.

[53] V. Jungnickel, L. Thiele, T. Wirth, T. Haustein, S. Schiffermuller, et.al. Coordinated multipoint trials in the downlink. *Proc. IEEE Global Communications Conference*, pages 1–7, Nov./Dec. 2009.

[54] M. Kang, L. Yang, and M.-S. Alouini. Capacity of MIMO channels in the presence of co-channel interference. *Wireless Communications and Mobile Computing*, 7(1):113–125, Mar. 2006.

[55] J. H. Kim, W. Zirwas, and M. Haardt. Efficient feedback via subspace-based channel quantization for distributed cooperative antenna systems with temporally correlated channels. *EURASIP Journal on Advances in Signal Processing*, 2008:13 pages, 2008.

[56] T. Koivisto, K. Schober, T. Kuosmanen, T. Roman, and M. Enescu. Reference signal design for flexible MIMO operation in LTE-Advanced downlink. *Proc. IEEE Vehicular Technology Conference*, pages 1–5, May 2010.

[57] K. Kim, I. H. Kim, and D. J. Love. Utilizing temporal correlation in multiuser MIMO feedback. *Proc. IEEE Asilomar Conference on Signals, Systems, and Computers*, pages 121–125, Oct. 2008.

[58] B. O. Lee, H. W. Je, O.-S. Shin, and K. B. Lee. A novel uplink MIMO transmission scheme in a multicell environment. *IEEE Transactions on Wireless Communications*, 8(10):4981–4987, Oct. 2009.

[59] B. O. Lee, H. W. Je, I. Sohn, O.-S. Shin, and K. B. Lee. Interference-aware decentralized precoding for multicell MIMO TDD systems. *Proc. IEEE Global Telecommunications Conference*, pages 1–5, Dec. 2008.

[60] Y. Liang and A. Goldsmith. Symmetric rate capacity of cellular systems with cooperative base stations. *Proc. IEEE Global Telecommunications Conference*, pages 1–5, Nov. 2006.

[61] Y. Liang, T. Yoo, and A. Goldsmith. Coverage spectral efciency of cellular systems with cooperative base stations. *Proc. IEEE Asilomar Conference on Signals, Systems and Computers*, pages 349–353, Oct. 2006.

[62] J. Lindblom, E. Karipidis, and E. G. Larsson. Selfishness and altruism on the MISO interference channel: The case of partial transmitter CSI.

IEEE Communications Letters, 13(9):667–669, Sept. 2009.

[63] D. J. Love, R. W. Heath, Jr., V. K. N. Lau, D. Gesbert, B. D. Rao, and M. Andrews. An overview of limited feedback in wireless communication systems. *IEEE Journal on Selected Areas in Communications*, 26(8):1341 – 1365, Oct. 2008.

[64] Y. Ma, D. Zhang, A. Leith, and Z. Wang. Error performance of transmit beamforming with delayed and limited feedback. *IEEE Transactions on Wireless Communications*, 8(3):1164–1170, 2009.

[65] A. F. Molisch, P. V. Orlik, Z. Tao, R. Annavajjala, J. Zhang, L. Dong, and T. Kuze. Base station cooperation. Technical report, IEEE 802.16 Working Group on Broadband Wireless Access Standards - Task Group m., July 2008.

[66] B. Mondal and R. W. Heath, Jr. An upper bound on SNR for limited feedback MIMO beamforming systems. *Proc. IEEE Information Theory Workshop*, pages 408–412, Oct. 2004.

[67] K. Murota. *Discrete Convex Analysis*. Society for Industrial and Applied Mathematics, 2003.

[68] B. L. Ng, J. S. Evans, S. V. Hanly, and D. Aktas. Transmit beamforming with cooperative base stations. *Proc. IEEE International Symposium on Information Theory*, pages 1431–1435, Sept. 2005.

[69] B. L. Ng, J. S. Evans, S. V. Hanly, and D. Aktas. Distributed downlink beamforming with cooperative base stations. *IEEE Transactions on Information Theory*, 54(12):5491–5499, Dec. 2008.

[70] R. Prakash and V. V. Veeravalli. Adaptive hard handoff algorithms. *IEEE Journal on Selected Areas in Communications*, 18(11):2456–2464, Nov. 2000.

[71] Q. Rentmeesters, P.-A. Absil, P. .V. Dooren, K. Gallivan, and A. Srivatsava. An efficient particle filtering technique on the Grassmann manifold. *Proc. IEEE Conference on Acoustics, Speech, and Signal Processing*, pages 3838–3841, Mar. 2010.

[72] J. C. Roh and B. D. Rao. Efficient feedback methods for MIMO channels based on parameterization. *IEEE Transactions on Wireless Communications*, 6(1):282–292, Jan. 2007.

[73] D. Samardzija and H. Huang. Determining backhaul bandwidth requirements of network MIMO. *Proc. European Signal Processing Conference*, pages 1494–1498, Aug. 2009.

[74] A. Sanderovich, O. Somekh, H. V. Poor, and S. Shamai (Shitz). Uplink macro diversity with joint multicell processing and limited backhaul capacity. *IEEE Transactions on Information Theory*, 55(8):3457–3478, Aug. 2009.

[75] W. Santipach and M. Honig. Asymptotic capacity of beamforming with limited feedback. *Proc. IEEE International Symposium on Information Theory*, pages 290–295, Jun./Jul. 2004.

[76] W. Santipach and M. Honig. Signature optimization for CDMA with limited feedback. *IEEE Transactions on Information Theory*, 51(10):3475 – 3492, Oct. 2005.

[77] S. Shamai (Shitz) and B. M. Zaidel. Enhancing the cellular downlink capacity via co-processing at the transmitting end. *Proc. IEEE Vehicular Technology Conference*, pages 1745–1749, May 2001.

[78] M. Sharif and B. Hassibi. On the capacity of MIMO broadcast channels with partial side information. *IEEE Transactions on Information Theory*, 51(2):506–522, Feb. 2005.

[79] O. Simeone, O. Somekh, H. V. Poor, and S. Shamai (Shitz). Downlink macro- diversity with limited backhaul capacity. *EURASIP Journal on Wireless Communications and Networking*, 2009:10 pages, 2009.

[80] O. Simeone, O. Somekh, H. V. Poor, and S. Shamai (Shitz). Local base station cooperation via finite-capacity links for the uplink of wireless networks. *IEEE Transactions on Information Theory*, 55(1):190–204, Jan. 2009.

[81] C. Simon, R. de Francisco, D. T. M. Slock, and G. Leus. Feedback compression for correlated broadcast channels. *Proc. IEEE Symposium*

on Communication and Vehicular Technology, pages 1–4, Nov. 2007.

[82] O. Somekh, O. Simeone, Y. Bar-Ness, and A. M. Haimovich. CTH11-2: Distributed multi-cell zero-forcing beamforming in cellular downlink channels. *Proc. IEEE Global Telecommunications Conference*, pages 1–6, Nov. 2006.

[83] O. Somekh, B. M. Zaidel, and S. Shamai (Shitz). Sum rate characterization of joint multiple cell-site processing. *IEEE Transactions on Information Theory*, 53(12):4473–4497, Dec. 2007.

[84] A. Srivastava and E. Klassen. Bayesian and geometric subspace tracking. *Advances in Applied Probability*, 36(1):43–56, Jan. 2004.

[85] C. C. Tan and N. C. Beaulieu. On first-order Markov modeling for the Rayleigh fading channel. *IEEE Transactions on Communications*, 48(12):2032–2040, Dec. 2000.

[86] A. J. Tenebaum, R. S. Adve, and Y. S. Yuk. Channel prediction and feedback in multiuser broadcast channels. *Proc. Canadian Workshop on Information Theory*, pages 67–70, May 2009.

[87] L. Thiele and M. Schellmann and S. Schiffermuller and V. Jungnickel and W. Zirwas. Multi-cell channel estimation using virtual pilots. *Proc. IEEE Vehicular Technology Conference*, pages 1211–1215, May 2008.

[88] M. Trivellato, S. Tomasin, and N. Benvenuto. Channel quantization and feedback optimization in multiuser MIMO-OFDM downlink systems.

Proc. IEEE Global Telecommunications Conference, pages 1–5, Mar. 2008.

[89] W. Turin, R. Jana, C. Martin, and J. Winters. Modeling wireless channel fading. *Proc. IEEE Vehicular Technology Conference*, volume 3, pages 1740–1744, Oct. 2001.

[90] M. Vath. *Integration Theory: A Second Course*. World Scientific Publishing Company, 2002.

[91] A. D. Wyner. Shannon-theoretic approach to a Gaussian cellular multiple-access channel. *IEEE Transactions on Information Theory*, 40(6):1713 – 1727, Nov. 1994.

[92] J. Xu, J. Zhang, and J. G. Andrews. On the accuracy of the Wyner model in cellular networks. *Proc. IEEE Global Communications Conference*, to appear, Dec. 2010.

[93] D. Yang, W. Liu, L.-L. Yang, and L. Hanzo. Channel prediction and predictive vector quantization aided channel impulse response feedback for SDMA downlink preprocessing. *Proc. IEEE Vehicular Technology Conference*, pages 1–5, Sept. 2008.

[94] H. Yigit, A. Kavak, and K. Kucuk. Capacity improvement for TDD-MIMO systems via AR modeling based linear prediction. *Wireless Personal Communications*, 52(2):411–418, Jan. 2010.

[95] W. Yu and T. Lan. Transmitter optimization for the multi-antenna downlink with per-antenna power constraints. *IEEE Transactions on Signal Processing*, 55(6):2646–2660, Jun. 2007.

[96] E. Zacarias, S. Werner, and R. Wichman. Decentralized limited-feedback multiuser MIMO for temporally correlated channels. *Journal of Electrical and Computer Engineering*, 2010:9 pages, 2010.

[97] H. Zhang and H. Dai. Cochannel interference mitigation and cooperative processing in downlink multicell multiuser MIMO networks. *EURASIP Journal on Wireless Communications and Networking*, 2004(2):222–235, 2004.

[98] H. Zhang, N. B. Mehta, A. F. Molisch, J. Zhang, and H. Dai. Asynchronous interference mitigation in cooperative base station systems. *IEEE Transactions on Wireless Communications*, 7(1):155–165, Jan. 2008.

[99] J. Zhang and J. G. Andrews. Adaptive spatial intercell interference cancellation in multicell wireless networks. *IEEE Journal on Selected Areas on Communications. Special issue on Cooperative Communications in MIMO Cellular Networks*, to appear, 2010.

[100] J. Zhang, R. Chen, J. G. Andrews, A. Ghosh, and R. W. Heath, Jr. Networked MIMO with clustered linear precoding. *IEEE Transactions on Wireless Communications*, 8(4):1910–1921, Apr. 2009.

[101] J. Zhang, R. W. Heath, Jr., M. Kountouris, and J. G. Andrews. Mode switching for the MIMO broadcast channel based on delay and channel quantization. *EURASIP Journal on Advances in Signal Processing, special issue on Multiuser Limited Feedback*, 2009:15 pages, 2009.

[102] J. Zhang, M. Kountouris, J. G. Andrews, and R. W. Heath, Jr.. Multimode transmission for the MIMO broadcast channel with imperfect channel state information. *IEEE Transactions on Communications*, submitted, Mar. 2010.

[103] Y. R. Zheng and C. Xiao. Simulation models with correct statistical properties for rayleigh fading channels. *IEEE Transactions on Communications*, 51(6):920–928, Jun. 2003.

Vita

Ramya Bhagavatula received the B.S. degree from the Birla Institute of Technology and Sciences, Pilani-Dubai, Dubai, United Arab Emirates, in 2005 and the M.S. degree from The University of Texas at Austin in 2006. She received the Best Student Paper award at the Spring 2007 IEEE Vehicular Technology Conference in Dublin, Ireland. She is also the recipient of the David Bruton Jr. Fellowship in 2007–2008 and 2009-2010, in addition to the Aileen S. Andrew Fellowship in 2007–2008. She has interned with companies like Qualcomm and Andrew Corporation. She also completed a project for Boeing to determine feasibility and placements of multiple antenna systems in aircraft. Her research interests include multicell cooperative transmission, limited-feedback strategies, multiple inputmultiple-output channel modeling, and antenna design.

Email address: ramya.bh@gmail.com

This dissertation was typeset with LaTeX[†] by the author.

[†]LaTeX is a document preparation system developed by Leslie Lamport as a special version of Donald Knuth's TeX Program.